

Energy management for automotive power nets

Citation for published version (APA):

Kessels, J. T. B. A. (2007). *Energy management for automotive power nets*. [Phd Thesis 1 (Research TU/e / Graduation TU/e), Electrical Engineering]. Technische Universiteit Eindhoven. <https://doi.org/10.6100/IR617399>

DOI:

[10.6100/IR617399](https://doi.org/10.6100/IR617399)

Document status and date:

Published: 01/01/2007

Document Version:

Publisher's PDF, also known as Version of Record (includes final page, issue and volume numbers)

Please check the document version of this publication:

- A submitted manuscript is the version of the article upon submission and before peer-review. There can be important differences between the submitted version and the official published version of record. People interested in the research are advised to contact the author for the final version of the publication, or visit the DOI to the publisher's website.
- The final author version and the galley proof are versions of the publication after peer review.
- The final published version features the final layout of the paper including the volume, issue and page numbers.

[Link to publication](#)

General rights

Copyright and moral rights for the publications made accessible in the public portal are retained by the authors and/or other copyright owners and it is a condition of accessing publications that users recognise and abide by the legal requirements associated with these rights.

- Users may download and print one copy of any publication from the public portal for the purpose of private study or research.
- You may not further distribute the material or use it for any profit-making activity or commercial gain
- You may freely distribute the URL identifying the publication in the public portal.

If the publication is distributed under the terms of Article 25fa of the Dutch Copyright Act, indicated by the "Taverne" license above, please follow below link for the End User Agreement:

www.tue.nl/taverne

Take down policy

If you believe that this document breaches copyright please contact us at:

openaccess@tue.nl

providing details and we will investigate your claim.

Energy Management for Automotive Power Nets

PROEFSCHRIFT

ter verkrijging van de graad van doctor aan de
Technische Universiteit Eindhoven, op gezag van de
Rector Magnificus, prof.dr.ir. C.J. van Duijn, voor een
commissie aangewezen door het College voor
Promoties in het openbaar te verdedigen
op woensdag 14 februari 2007 om 16.00 uur

door

Johannes Theodorus Bernard Anna Kessels

geboren te Venray

Dit proefschrift is goedgekeurd door de promotoren:

prof.dr.ir. P.P.J. van den Bosch

en

prof.dr.ir. M. Steinbuch

CIP-DATA LIBRARY TECHNISCHE UNIVERSITEIT EINDHOVEN

Kessels, Johannes T.B.A.

Energy management for automotive power nets / by Johannes Theodorus Bernard Anna Kessels. - Eindhoven : Technische Universiteit Eindhoven, 2007 - Proefschrift.

ISBN-10: 90-386-1963-4

ISBN-13: 978-90-386-1963-7

NUR 951

Trefw.: energiemangement / hybride voertuigen / brandstofverbruik / regelsystemen ; optimalisering.

Subject headings: energy management systems / hybrid electric vehicles / fuel economy / optimal control.

Printed by Universiteitsdrukkerij, Technische Universiteit Eindhoven.

Energy Management for Automotive Power Nets

*Vier jaar bevlogen onderzoek,
Vier jaar samengevat in een boek.*

*Vier jaar aan nieuwe dingen mogen wennen,
Vier jaar de wereld een beetje beter leren kennen.*

Samenstelling promotiecommissie:

prof.dr.ir. A.C.P.M. Backx (voorzitter)

prof.dr.ir. P.P.J. van den Bosch

prof.ir. O.H. Bosgra

dr.ir. A.G. de Jager

dr.ir. D.B. Kok

dr.ir. J.P. Pauwelussen

prof.dr.ir. M. Steinbuch

prof.dr.ir. A.J.A. Vandenput



The research reported in this thesis is part of the research program of the Dutch Institute of Systems and Control (DISC).

The author has successfully completed the educational program of the Graduate School DISC.

Contents

1	Introduction	1
1.1	Research scope	2
1.1.1	Hybrid vehicle configurations	2
1.1.2	Energy efficiency	5
1.1.3	Concepts for energy management	6
1.2	Thesis motivation	9
1.2.1	Positioning of this thesis	9
1.2.2	Problem definition	11
1.2.3	Modeling assumptions	12
1.2.4	Outline thesis	13
2	Simulation environment	15
2.1	Quasi-static vehicle modeling for EM	16
2.1.1	Internal combustion engine	16
2.1.2	Drive train and driver	20
2.1.3	Electric machine	22
2.1.4	Battery model	23
2.2	Dynamic CarSim simulation environment	26
2.2.1	Drive train model with driver	26
2.2.2	Battery model	30
2.3	Conclusions	33
3	Energy management for hybrid electric vehicles	35
3.1	Energy management for S-HEV	36
3.1.1	Vehicle model	36
3.1.2	Strategy analysis	40
3.1.3	Design rules	43
3.1.4	Optimal strategy	45
3.1.5	On-line adaptive strategy	47
3.1.6	On-line optimal strategy	52
3.2	Energy management for P-HEV	53
3.2.1	Vehicle model	54
3.2.2	Strategy outline	56

3.2.3	On-line adaptive strategy	58
3.3	Energy management for S/P-HEV	62
3.3.1	Electronically-controlled CVT	62
3.3.2	Planetary gear train	63
3.3.3	Vehicle model	65
3.3.4	On-line adaptive strategy	67
3.4	Energy management including battery wear	75
3.5	Conclusions	77
4	Simulation results	79
4.1	Simulation environment	80
4.1.1	Description of S-HEV	80
4.1.2	Description of P-HEV	81
4.1.3	Description of S/P-HEV	82
4.2	Simulation results	82
4.2.1	Results S-HEV	82
4.2.2	Results P-HEV	84
4.2.3	Results S/P-HEV	87
4.3	Evaluation	89
4.3.1	Conclusions	91
4.3.2	Recommendations	92
5	Energy management with electronic horizon	93
5.1	Road information	93
5.2	Energy management with electronic horizon	95
5.2.1	Statistic road information	95
5.2.2	Energy scheduling between road segments	99
5.3	Simulation results	101
5.3.1	Strategy evaluation	103
5.3.2	Discussion	105
5.4	Conclusions	106
6	Case-study: Conventional vehicles	107
6.1	Introduction	108
6.2	Vehicle control model	110
6.3	Problem definition	112
6.4	Quadratic programming	113
6.4.1	Model reduction	113
6.4.2	QP formulation	114
6.4.3	Model predictive control	116

6.5	On-line strategy	117
6.5.1	Strategy analysis	117
6.5.2	Optimal performance	120
6.5.3	Adaptive strategy	120
6.6	Experimental validation	121
6.6.1	Simulation environment	121
6.6.2	Vehicle implementation	121
6.6.3	Evaluated strategies	122
6.7	Strategy results	123
6.7.1	Influence of prediction horizon	123
6.7.2	Results from experimental validation	125
6.8	Evaluation & Discussion	127
6.9	Conclusions	131
7	Conclusions & Recommendations	133
7.1	General observations	133
7.2	Conclusions	134
7.3	Recommendations	137
A	Bandwidth of energy management strategy	139
A.1	Closed-loop stability	139
A.1.1	Kharitonov theorem	142
A.1.2	Model components with losses	143
A.2	Closed-loop bandwidth	144
A.2.1	Power spectrum	145
A.2.2	Example NEDC driving cycle	146
	Bibliography	149
	Summary	155
	Samenvatting	157
	Dankwoord	159
	Index	161
	Curriculum Vitae	163

Contents

1

Introduction

Fossil fuels in the earth's crust are formed from the remains of plants and animals, that lived millions of years ago. Coal, oil (petroleum), and natural gas are the main elements of fossil fuels and together with nuclear and renewable energy, they cover the world's primary energy demand.

Since the oil crisis in 1973, the world became aware of the fact that fossil fuels are a precious product on earth. Within a time span of almost thirty-five years, the average price for a barrel of crude oil on the US market rose from approximately \$3.29 up to \$54.52 in 2005. Also last year, the oil prices have been historically high with peaks above \$75.00 during the summer of 2006. As a result, the authorities and the industry have a strong interest in technological improvements for the production, distribution and consumption of energy around the world.

Within the scope of this thesis, oil takes a special position, as it can be separated into fractions for the production of gasoline. For this reason, oil is currently the primary energy source for the transport sector. As stated by the International Energy Agency, the transport sector requested 16% of the world primary energy demand¹ in 2002, and looking at the transport sector itself, the largest energy request comes from road vehicles (75%), whereas other transportation methods stay far behind, see [63] for a detailed overview. Given the fact that in 2006 the world's average oil request was close to 85 million barrels per day, it is clear that transport has a large impact on the world's oil production.

¹These figures are on-line available at the International Energy Agency (IEA): "World Energy Outlook 2004", page 68, www.worldenergyoutlook.org.

Suppose that road vehicles improve their fuel economy only by 1%. Then the world's oil demand reduces with 102.000 barrels of oil each day. Hence, a small improvement in the energy efficiency of vehicles corresponds to a huge reduction in primary energy usage. This makes the research area of Energy Management (EM) for automotive vehicles really appealing.

This thesis focusses on EM strategies for automotive power nets. Currently, the electric power demand in road vehicles increases rapidly. Reasons for this trend are the high standards on safety and comfort, as well as the replacement of mechanical or hydraulic systems by electromechanical devices, see [71, 15]. In addition, the Hybrid Electric Vehicle (HEV) has appeared to the market, *e.g.*, the Toyota Prius and the Honda Civic Hybrid. In these vehicles, the power train combines at least two power sources (*i.e.*, the traditional combustion engine and an electric motor), and this concept contributes to a high electric power demand. In general, these new technologies have the potential for improving the overall energy efficiency of the vehicle. Nevertheless, a suitable strategy will be required to control all these new facilities, leading to the central theme in this thesis: Energy Management.

1.1 Research scope

The entire process starting from the production of fuel to actually driving the vehicle is complex. At intermediate steps, there are many opportunities to improve the energy efficiency, but it is important to keep the scope of the research focussed. This section provides an overview of possible directions to improve the vehicle's fuel efficiency. Furthermore, it shows how the actual fuel efficiency gets affected by an alternative vehicle configuration or with EM.

1.1.1 Hybrid vehicle configurations

In a traditional vehicle, the Internal Combustion Engine (ICE) provides propulsion power to the drive train. Since the speed and torque characteristics of an ICE do not match with the requirements at the wheels, a gearbox is used. Over the years, this has become an approved method, although the ICE is frequently operated in less preferred operating points. To overcome this problem, one could install an alternative power source (*e.g.*, an electric motor) that better fits with the power requirements from the drive train. It is also possible to keep the traditional ICE installed and add

a secondary power source to cover the total power demand. According to this line of reasoning, three different concepts are discussed below: electric vehicles, fuel cell hybrid vehicles and hybrid electric vehicles. It turns out that EM takes a central role in all these approaches. The hybrid electric vehicles offer the highest flexibility for an EM system and therefore, the research in this thesis concentrates on this configuration.

Electric vehicle (EV)

In an EV, the primary energy source is the battery and an electric motor is present for vehicle propulsion. An EV is not charge sustaining, which means that its battery needs to be charged from an external device. In many cases, battery charging takes place from the grid. That is why people often call the EV a “plug-in” car.

Fuel cell hybrid vehicle (FCHV)

From a mechanical point of view, there is no difference between the propulsion system of an FCHV and an EV. Both vehicles provide power to the wheels solely by the electric motor. However, the electric energy supply system is different. Besides the battery, also a fuel cell is present to supply electric power. The fuel cell generates electric power from hydrogen (H_2) stored in the fuel tank. The vehicle becomes charge sustaining by charging the battery with energy from the fuel cell.

Note that there is a difference between a hydrogen FCHV and a hydrogen ICE vehicle. The latter refers to a traditional vehicle configuration, but the ICE has been modified to run on pure hydrogen. This means that hydrogen goes into the fuel tank and after the combustion process, water comes out of the tail-pipe. The hydrogen ICE vehicles can be valuable for a technology push of an hydrogen infrastructure.

In addition, also fuel cell vehicles are proposed using a reformer for producing hydrogen. Like traditional vehicles, gasoline goes into the fuel tank and the reformer takes care of the conversion into H_2 gas, and can be directly used by the fuel cell stack. Nevertheless, the energy efficiency of this vehicle configuration turns out to be less promising [84].

Hybrid electric vehicle (HEV)

An HEV combines an ICE and an electric machine in its propulsion system. The terminology HEV does not refer to one single vehicle topology, but covers a wide range of solutions. In literature, mainly

three HEV-classes are distinguished: Series- (S), Parallel- (P), and Series/Parallel- (S/P) HEVs.

In an S-HEV, there is no mechanical connection between the ICE and the drive train. This means that the ICE can run continuously in its preferred operating range, whereas the drive train is driven by an electric machine. For the electric power request, it relies on the battery plus the generator. The generator is driven by the ICE and maintains a suitable energy level in the battery. A drawback of this configuration is that energy is first converted from mechanical power to electric power with the generator, and then back to mechanical power by the electric machine, both introducing losses.

The P-HEV establishes a parallel connection between the ICE and the electric machine, and both systems are allowed to give tractive force to the drive line. The power through the electric machine can be positive as well as negative. This allows the electric machine to operate in motor mode and generator mode. At a top-level view, the P-HEV configuration looks similar to a conventional vehicle, although the electric machine in a conventional vehicle operates only in generator mode.

According to the size of the electric machine and the power net voltage, the P-HEVs are often classified into four groups [39]: micro, mild, medium, and full. The micro HEV offers the smallest hybridization with an electric machine typically in the range of 2 - 4 [kW]. The mild or medium HEVs are recognized by their increased power net voltage (typically ≥ 42 [V]). Nevertheless, the added value of the electric machine is still limited to assisting the ICE, rather than driving pure electric. This is different with a full HEV, where electric drive is fully supported, by using a higher battery voltage and a large electric machine.

Finally, the last vehicle configuration is an S/P-HEV. As already indicated by its name, it combines the topology of a series and a parallel HEV. In principle, these types of vehicles have the highest complexity since power to the drive train can follow various trajectories. Examples for these vehicle types are the Ford Hybrid Escape and the Toyota Prius.

The vehicle configurations listed above are shown in Fig. 1.1. Through a careful technology selection for individual components, each vehicle op-

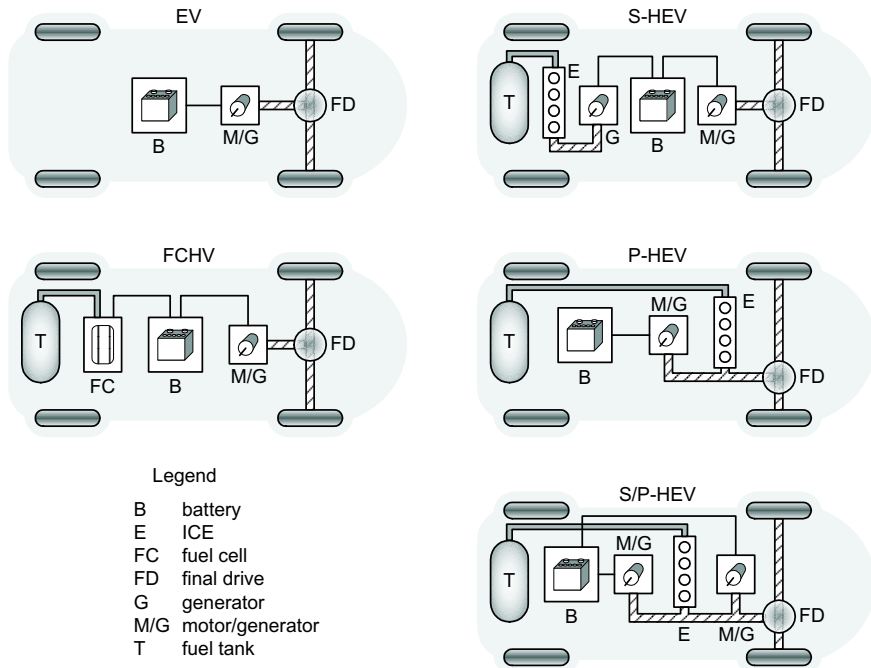


Figure 1.1: Alternative vehicle configurations

timizes its energy efficiency and subsequently, extends the vehicle mileage. The next section provides a survey of the energy efficiency for these vehicles.

1.1.2 Energy efficiency

In the transportation sector, the energy efficiency of vehicles falls apart into two fractions. First, one has to consider the efficiency of the fuel manufacturing plant (well-to-tank efficiency) and second, there is the efficiency of the vehicle itself (tank-to-wheel efficiency). Altogether, the overall efficiency (well-to-wheel efficiency) is equal to the product of both efficiencies.

Table 1.1 indicates the corresponding efficiency for three vehicle configurations: the traditional gasoline vehicle, the HEV such as the Toyota Prius, and the FCHV with hydrogen for fuelling. What should be noticed from this table is the excellent well-to-tank efficiency for gasoline. Over the years, the manufacturing process has become fully optimized and therefore, significant improvements are not very likely to happen in the near future. This is different with natural gas, where new technologies will be able to




	Well-to-tank efficiency (%)	Tank-to-wheel efficiency (%)	Well-to-wheel efficiency (%)			
			0	10	20	30
Traditional gasoline car	88	16				
Hybrid electric vehicle	88	37				
Fuel cell hybrid vehicle	58	50				

Table 1.1: Overall fuel efficiency, source: [21]

raise the well-to-tank efficiency above 70% for hydrogen.

Another important observation from Table 1.1 is the great diversity of tank-to-wheel efficiencies. It can be seen that the present generation of HEVs achieves a superior tank-to-wheel efficiency, compared to the traditional vehicles. As already proven by HEVs that are nowadays moving through the streets, this high tank-to-wheel efficiency translates into an extended vehicle mileage. Moreover, Table 1.1 provides only figures for an HEV with a gasoline ICE, but in [84] it is reported that HEVs with a diesel engine will offer an improved well-to-wheel efficiency of at least 5%.

In spite of the higher tank-to-wheel efficiency of an FCHV, the HEV currently dominates the hydrogen technology. However, car manufacturers expect the tank-to-wheel efficiency of a FCHV to improve approximately 10% in the near future [21]. Together with an improved well-to-tank efficiency, this will put the FCHV in a leading position.

1.1.3 Concepts for energy management

The dominant position for the tank-to-wheel efficiency in an HEV comes in the first place from the selected vehicle topology and the improved component technology. Nevertheless, without an intelligent EM system, this high energy efficiency is probably not reachable under normal driving conditions. This section provides an overview of the basic principles behind an EM system.

Regenerative braking

In a traditional vehicle, the mechanical friction brakes become active when the driver wants to decelerate the vehicle. From an energy point of view, this is certainly not an economic solution, since all kinetic energy is wasted into heat. To recover the energy that comes

available during braking periods, one can operate the electric machine in generator mode. This way, the electric machine absorbs power from the drive train and stores it into the battery. In terms of fuel economy, this is the most economical way to charge the battery, since it requires no additional fuel.

Engine stop/start

The ICE of a traditional vehicle runs frequently idle during city trips. A simple method to save fuel, is to stop the engine at those moments when no power is needed. However, for driver comfort a quick vehicle response is preferred when the driver wants to move on. Given the fact that a powerful electric machine is present in most HEVs, a smooth engine cranking will be no problem. Moreover, the electric machine could also establish an electric drive during vehicle launch. This offers additional freedom for keeping the engine off.

Motor assist

There are several reasons why the fuelmap of an ICE incorporates non-linear behavior in specific operating ranges. Consequently, some operating points are more beneficial to produce power than others. In case of an HEV, there exists freedom in the amount of power that should be delivered by the ICE versus the power from the electric machine. This means that at moments when the ICE enters an un-economic operating area, motor assist takes place with power taken from the battery. Conversely, the ICE produces additional power in economic operating points to charge the battery.

Load scheduling

Except for the mechanical vehicle load, there are also electric loads active in the vehicle. Some of these loads are time-critical, but there are also loads where the driver will not notice different behavior if their energy request is scheduled in time. *E.g.*, heating and cooling functions are good examples for these loads. With an EM system, they become only active in economic operating points.

Very often, these individual concepts are considered as a separate subsystem of an EM system. However, in terms of energy efficiency it is desirable to develop a general solution which includes all possible EM facilities. This automatically addresses the main contribution of this thesis: the development of an on-line EM system, suitable for all HEVs as well as vehicles

with a traditional power train. This system provides a full integration of the concepts given above.

To develop this EM system, it is important to have a good knowledge about the parameters that influence the actual fuel consumption of the vehicle. In the first place, this is the selected vehicle configuration, but also other effects play a dominant role such as component sizing, the driver's power demand, driving cycle characteristics, etc. Nevertheless, the maximum fuel benefits for any EM system are theoretically bounded by two engine characteristics:

1. The fuel consumption of the ICE when it runs at idle speed;
2. Variations in the slope of the fuelling-curves, when the ICE changes its operating point.

This is explained as follows. When the ICE runs at idle speed, it produces no mechanical power (measured at the crankshaft), although a small amount of fuel is still required. Without considering other side-effects, one can switch off the engine and eliminate this fuel offset to save fuel.

The second ICE characteristic relates to the following observation. Injecting more fuel into the engine leads to extra mechanical power. However, the exact relation between fuel injection and power depends on many tuning parameters and the corresponding fuel curves express usually non-linear behavior. These non-linearities translate into opportunities for the EM system by shifting the operating point of the ICE to areas that require relative less fuel. Graphically, this is elucidated in Fig. 1.2, where three artificial fuel curves are shown. The curves A and B express a linear relation between engine power and fuel use, whereas curve C incorporates some non-linearities. Furthermore, B and C have an offset at zero power, which denotes the fuel consumption at idle speed.

For all basic EM concepts, the potential fuel benefit is summarized in Table 1.2. One can see that regenerative braking is always profitable, since it provides electric energy without additional fuel costs. Furthermore, it is trivial that the potential of engine stop/start is directly related to the height of the fuel offset during idle speed. Curve A has no offset, leaving no stop/start potential for EM. Finally, the non-linear behavior in curve C allows the EM system to apply motor assist or load scheduling. Because more fuel is required at high power levels, that area should be avoided to produce (electric) power.

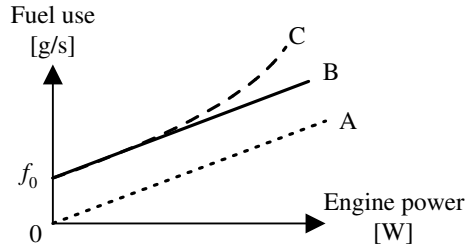


Figure 1.2: Example of three artificial fuel curves

	<i>Regen braking</i>	<i>Engine stop/start</i>	<i>Motor assist</i>	<i>Load scheduling</i>
Curve A	Yes	No	No	No
Curve B	Yes	Yes	No	No
Curve C	Yes	Yes	Yes	Yes

Table 1.2: Fuel benefit from EM concept

1.2 Thesis motivation

In November 2001, the Ford Motor Company and the Technische Universiteit Eindhoven (TU/e) set up a multidisciplinary research project entitled: “The development of an energy and power management system for conventional and future vehicle power nets”.

Since the start of the project, the TU/e deployed two PhD students. The first PhD student started in February 2002 and had a background in mechanical engineering. His research was completed recently with the thesis entitled: “Energy management for vehicular electric power systems” [52]. The second PhD student started in February 2003 and has a background in electrical engineering. By means of this thesis, the author completes his research.

1.2.1 Positioning of this thesis

In recent years, a lot of research is carried out in the field of energy management for HEVs and EVs. To position the work presented in this thesis, a short overview of existing literature will be given.

Strategies that are based on heuristics can be easily implemented in a

real vehicle by using a rule-based strategy [10, 20] or by using fuzzy logic [10, 72]. Although these strategies can offer a significant improvement in energy efficiency, it is clear that they do not guarantee an optimal result in all situations. Consequently, strategies emerged that are based on optimization techniques.

To find the global optimal solution, control techniques such as linear programming [78], quadratic programming [77], optimal control [25], and especially dynamic programming (DP) [4, 7, 36, 55] have been studied. In general, these techniques do not offer a causal solution, because they assume that the future driving cycle is entirely known. Moreover, the required calculations put a high demand on computational resources and prevent an on-line implementation. Nevertheless, their result can be used as a benchmark for the performance of other strategies, or to derive rules for a rule-based strategy.

A different approach is taken in [47, 46, 54]. Instead of considering one particular driving cycle for calculating an optimal control law, a set of driving cycles is considered, resulting in a stochastic optimization approach. The solution is calculated off-line and stored in a state-dependent look-up-table. This look-up-table provides a quasi-static control law which is directly suitable for on-line vehicle implementation. A difficulty will be to cover a real-world driving situation with a set of individual driving cycles.

If only the present state of the vehicle is considered, optimization of the operating points of the individual components can still be beneficial. Typically, the proposed methods define an optimization criterion which minimizes the vehicle fuel consumption or exhaust emissions. A weighting factor can be included to prevent drift in the battery from its nominal energy level and guarantee a charge sustaining solution. This is done in [31], but it remains difficult to select a weighting factor that is mathematically sound. An alternative approach is to extend the objective function with a fuel equivalent term. This term includes the corresponding fuel use for the energy exchange with the battery in the optimization criterion, see [19, 37, 56, 61, 65, 74]. Mathematically, this concept is correct and is taken as a starting point for the solution methods presented in this thesis. Furthermore, this solution also emerges when considering a sub-class of the optimal control problem, see [14, 25].

One step further is to incorporate the optimization into a Model Predictive Control (MPC) framework [7, 83], such that the energy management strategy will be able to anticipate on upcoming events. A disadvantage of this approach is that it requires knowledge about the future power de-

mand of the vehicle. The quality of the prediction information as well as the length of the prediction horizon determine the success of the control strategy.

After considering the optimization based methods described above, the following observations are made. First, many optimization techniques suffer from complex calculations which are undesirable for on-line vehicle implementation. Although techniques exist to overcome this drawback (*e.g.*, by training a neural network to mimic the complex optimization algorithm on-line, see [60]), they lose optimality through their approximation. A second observation is that accurate information is needed about the future driving cycle and the vehicle status. Especially the strategies with a fuel equivalent term require detailed information about the expected energy losses in vehicle components, to determine a proper weighting factor.

This thesis presents a causal on-line EM system, which puts aside both drawbacks mentioned above. The EM system remains free from complex optimization algorithms and it does not rely on prediction information, but still mimics the optimal solution. It is shown that the proposed concept is suitable for the series, parallel and series/parallel HEV. Moreover, it also applies to vehicles with a conventional drive train.

The underlying EM strategy has been derived from the optimal control problem, but differs from existing solutions by providing a mathematical as well as a physical interpretation for the fuel equivalent term. This also explains the success of the strategy, because it utilizes only vehicle characteristics which are important for EM.

1.2.2 Problem definition

The primary goal of the EM system is to minimize the vehicle's fuel consumption under all driving situations. To that end, the EM strategy optimizes the powerflow of the electric power net in a fuel efficient way.

The components connected to the power net are the battery, the electric machine (or generator), and the auxiliary loads. When the power request from the driver is known, it follows that the EM system has to optimize two decision variables. The first variable corresponds to the power from the electric machine, whereas the second variable decides whether the ICE is turned on or off.

Although the vehicle is a complex dynamical system, the control objective of the EM system fits into a static optimization problem:

$$\min_x J(x), \quad \text{subject to } G(x) \leq 0. \quad (1.1)$$

Here, $J(x)$ is called the objective function, whereas $G(x)$ denotes the constraints that have to be satisfied for the decision variables x . This mathematical framework is used to calculate the global optimal solution, where the EM system achieves the best possible fuel economy. Unfortunately, this does not lead to a causal strategy, since it requires exact knowledge about the entire future driving cycle. The main research question is to develop a causal EM system, with similar behavior as the global optimal solution, but without the need for having prediction information. Moreover, complex optimization routines should be avoided, to guarantee an on-line vehicle implementation.

In the end, the performance of the EM system has to be compared to a baseline situation. Unfortunately, vehicle manufacturers are hesitating when giving information about their EM strategy. Moreover, technical details of vehicle components are also lacking, so there are many uncertainties when validating a baseline vehicle model. For the S-HEV and the P-HEV, the baseline situation implies a solution where the battery is never charged or discharged. This situation is compared to the situation with an EM strategy. Unfortunately, the S/P-HEV offers still many solutions, while the battery power is zero. For this vehicle configuration, there does not exist a unique baseline strategy, given only the requirement that the battery power is zero. Hence, a comparison with the EM strategy is not possible.

Finally, this thesis will not discuss the decision process about which vehicle technology to use and it does not make a statement about a suitable component sizing. For this, the reader is referred to other work, *e.g.*, [26, 35].

1.2.3 Modeling assumptions

Vehicles and their environment are complex systems and apparently, no model can describe accurately the entire vehicle behavior, including its surrounding environment, in any situation. Nevertheless, models are of great help when developing an EM strategy. Although their accuracy might be limited in general, they can be sufficiently accurate for a dedicated application. This thesis uses power-oriented vehicle models, taking into account the following assumptions:

- Quasi-static maps can be used to describe the process of energy conversion in the ICE, the electric machine and the battery. Especially for the ICE and the battery, ongoing research must reveal the situations where this assumption is valid. Nevertheless, it is expected that

on a time-scale of seconds and minutes, as used by the models in this thesis, their dynamical behavior can be represented accurately with a quasi-static map. For motivating examples, the reader is referred to [34].

- Thermal effects of the ICE have been excluded from the engine model. All driving cycles start with a pre-heated ICE, and engine stop/start has a negligible effect on engine temperature, because of its short duration.
- The ICE requires no extra fuel during the cranking phase. This assumption will be justified in Chapter 2.
- The electric loads in the vehicle are power based such that their power demand is independent from the voltage level of the power net. Their total power demand can be estimated on-line.
- Information about the energy status of the battery is on-line available.
- Battery wear is a slow varying process and is not included in the battery model. Extra costs for replacement of the battery are neglected by the EM system, although they easily can be included, see Section 3.4.
- The mechanical power demand, typically measured at the transmission side of the drive train and not at the wheel-side, can be estimated on-line.

The necessity of these assumptions becomes clear in the next chapters.

1.2.4 Outline thesis

The research described in the remaining chapters is structured as follows. In Chapter 2, the simulation models are explained for all vehicle components. In addition, this chapter describes the simulation environment which is used for analyzing an EM strategy.

Chapter 3 demonstrates the EM system for the power net in three different vehicle classes: S-HEV, P-HEV and S/P-HEV. This chapter shows an extensive analysis on how EM improves the vehicle fuel economy. Next, an optimal causal EM strategy is presented for each vehicle class.

The EM strategies developed in Chapter 3 are tested and evaluated in a simulation environment. The results are summarized in Chapter 4.

Amongst other things, this chapter visualizes the benefits of each EM feature, with respect to fuel economy.

So far, the on-line EM strategies do not include any information about the future driving cycle. A method to utilize road predictions is presented in Chapter 5. By means of simulations, this chapter qualifies the added value of an electronic prediction horizon.

As a case-study, Chapter 6 presents a practical application of the EM concept as proposed in this thesis. For a series-production vehicle with a traditional drive train, it is shown how the EM strategies from Chapter 3 can be applied with a minimum investment for the vehicle hardware. Vehicle experiments on a roller-dynamometer demonstrate the actual fuel benefits.

Finally, an overview of the main conclusions from this thesis is given in Chapter 7. Moreover, this chapter ends with recommendations on how to continue the research from this thesis.

2

Simulation environment

This chapter describes the simulation environment that has been developed for testing and analyzing EM strategies. The current simulation environment covers two vehicle configurations: a traditional vehicle configuration (*e.g.*, the Ford Mondeo) and an HEV.

The simulation environment incorporates appropriate models for all essential vehicle elements, including the driver. In addition, also the EM system is part of the simulation environment. Because the EM strategy applies a model-based control algorithm, it utilizes a control model to decide on the controlled variables. Both the control model and the simulation model represent the same vehicle, although the control model includes less details. The overall model structure is visualized in Fig. 2.1. Since the EM strategy takes its decisions by evaluating on-line the control model, the control model has a limited complexity.

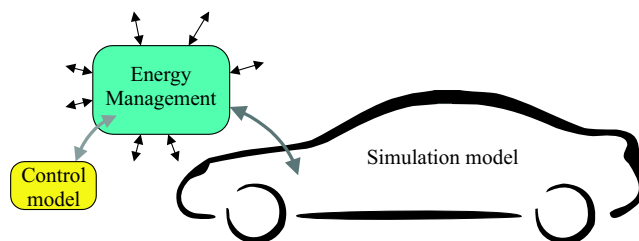


Figure 2.1: Structure of simulation model with EM system

In the project, the majority of the modeling activities focussed on a Ford Mondeo vehicle with a 2.0ℓ gasoline engine and a 5-speed manual transmission. A quasi-static control model has been derived as well as a dynamic simulation environment named CarSim. A description of the control model can be found in Section 2.1 whereas the simulation environment CarSim is discussed in Section 2.2. This latter simulation environment has been developed as a separate work-package within the research project and an earlier publication appeared in [41]. In this thesis, the application of the CarSim environment can be found in Chapter 6.

Contrary to the Ford Mondeo vehicle, an HEV was not physically available within this research project for doing vehicle experiments. For that reason, the HEV models have a limited model complexity and only quasi-static models are developed in Section 2.1. From a practical point of view, significant time savings are achieved by applying an identical control model and simulation model. Nevertheless, for a thorough strategy evaluation, one has to verify if the simulation model is sufficiently accurate with respect to reality.

2.1 Quasi-static vehicle modeling for EM

Due to the complexity of a vehicle, the vehicle model consists of complete subsystems, rather than individual components. This section describes the following subsystem: the internal combustion engine, the drive train, the electric machine, the battery and the electric loads. By connecting these model components in a proper way, the preferred vehicle configuration is established (*i.e.*, vehicles with a traditional drive train as well as HEVs).

2.1.1 Internal combustion engine

The model for the internal combustion engine (ICE) expresses the relation between the operating point of the ICE and the actual fuel consumption. The operating point is defined by two parameters: engine speed ω [rad/s] and engine torque τ_m [Nm]. Both quantities are specified at the engine crankshaft. For practical reasons, the corresponding fuel consumption $f(\tau_m, \omega)$ [g/s] is often measured on an engine test-bench. On this test-bench, the ICE runs sufficiently long in a steady operating point, such that all the thermal-dynamic effects in the ICE and the coolant temperature are excluded from the measurement. After measuring the actual fuel consumption over a short interval, the entire procedure is repeated for another op-

erating point. All measurement results are translated into a 2-dimensional look-up-table. This way, a quasi-static fuel map is established.

To visualize the measurement data, fuel maps are often represented in terms of Brake Specific Fuel Consumption (BSFC). The name BSFC originates from the classical engine test-bench where a mechanical brake is connected to the crankshaft and defines the operating point of the ICE. Mathematically, the BSFC expresses the ratio between the actual fuel consumption f and the power P_m [W] at the crankshaft:

$$\text{BSFC}(\tau_m, \omega) := \frac{f(\tau_m, \omega)}{P_m} \times 3600 \times 10^3 \quad [\text{g/kWh}]. \quad (2.1)$$

An example of a map for a 2.0ℓ Spark Ignition (SI) engine is shown in Fig. 2.2. Note that the BSFC is inversely proportional to the efficiency of the ICE. This is explained as follows. The chemical energy content of fuel is defined by its Lower Heating Value h_f [J/g]. Typically, $h_f = 44.5$ [kJ/g] for gasoline, which means that each gram of fuel carries 44.5 [kJ] of energy. The ICE efficiency η_{ice} equals the ratio between the mechanical output power and the chemical input power:

$$\eta_{ice} := \frac{P_m}{P_{ch}} = \frac{P_m}{h_f f(\tau_m, \omega)} = \frac{3600 \times 10^3}{h_f \text{BSFC}(\tau_m, \omega)} \quad [-]. \quad (2.2)$$

Instead of measuring the actual fuel consumption, it is also possible to measure the tail pipe emissions and analyse the contribution of particular exhaust gas products. Tail pipe emissions are extremely dominant in the procedure of vehicle homologation, because environmental regulations allow only a limited amount of carbon monoxide (CO), oxides of nitrogen (NOx) and hydrocarbons (HC) for vehicles with a gasoline engine. For a diesel engine, these regulations focus on particulate matter (PM) and NOx emissions¹.

Based on the applied measurement procedure, the obtained fuel and emission maps are preferably used in a static engine model, where the engine operating point remains fixed. However, these maps are also used in quasi-static models, where the ICE operating point changes smoothly according to the power demand of the driver. For example, the simulation environment ADVISOR [85] takes a similar approach. Nevertheless, it is important to realize that the emission maps of an SI engine are actively controlled

¹Nowadays, all new passenger cars sold within the European Union have to comply with the EURO-5 standard as specified in directive 70/220/EEC and additional amendments. In addition, more stringent regulations have been announced for the year 2008.

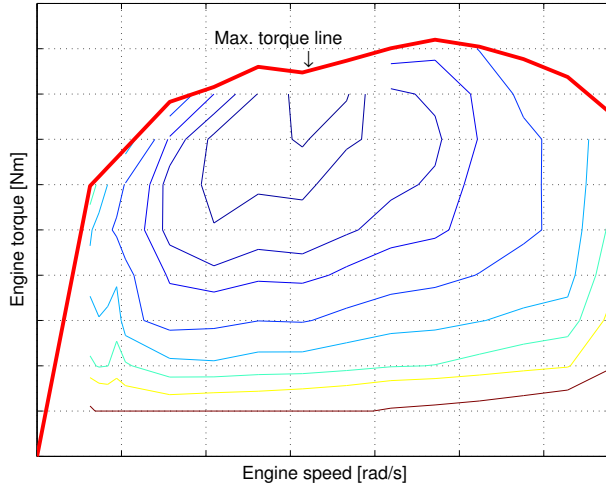


Figure 2.2: Outline of BSFC curves for 2.0 ℓ SI engine [g/kWh]

by the Engine Control Unit (ECU). Because the dynamic behavior has been excluded from the measurement procedure, the emission maps do not accurately describe the ICE under highly dynamic conditions. Finally, little information is known about the validity of these maps, when the engine needs to be serviced, or how they match with similar series production engines. This will be a topic for further research.

Engine stop/start

An attractive method to reduce the fuel consumption is by applying engine stop/start. With engine stop/start, the ICE shuts down when no mechanical power is needed. This situation occurs for example when the vehicle is standing still. Turning off the ICE is profitable since it eliminates the required fuel to run idle. On the other hand, engine cranking requires extra fuel, and this gives a trade-off whether engine stop/start should be done.

Experiments with a similar 2.0 ℓ ICE in a vehicle with a conventional starter, learn that engine cranking at ambient temperature takes approximately 1 [s], see [18, 70]. Within this period, the engine starts to crank from standstill, speeds up quickly to 1500 [rpm] if the engine fires, then slows down toward idle speed. To guarantee a good startability, significantly more fuel is dumped into the intake port during the first engine cycles. Especially for a cold engine start this extra fuel is necessary, although it

contributes to excessive hydrocarbon (HC) emissions. In [57] it is shown that for a hot engine start, each cylinder receives approximately 600 [mg] fuel over the first three cycles, whereas the next cycles require only 18 [mg] to run idle. Hence, for this particular situation, engine stop/start will be profitable if the ICE remains off at least 11 cycles. This requirement should be taken into account by the EM system.

A different situation appears for HEVs. These vehicles have typically no starter, but use an Integrated Starter/Generator (ISG) instead. This electric machine is usually more powerful than a traditional starter and therefore, the ISG can start the ICE in less than 250 [ms]. Moreover, it is sufficient to supply only enough fuel to maintain idle during the first engine cycles, see [40]. As a result, an EM system can apply engine stop/start with no additional fuel costs. On the other hand, the ISG consumes energy from the battery during the starting period. These starting periods take usually place when the vehicle drives off, and the ISG delivers already the required propulsion power. Compared to the propulsion power, a starting period over a small time interval requires limited energy. Therefore, this thesis uses the assumption that an EM strategy can apply engine stop/start without extra fuel costs and without using extra energy from the battery.

Engine drag torque

A topic that has not been addressed so far is the fuelling behavior of the ICE during braking periods. This behavior is mainly determined by the ECU, and it has been tuned for a smooth engine operation during braking. Still these characteristics are important for an EM system, since they immediately affect the capability for a regenerative braking strategy. In a traditional vehicle, the ICE provides a braking torque to the drive train, as soon as the driver releases the accelerator pedal. At those moments, the crankshaft torque becomes negative, since kinetic energy from the vehicle is absorbed by the ICE. Unfortunately, only two points are measured for this negative torque range. The first point is at zero torque when the engine delivers no power. For different speeds, one can measure the corresponding fuel consumption. The second point corresponds to the situation that the ECU injects no fuel and the ICE keeps running from an external power offered to the crankshaft. This so-called fuel cut-off phase occurs, amongst others, when the vehicle goes down-hill. Measuring the actual power absorbed by the ICE provides insight into the drag torque of the ICE. Finally, both points are used to estimate the fuelling behavior of the

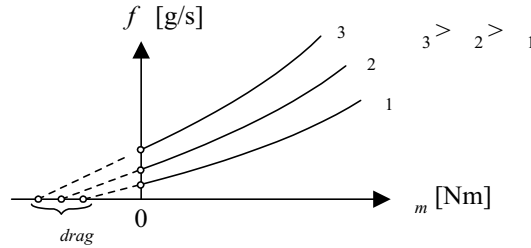


Figure 2.3: Linear interpolation in negative torque area

ICE in the area in-between, using linear interpolation. This procedure is elucidated in Fig. 2.3 with separate fuel curves for different engine speeds.

It is clear that the method from above is not perfectly sound. However, more information is currently not available from the documentation of the ECU. Moreover, accurate measurement data is not easily obtained because an engine test-bench would be required, rather than a roller dynamometer test-bench which is currently available.

2.1.2 Drive train and driver

The longitudinal vehicle dynamics are modelled by the drive train and the driver. The drive train delivers the propulsion power from the ICE to the wheels, whereas the driver controls the actual vehicle speed. The drive train model encompasses the following components: the vehicle chassis, the final drive gear ratio, a gearbox and the clutch.

In literature, basically two modeling approaches are distinguished for describing the vehicle drive train in combination with the driver: a forward vehicle model and a backward vehicle model. The forward vehicle model is the most accurate model, but has a high level of complexity. The name forward vehicle model originates from the method how the actual vehicle speed is calculated. Starting with a desired throttle position from the driver, the ICE provides torque to the drive train and consequently, the vehicle achieves a certain speed. Contrary to the forward vehicle model, the backward vehicle model is less complex. It uses a given speed profile of the wheels and calculates *back* what the corresponding operating point of the engine has to be. Because the dynamic behavior of individual components and the influence of the driver is neglected, the backward vehicle model is computationally less demanding. This section discusses the drive train

<i>Quantity</i>	<i>Symbol</i>	<i>Value</i>	<i>Unit</i>
Vehicle mass	m	1400	kg
Frontal area	A_d	2.0	m ²
Air drag coefficient	C_d	0.3	-
Rolling resistance	C_r	0.015	-
Air density	ρ	1.2	kg/m ³
Gravity	g	9.8	m/s ²
Wheel radius	w_r	0.3	m
Final drive ratio	f_r	4.0	-
Gear ratio	g_r	3.4 - 2.1 - 1.4 - 1.0 - 0.77	-

Table 2.1: Parameter list for drive train model

model with a backward vehicle model. More details about the forward vehicle model as it is available in the CarSim simulation environment, are given in Section 2.2.1.

A typical aspect of the backward vehicle model is that a quasi-static model is used to describe the relation between the vehicle speed and the required propulsion power. Consider, for convenience, a vehicle with a traditional drive train and a manual transmission. For a given vehicle speed $v(t)$ [m/s] with a selected gear ratio $g_r(t)$ [-], and road slope $\alpha(t)$ [rad], the corresponding engine speed $\omega(t)$ [rad/s] and drive train torque $\tau_d(t)$ [Nm] are calculated using the following formulas [34]:

$$\omega(t) = \frac{f_r}{w_r} g_r(t) v(t), \quad (2.3)$$

$$\tau_d(t) = \frac{w_r}{f_r} \frac{1}{g_r(t)} F_d(t), \quad (2.4)$$

with

$$F_d(t) = m \dot{v}(t) + \frac{1}{2} \rho C_d A_d v(t)^2 + m g [\sin(\alpha(t)) + C_r \cos(\alpha(t))]. \quad (2.5)$$

Then the power required by the drive train is equal to:

$$P_d(t) = \omega(t) \tau_d(t) = v(t) F_d(t). \quad (2.6)$$

A description of all parameters is given in Table 2.1. Furthermore, this table provides also the parameter values for a mid-sized vehicle such as the Ford Mondeo.

A difficulty when modeling the drive train is the validation procedure. In general, vehicle measurements cover only the engine speed, the wheel speed and possibly the torque at the wheels. However, the torque delivered by the ICE is typically not measured but estimated by the ECU. This means that there will always be an uncertainty in the parameter list from Table 2.1. Furthermore, friction losses from the drive train are not explicitly present in (2.6), so they also appear as a disturbance on this parameter list.

Finally, a backward vehicle model assumes a perfect tracking of the vehicle speed according to the requested speed profile from the driver. This way, the driving cycle reduces to a static look-up-table, describing the vehicle speed and the gear position. This approach explicitly assumes that control actions from the EM system do not affect the speed of the vehicle, nor other aspects on driveability.

2.1.3 Electric machine

Based on the selected vehicle configuration, the simulation environment distinguishes two models for the electric machine: a generator model for the Ford Mondeo and a motor/generator model for HEVs. The generator model converts power from the mechanical domain into the electric domain, whereas the motor/generator can handle power in both directions.

Similar to the ICE model, also the electric machine uses a static look-up-table to describe the relation between its input and output signals. At the mechanical side, the signals of interest are speed and torque with their product equal to the mechanical power P_{em} [W]. The electric side considers electric power P_e [W] without notion of voltage and current. The simulation model assigns a positive value to P_e and P_{em} when the electric machine operates in generator mode. On the other hand, P_e and P_{em} become negative valued during motor mode. According to the nominal powerflow, the corresponding efficiencies are defined:

$$\text{Motor mode: } \eta_{mm}(\tau_{mm}, \omega) = \frac{P_{em}}{P_e} = \frac{\tau_{mm} \omega}{P_e} \quad [-] \quad (2.7)$$

$$\text{Generator mode: } \eta_{gm}(\tau_{gm}, \omega) = \frac{P_e}{P_{em}} = \frac{P_e}{\tau_{gm} \omega} \quad [-] \quad (2.8)$$

For a belt-driven 1.6 [kW] generator, an efficiency map is shown in Fig. 2.4a. This model has been used for simulations with the Ford Mondeo vehicle. A similar map can also be constructed for the electric machine in an HEV, although it needs extensions for operating in motor mode as well as rotations at low speeds.

The research described in this thesis will consider only simplified models for the electric machine in an HEV. This model also includes the losses from the electric power converter. For the mechanical losses, consider the map shown in Fig. 2.4b. The information shown in this figure is identical to Fig. 2.4a, but now separate curves are used to express the relation between input- and output power at different generator speeds. It turns out that the losses increase almost proportionally when the input power increases. Moreover, the main reason for large changes in the efficiency map from Fig. 2.4a is due to the static friction losses at zero power. Without these friction losses, the efficiency of the generator remains nearly constant.

Here it is assumed that the electric losses as well as the mechanical losses can be added into one average efficiency. This way, the efficiencies in motor mode and generator mode are fixed, and the model of the electric machine boils down to one single expression:

$$P_{em} = \max(\eta_{mm}P_e, \frac{1}{\eta_{gm}}P_e). \quad (2.9)$$

Note that (2.9) does not provide a good description of the friction losses at zero power. In [52] it is shown how these losses can be included as a speed dependent off-set term, but this extension is neglected in this thesis. The power limitations of the electric machine are taken into account at the mechanical side:

$$P_{em\min} \leq P_{em} \leq P_{em\max}. \quad (2.10)$$

2.1.4 Battery model

Lead-acid batteries have been used in road vehicles for more than 50 years. Due to its complex chemical behavior, batteries are nowadays still subject to on-going research. Moreover, the battery usage in the past has a large influence on its present status. An excellent survey on this topic is given by Jossen in [38]. Recently, publications appeared in the field of State Of Health [24] and overcharging [79].

For the control model, there exists a trade-off between the accuracy of the battery model versus the required simulation time. The EM strategies presented in this thesis use a power-oriented battery model. This way, the complex relation between voltage and current is excluded from the battery model and an on-line implementation of the EM system is guaranteed. It should be mentioned that the CarSim library includes an accurate dynamic battery model, which calculates the voltage and the current profile at the

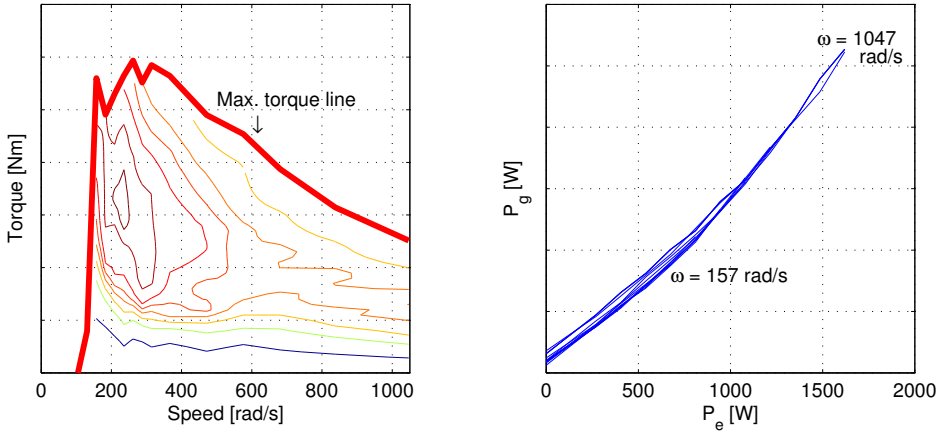


Figure 2.4: Generator model: (a) efficiency map and (b) power curves

battery terminals. However, due to its high level of complexity, it is not feasible to include this model in the control model of the EM system.

The battery model consists of two subsystems: a static efficiency block and a dynamic energy storage block, see Fig. 2.5. The efficiency block incorporates the energy losses during charging and discharging, whereas the energy storage block keeps track of the actual energy level E_s in the battery. At this point an integrator is used:

$$E_s(t_e) = E_s(0) + \int_0^{t_e} P_s(t) dt \quad [\text{J}]. \quad (2.11)$$

To indicate the actual charging level of the battery, the definition State of Charge (SOC) is often used in literature. However, the physical background of this definition has a strong relation with battery models based on current and voltage, see Section 2.2.2. Because the proposed battery model is power based, the definition State of Energy (SOE) is more appropriate. Given a theoretical energy capacity E_{cap} [J] of the battery, the SOE expresses the relative energy status:

$$SOE := \frac{E_s}{E_{cap}} \times 100 \quad [\%]. \quad (2.12)$$

Depending on the control strategy from the EM system, three different representations of the internal battery losses are taken into account, which approximate the relation between the power P_b at the battery terminals

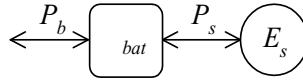


Figure 2.5: Battery model

and the net internal power P_s . Their application will become clear when discussing the individual strategies in Chapter 3 and Chapter 6.

- **Linear losses**

When considering linear losses, the battery is modelled through an efficiency number $0 \leq \eta_{bat} \leq 1$. This parameter expresses the overall losses during a combined cycle of charging and discharging. Physically, one can make a distinction between the losses that occur during charging ($P_s \geq 0$) and discharging ($P_s < 0$). Denoting these losses through the parameters $\eta^+ \leq 1$ and $\eta^- \leq 1$, respectively, with $\eta_{bat} = \eta^- \eta^+$ results in the following parametrization:

$$P_b \approx \max(\eta^- P_s, \frac{1}{\eta^+} P_s). \quad (2.13)$$

A typical static charge/discharge curve with (piece-wise) linear losses is shown in Fig. 2.6a.

- **Quadratic losses**

It is reasonable to believe that the battery losses increase more than proportional when the battery power increases. Therefore it makes sense to incorporate quadratic losses in the battery model by means of a second order polynomial:

$$P_b \approx \beta P_s^2 + P_s. \quad (2.14)$$

Fig. 2.6b shows a static map of a battery with quadratic losses.

- **Combination of linear and quadratic losses**

Finally, it can be attractive to consider a battery model with linear as well as quadratic losses (see Quadratic Programming in Section 6.4). This leads to the following parametrization:

$$P_b \approx \beta P_s^2 + \max(\eta^- P_s, \frac{1}{\eta^+} P_s). \quad (2.15)$$

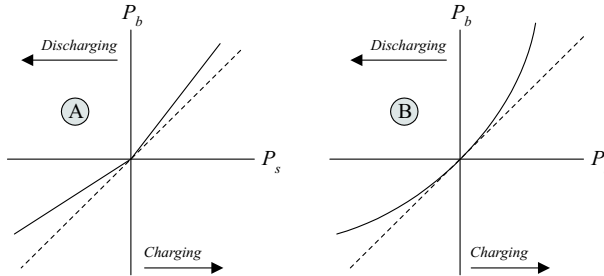


Figure 2.6: Battery model: (a) Linear losses and (b) Quadratic losses

These loss-models can be used in combination with the energy storage buffer E_s from (2.11). It is assumed that battery aging goes relative slowly and possible effects from battery wear can be included by updating the model.

2.2 Dynamic CarSim simulation environment

For the evaluation of an EM system in a conventional vehicle, an advanced simulation environment named CarSim has been developed in Matlab Simulink. This simulation environment offers a flexible workspace for testing and analyzing EM strategies. In principle, CarSim consists of a Simulink library holding all necessary components to construct the vehicle model. The library blocks introduce a modular approach, such that vehicle components can be easily exchanged. This section will describe only two components of the CarSim library: the drive train model with the driver and the battery model. These components have a complex dynamic behavior and their implementation will be discussed in the remainder of this section. The implementation of the other CarSim models is done in a similar way as the description given in Section 2.1.

2.2.1 Drive train model with driver

The CarSim-library makes use of a forward vehicle model, covering the longitudinal dynamics of the vehicle. A forward facing vehicle model is characterized by the fact that a driver model controls actively the vehicle speed by means of the pedal position for throttle, brake and clutch. Depending on the throttle-position, the ICE provides torque towards the drive

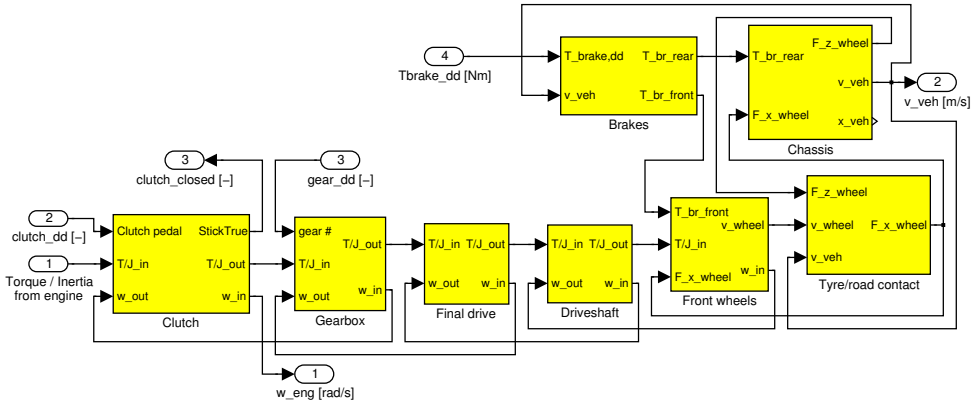


Figure 2.7: Drive train model in CarSim

train. Next, the drive train model describes the relation from the engine torque to the vehicle speed by means of the following components: the clutch, transmission, final drive, drive shafts, wheels, brakes and chassis. They are mutually connected as shown in Fig. 2.7. This causal structure is based on the ADVISOR scheme [85] but differs from it by being forward facing.

Each element of the drive train is modelled as a separate subsystem. In Fig. 2.7, the torque and the cumulative inertia of the preceding components are passed through from left to right. This means that the available engine torque is decreased by the torque losses in the drive train components while the lumped inertia is the sum of the individual drive train component inertias. In the end, the resulting vehicle speed is calculated in the chassis block. Next, the corresponding rotational speeds of the components are passed through from right to left. Finally, this leads to the engine speed as calculated in the clutch block. The main characteristics of each component are given below, whereas details about the experimental validation can be found in [41].

Clutch: The clutch model encompasses two discrete modes: stick and slip. The stick-mode describes the situation that the clutch is closed. In this mode, there is no speed difference between the input and output shaft. Furthermore, possible losses are excluded in stick-mode. In slip-mode, the clutch is slipping or completely open. The torque

losses in slip mode have been modelled based on experimental data.

Gearbox: The gearbox covers a 5-speed manual transmission, but to include the neutral gear, its model contains 6 modes. The corresponding gear ratios can be found in Table 2.1. The torque losses depend on the selected gear number as well as the input torque received from the clutch. Physical measurement data provided by its manufacturer has been used to calculate these losses.

Final drive: The final drive establishes a fixed ratio between the speed of the primary shaft (connected to the gearbox) and the secondary shaft (drive shafts). Its gear ratio is also given in Table 2.1. The torque losses are calculated according to the speed of the primary shaft. Again, data from the manufacturer has been used to determine these losses.

Drive shaft: The vehicle under consideration is a front-wheel driven vehicle. The drive shaft transports torque from the final drive to the front wheels. The torque and speed relations are calculated with a parallel spring and (weak) damper system.

Front wheels: The front wheels translate the torque from the drive shaft τ_{in} into a rotational wheel speed ω_{wheel} . The other forces acting on the front wheels are the rolling resistance τ_{roll_front} , the torque applied by the brakes τ_{br_front} and the force from the road contact $F_{w_contact}$. Given the inertia of the wheels J_w , the wheel speed satisfies the following differential equation:

$$\dot{\omega}_{wheel} = \frac{\tau_{in} - w_r F_{w_contact} - \tau_{roll_front} - \tau_{br_front}}{J_w}, \quad (2.16)$$

with the wheel radius w_r taken from Table 2.1.

Brakes: The brakes offer a desired braking force to the front and rear wheels. Unfortunately, the vehicle signals contain only a discrete on/off signal for the brake-lights, whereas the exact position of the brake pedal is not available for measurement. For the moment, a linear function has been selected for describing the relation between the position of the brake-pedal and the brake-torque applied to the wheels. Note that vehicles with an EM system apply first regenerative braking, whereas the friction brakes are only used when the

electric machine cannot recover more energy. This means that regenerative braking starts when the driver releases the throttle pedal. The mechanical brakes become only active when more vehicle braking is desired. As a result, the simplified relation between brake pedal and brake torque has no further consequences for the EM system.

Tire/Road contact: The contact between the tires and the road defines the final force $F_{w_contact}$ transferred to the road. The wheel-slip κ is estimated from the difference between the wheel speed and the actual vehicle speed. Next, this wheel-slip is used to calculate the tire friction coefficient μ using the “magic formula” from Pacejka [64]. The parameter values for the magic formula are taken from ADVISOR [85]. Finally, the force transferred to the road equals the product between μ and the normal wheel force F_{w_normal} (induced by the vehicle mass acting on the front wheels):

$$F_{w_contact} = \mu F_{w_normal} \quad (2.17)$$

Chassis: The chassis-block calculates the actual vehicle speed v_{veh} . Therefore, the force applied by the front wheels to the road $F_{w_contact}$ is reduced by the vehicle air drag F_{drag} and possibly an extra load from road inclination F_{climb} . Furthermore, the rear wheels introduce an additional rolling resistance F_{roll_rear} and a braking torque τ_{br_rear} during vehicle deceleration. Altogether, the actual vehicle speed is calculated as follows:

$$\dot{v}_{veh} = \frac{F_{w_contact} - F_{drag} - F_{climb} - F_{roll_rear} - \tau_{br_rear}/w_r}{m}, \quad (2.18)$$

with m and w_r taken from Table 2.1.

Now that all components of the drive train model are discussed, the driver model will be explained. Similar to a real vehicle, this driver model operates the throttle, clutch and brake pedal, such that the vehicle follows a desired speed profile. In a conventional vehicle, a belt-driven generator is permanently connected to the crankshaft of the ICE. Therefore, the available power from the ICE changes when the EM strategy selects a different setpoint for the generator. As a result, the driver notices possible actions from the EM system as a disturbance on the actual vehicle speed (assuming no feed-forward compensation from the strategy itself).

Basically, the driver model applies a feedback Proportional Integral (PI) controller, taking the actual vehicle speed and the desired vehicle speed as

input signals (including a selected gear position as specified in the driving cycle). The output signals are a desired propulsion torque from the engine, a braking torque for the brakes, and the position of the clutch. An additional interface has been created to convert the torque signals into a suitable position for the throttle, the clutch and the brake pedal.

The initial parameter settings for the PI controller are derived from general driver characteristics found in literature (see [2] and the references therein). For calculating the position of the brake pedal, no further mappings are required since the actual pedal position is not available in the measurement data. The throttle and the clutch signals require a more advanced approach. These signals are generated by a mode-switching system, using four separate modes: stop, launch, shifting, or driving. Each mode activates its own settings for the parameters of the PI controller, and this enables the driver model to maintain the vehicle speed within the required tolerance window.

The question might appear if a PI controller is the best solution to represent the behavior of a real-world driver. In fact, a real driver always looks ahead of the vehicle and this way, he or she relies heavily on feed-forward input signals. Compare this to a driver with only feedback information available. The only input for this driver would be the rear-view mirror, so control actions are started when the vehicle has already left its preferred direction. From a control point of view, it would be more realistic to use a driver model that includes a feed forward signal. However, this would require additional research to determine the exact amount of feed forward information as seen by a real-world driver. This research is outside the scope of this thesis.

2.2.2 Battery model

Most road vehicles are nowadays equipped with a lead-acid SLI-battery (Start, Light, and Ignition). Unfortunately, the lifetime of a battery reduces when the energy throughput increases, whereas intensive battery usage is one of the main side-effects of an EM system. A battery type that is less sensitive to this sort of battery wear is the Valve-Regulated Lead-Acid (VRLA) battery. In terms of energy throughput, the expected lifetime of a VRLA battery exceeds more than three times the life expectancy of an SLI-battery. For this reason, the VRLA battery has been selected for the research with conventional vehicles.

Vehicle simulations over an extended time horizon (approximately 20

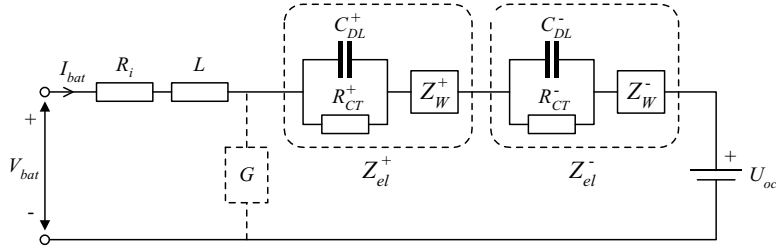


Figure 2.8: Electric circuit of VRLA battery model

minutes for a typical European driving cycle) put a high demand on the accuracy of the fast and slow dynamical elements in the battery model. An impedance-based non-linear battery model as described by Buller et al. [16] is able to fulfill these requirements for a VRLA battery. This model has been implemented in the CarSim library. The block diagram is shown in Fig. 2.8 and the main characteristics of the components are summarized below. For more details about the battery dynamics, the interested reader is referred to an excellent survey in [38].

Open circuit voltage U_{oc}

A 12 [V] lead acid battery is build from a series connection of six electrochemical cells with a nominal voltage of 2.0 [V]. This nominal voltage determines the open circuit voltage U_{oc} of the battery when it is in rest. In this steady state, U_{oc} turns out to be an accurate indication for the SOC of the battery [6]. The battery model keeps track of the SOC by integration of the current-flow and a suitable mapping from SOC to U_{oc} is derived from experimental data.

Internal resistance R_i

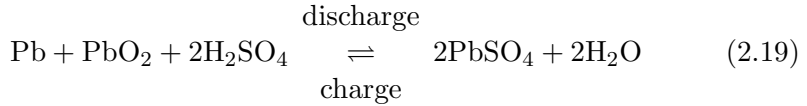
The internal ohmic resistance R_i represents the sum of the resistance of the battery terminals, the transition between the electrodes and the electrolyte, and the electrolyte itself. The actual value of R_i depends on the battery temperature and the SOC.

Inductance L

The inductance L of the battery is mainly determined by the geometric construction of each cell in the battery. For this reason, the value of L does not depend on changes in temperature or SOC. A fixed parameter value for L has been determined from the measurement data.

Impedance for positive electrode Z_{el}^+ and negative electrode Z_{el}^-

The negative electrode is constructed from porous lead Pb whereas the positive electrode is created from lead dioxide PbO_2 . Both electrodes are immersed in an aqueous solution of sulphuric acid H_2SO_4 . As the battery discharges, electrons are drawn from the negative battery terminal and find their way through the electric circuit towards the positive battery terminal. Within the battery, the sulphuric acid from the electrolyte is consumed and water is formed. At the same moment, the lead-material from the electrodes changes into lead sulfate $PbSO_4$. When charging the battery, this chemical process is reversed. The overall process is denoted in the following equation [82]:



When charging or discharging the battery, a charge zone is formed on the layer between the electrodes and the electrolyte. This zone determines the dynamic behavior of the battery, as it behaves as a capacitor. This so-called double-layer capacitance occurs in parallel to the electrochemical charge transfer reaction. Typically, the charge transfer reaction is described by a non-linear resistance R_{CT} .

Except for the double-layer capacitance, also the mass transport of ions through the electrolyte of the battery influences the dynamic behavior of the battery. In most cases, this mass transport is caused by diffusion (*i.e.*, the gradient in the concentration of the electrolyte gives rise to movement of the ions) and a valid representation for this phenomenon is given by a Warburg impedance Z_W . All together, each electrode contains three model elements: a double layer capacitor C_{DL} , a charge transfer resistance R_{CT} and a Warburg impedance Z_W . The equivalent circuit is elucidated in Fig. 2.8.

Since the material of the positive and negative electrodes are different, also the dynamic behavior of C_{DL} and R_{CT} will be different. As both elements are connected in parallel, they form a low-pass filter with a typical cut-off frequency for the positive and negative electrode at 10 [Hz] and 100 [Hz], respectively [38]. As a result, current signals above 100 [Hz] will not flow through the charge transfer resistance.

Gassing reactions G

In case of overcharging, gassing reactions are initiated by the water in the battery. It falls apart into oxygen at the positive electrode and hydrogen at the negative electrode. These reactions are irreversible if one of the gasses is released from the battery. Therefore, the VRLA batteries are designed to promote the chemical recombination of oxygen at the negative electrode to minimize water loss. These side-reactions become dominant when charging the battery near 100% SOC or at a high voltage level. Since an EM system does not operate the battery in this area, these reactions are excluded from the battery model.

The battery model is able to simulate the voltage response of a VRLA battery during highly dynamic current profiles over various SOC levels. However, charge acceptance of the battery is not included in the model, so simulation results might be too optimistic about the amount of power that can be accepted by the battery. Also the influence of temperature and battery aging is not taken into account. More information about this battery model and its validation procedure is presented in [16].

2.3 Conclusions

Two simulation environments have been derived. One simulation environment has a reduced model complexity and uses quasi-static models for the drive train (backward facing), the electric machine and the ICE. The available model components allow for vehicle configurations with a traditional drive train as well as HEVs. Through its limited complexity, this environment can be used both as a control model and as a simulation model. The results presented in Chapter 3 and 5 are obtained from this simulation environment.

The other simulation environment is called CarSim and offers a complex dynamic simulation model only for vehicles with a traditional drive train. The forward facing drive train model has been validated against results from vehicle experiments. This simulation environment will be used in Chapter 6.

3

Energy management for hybrid electric vehicles

Over the years, the automotive industry has put much effort in developing vehicles that satisfy today's high standards on safety and comfort, and simultaneously comply with strict environmental regulations. One of the leading technologies that nowadays becomes generally accepted is a Hybrid Electric Vehicle (HEV). By applying a secondary power source, these vehicles offer a significant improvement in fuel economy compared to a vehicle with a traditional drive train.

These vehicles require an advanced Energy Management (EM) strategy to control the power of the secondary power source. In literature, many solutions to this problem have been presented, covering heuristic approaches [10, 20] as well as advanced strategies based on optimization techniques [51, 55, 61, 73]. Especially the optimization concept offers an excellent solution to the stated EM problem. However, it remains difficult to achieve robust performance when an exact prediction of the future driving cycle is not available.

This chapter presents a proven concept for an adaptive EM system, suitable for the series (S), parallel (P) and series/parallel (S/P) HEV topologies. Without the need for having exact predictions about the future driving cycle, the proposed EM system achieves a performance very close to the optimal non-causal strategy. The success of the EM system originates from the fact that it exploits only typical vehicle characteristics which are relevant for EM. These characteristics, as well as their relation with the EM system will also be treated in this chapter.

As indicated above, this chapter considers three HEV topologies. The S-HEV does not have a mechanical connection between the internal com-

bustion engine (ICE) and the wheels and the EM strategy will be discussed in Section 3.1.1. Next, Section 3.2 focusses on the EM strategy for a P-HEV. In a P-HEV, the ICE and the electric machine can both give tractive force to the wheels, offering freedom for an EM strategy. An earlier publication of the work described in this section appeared in [45]. The third vehicle configuration is the S/P-HEV, and its EM strategy will be explained in Section 3.3. The S/P-HEV has maximum freedom for EM, due to its versatile powersplit device.

Except for the benefits in fuel economy, an EM strategy also introduces extra costs, due to an intensified battery usage. In addition to the EM strategies from the preceding sections, Section 3.4 presents a general method to include the costs for an early replacement of the battery. Finally, this chapter ends with the conclusions in Section 3.5.

3.1 Energy management for S-HEV

3.1.1 Vehicle model

The vehicle topology of an S-HEV is shown in Fig. 3.1. The mechanical power P_m from the combustion engine is directly converted into electric power P_g with the generator. Next, the electric machine utilizes this power and provides mechanical power P_{em} to the drive train for vehicle propulsion. Furthermore, the electric load demand equals P_L . In case P_e plus P_L are not balanced with P_g , there is a power exchange P_b with the battery. The characteristic behavior of the components is further discussed below. Note that the arrows in Fig. 3.1 define the powerflow in positive direction.

Drive Train model

The power demand P_d from the drive train is calculated with the quasi-static backward-facing vehicle model described in Chapter 2. Given a preferred speed profile, this model calculates the mechanical power request P_d according to:

$$P_d = \omega_d \tau_d \quad [\text{W}], \quad (3.1)$$

with ω_d [rad/s] and τ_d [Nm] defined in (2.3) and (2.4), respectively.

Electric Machine

The electric machine can operate in two modes: motor mode ($P_{em} \leq 0$) and generator mode ($P_{em} > 0$). There is a rigid connection between the

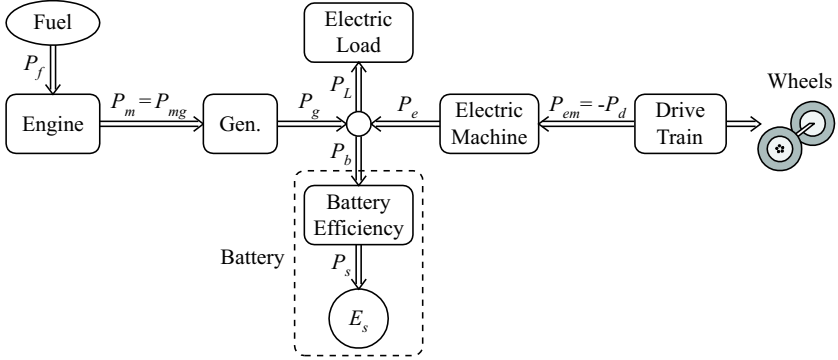


Figure 3.1: Topology of an S-HEV (arrows define positive powerflow)

drive train and the electric machine. This way, the electric machine is able to supply power to the drive train (motor mode) but it also can recover kinetic energy in generator mode during regenerative-braking phases. For convenience, the description for the power losses in the electric machine is repeated here from (2.9).

$$P_{em} = \max(\eta_{mm}P_e, \frac{1}{\eta_{gm}}P_e) \quad [\text{W}]. \quad (3.2)$$

The power limitations of the electric machine are assumed to be fixed:

$$P_{emmin} \leq P_{em} \leq P_{emmax}. \quad (3.3)$$

Electric power net

The power net accumulates the powerflow from all electric devices. For simplicity, it is assumed that the required power converters (including their energy losses) are incorporated in the generator, the electric machine and the electric load. This way, the power net reduces to the following power balance:

$$P_g + P_e = P_b + P_L. \quad (3.4)$$

Generator

Mechanical power from the engine is converted into electric power by the generator. The generator allows electric power only in one direction, so $P_g \geq 0$. In agreement with the electric machine, the losses are proportional

with power. By defining the efficiency $\eta_g \leq 1$, a linear generator model appears:

$$P_g = \eta_g P_{mg} \quad [\text{W}]. \quad (3.5)$$

Internal Combustion Engine

In literature, the fuel consumption of an ICE is usually represented with a static non-linear map, describing the relation between fuel use, the crankshaft torque τ_m and the engine speed ω . However, it is also possible to define the fuel consumption as a function of engine power and speed:

$$\text{fuelrate} = f(\tau_m, \omega) = f(P_m \mid \omega) \quad [\text{g/s}]. \quad (3.6)$$

The notation with the conditional-operator \mid is introduced here to emphasize the dependency of $f(P_m)$ on ω . The advantage of this notation becomes clear when explaining the control objective of an EM strategy. Similar to the definition in Chapter 2, the efficiency of the ICE is calculated with help of the lower heating value of fuel h_f [J/g]:

$$\eta_{ice}(P_m \mid \omega) = \frac{P_m}{P_f} = \frac{\omega \tau_m}{f(P_m \mid \omega) h_f} \quad [-]. \quad (3.7)$$

A typical efficiency map of a 2.0ℓ Spark Ignition (SI) engine is shown in Fig. 3.2.

Instead of considering the engine efficiency over its entire operating range, one can also focus on variations in efficiency for a fixed engine power P_m . The actual value of P_m is determined by τ_m and ω . In an S-HEV, there is no mechanical connection between the ICE and the wheels, so the ICE can run in several operating points (τ_m, ω) and still deliver equal power $P_m = \tau_m \omega$. From an efficiency point of view, it will be beneficial to operate the engine only in those operating points that entail minimum fuel use for a given power demand. The set of operating points that fulfills this criterion is called the *e-line* (economy line). For every power request P_m , the e-line operating point $(\tau_m, \omega)_{e\text{-line}}$ equals:

$$\begin{aligned} (\tau_m, \omega)_{e\text{-line} \mid P_m} &= \arg \max_{(\tau_m, \omega) \in \mathcal{Q}(P_m)} \eta_{ice}(\tau_m, \omega) \\ &= \arg \min_{(\tau_m, \omega) \in \mathcal{Q}(P_m)} f(\tau_m, \omega), \end{aligned} \quad (3.8)$$

with

$$\mathcal{Q}(P_m) = \{ (\tau_m, \omega) \mid P_m = \omega \tau_m \}. \quad (3.9)$$

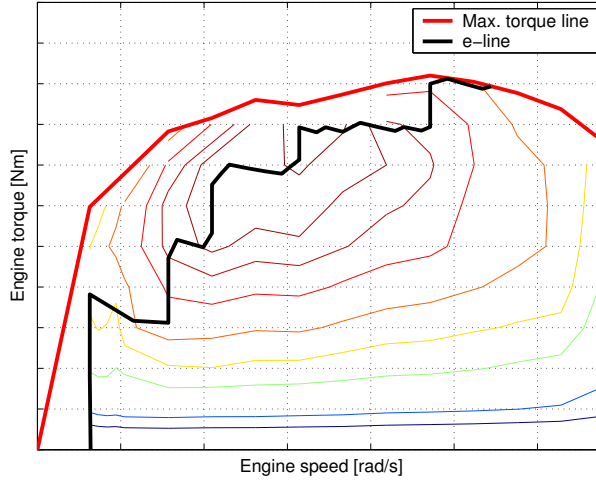


Figure 3.2: Outline of engine efficiency map and e-line

The efficiency map shown in Fig. 3.2, also presents the corresponding e-line. Recall that this efficiency map is measured at fixed grid points. Due to linear interpolation, the e-line expresses non-smooth behavior. The associated fuel consumption follows from the substitution of (3.8) in (3.6):

$$f_{e\text{-line}}(P_m) = f(\tau_m, \omega)_{e\text{-line}|P_m} \quad [\text{g/s}]. \quad (3.10)$$

Finally, to express whether the engine is running or not, a discrete variable $S \in \{0, 1\}$ will be added. Altogether, the fuel consumption of the ICE depends on two variables:

$$fuelrate(P_m, S) = \begin{cases} 0 & \text{if } S = 0 \\ f_{e\text{-line}}(P_m) & \text{if } S = 1 \end{cases} \quad [\text{g/s}]. \quad (3.11)$$

Note that a penalty for engine stop/start is not included in the model.

Battery model

The battery model consists of a static efficiency map in combination with an energy storage buffer. The efficiency map incorporates piece-wise linear losses, according to the description in Section 2.1.4. Together with an integrator for the energy buffer, the battery model consists of two equations:

$$P_b = \max(\eta^- P_s, \frac{1}{\eta^+} P_s), \quad (3.12)$$

$$E_s(t) = E_s(0) + \int_0^t P_s(\tau) d\tau. \quad (3.13)$$

3.1.2 Strategy analysis

A typical characteristic of the S-HEV, is that there is no mechanical connection between the drive train and the ICE or the generator. Therefore, the engine can operate on the e-line all the time. Now suppose that the ICE runs on the e-line and that the generator supplies exactly the power requested by the drive train and the electric loads. This means that the battery power is zero (*i.e.*, $P_b = 0$) and for convenience, this situation is called *Baseline* (BL). However, from an energy efficiency point of view, it might be attractive to generate additional power and store the surplus energy in the battery. Likewise, it could be profitable to produce less electric power and retrieve the remaining part from the battery. These situations are referred to as *Charging mode* (C) and *Power supply management* (PSM), respectively. Finally, there is also an option to turn-off the ICE and rely completely on the battery to fulfill the power request. This mode is called *Motor only* (MO).

From an EM strategy it is expected that it selects the most economic mode and, if necessary, decides on the generator power. To obtain insight into this decision process, the fuel map of the ICE has to be taken into consideration. To that end, the e-line shown in Fig. 3.2 is drawn again in Fig. 3.3 but now as a function of power P_m . This figure reveals four areas where there exists an almost linear (affine) relation between the function $f_{e-line}(P_m)$ and P_m . Typically, the slope λ of this curve remains almost constant within these areas and equals the following definition:

$$\lambda(P_m) = \frac{\partial f_{e-line}(P_m)}{\partial P_m} \quad [\text{g/J}]. \quad (3.14)$$

Intuitively, it is clear that λ expresses the additional fuel massflow to produce a small amount of mechanical power, given a certain power level P_m . Hence, λ expresses the incremental fuel cost. With help of this definition, the e-line curve can be approximated as a piece-wise affine function:

$$f(P_m) \approx f_i + \lambda_i P_m \quad \text{for } P_m \in \Omega_i, \quad (3.15)$$

with $i = 0, \dots, N_f$ and where $\Omega_i, \dots, \Omega_{N_f}$ are line segments:

$$\Omega_i = \{P_m | P_{m_i} \leq P_m \leq P_{m_{i+1}}\}. \quad (3.16)$$

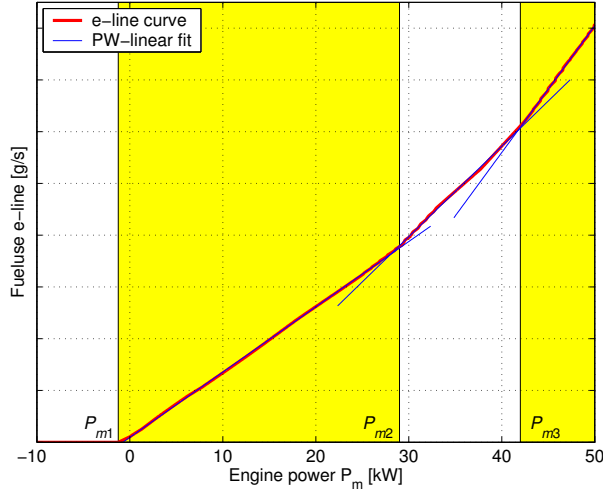


Figure 3.3: Fuel consumption of e-line curve and piece-wise linear fit

For this particular engine it is sufficient to take $N_f = 3$. Hence, the e-line is approximated as:

$$f(P_m) \approx \begin{cases} 0 & \text{if } P_m < P_{m1} \\ f_1 + \lambda_1 P_m & \text{if } P_{m1} \leq P_m < P_{m2} \\ f_2 + \lambda_2 P_m & \text{if } P_{m2} \leq P_m < P_{m3} \\ f_3 + \lambda_3 P_m & \text{if } P_m \geq P_{m3} \end{cases} \quad (3.17)$$

This parametrization is also elucidated in Fig. 3.3. Note that an S-HEV never operates the ICE in the negative power range. This is because the powerflow through the generator is limited to one direction. Hence, $P_m \geq 0$.

To get insight into the importance of λ for EM, this parameter is compared to the engine efficiency η_{ice} in Fig. 3.4. For convenience, λ in Fig. 3.4a has been multiplied with $h_f = 44.5$ [kJ/g] to obtain a suitable scaling. The maximum efficiency of the ICE equals approximately 34%, so producing energy there requires almost three times more chemical energy. Hence, $\lambda h_f \sim 2.9$ [J/J].

The curves in Fig. 3.4a and b are drawn from the information shown in Fig. 3.3. Although numerical differentiation of the e-line introduces noise for λh_f in Fig. 3.4a, still the distinctive areas between P_{m1} , P_{m2} and P_{m3} are visible. Furthermore, the information shown in this figure is independent from the fuel offset f_1 .

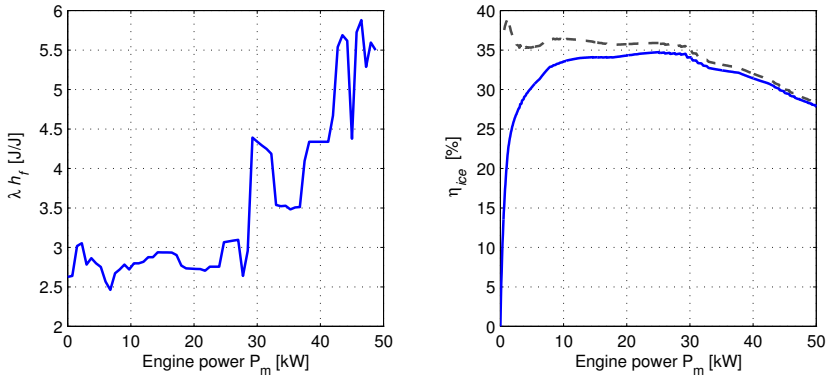


Figure 3.4: E-line: (a) incremental cost and (b) engine efficiency

This is different in Fig. 3.4b. Here, the piece-wise linear behavior is not visible and the efficiency η_{ice} varies over a large range. Moreover, the sharply rising efficiency at low engine powers suggest that the ICE exhibits extreme non-linearities in this area. However, for energy conversion this is not true and these variations are due to the fuel offset f_1 . This is elucidated by the dashed curve in Fig. 3.4b, which shows only small variations for the efficiency of the e-line when f_1 has been eliminated. This observation confirms that the efficiency map is less instructive for developing an EM system.

In (3.17) there are two aspects that make it profitable for an EM strategy to shift the engine's operating point towards a different location than BL. First, the slope of the fuel curve increases when P_m rises, so $\lambda_3 > \lambda_2 > \lambda_1$. This means that the production of mechanical power requires more fuel when P_m becomes larger. Moreover, it might be economically attractive to apply PSM here and avoid situations where the engine power is high. Off course, the energy that is taken from the battery during PSM needs to be compensated. Typically, this is done by applying C in the area where λ_1 holds. Deciding whether PSM and C have the potential to reduce the overall fuel consumption depends on the energy losses in the battery. This will be shown in the next section.

The second reason for changing the engine's operating point is initiated by the fuel offset f_1 . Turning off the engine in MO mode eliminates the constant fuel term f_1 and the battery becomes the primary power source. When the engine is switched on again, the battery needs to be charged.

Although this charging requires an additional fuel use, the fuel savings from MO need to be higher to obtain a positive result. The next section provides a design rule when it is profitable to switch the engine off.

3.1.3 Design rules

Not only the characteristics of the combustion engine, but also the efficiency of the battery plays a dominant role in the overall performance of an EM strategy. Given this parameter, it becomes possible to provide design rules about when to apply PSM, C or MO. The analysis makes use of the approximated fuel map in (3.17) and considers different situations for the engine power P_m .

Suppose that the current situation is BL and that the engine power is high and exceeds P_{m3} . Furthermore, it is realistic that the engine power drops below P_{m2} in the near future. This would be an opportunity to apply now PSM and afterwards C. If PSM reduces the engine power with ΔP_m^{PSM} , then the fuel consumption reduces according to (3.17):

$$\Delta f^{PSM} = f(P_m) - f(P_m - \Delta P_m^{PSM}) \approx \lambda_3 \Delta P_m^{PSM}, \quad (3.18)$$

and the corresponding net battery power during PSM is calculated from (3.5) and (3.12):

$$\Delta P_s^{PSM} = \frac{1}{\eta^-} \Delta P_b^{PSM} = \frac{\eta_g}{\eta^-} \Delta P_m^{PSM}. \quad (3.19)$$

Following a similar reasoning, C adds ΔP_m^C to the engine power, so the fuel consumption increases with:

$$\Delta f^C = f(P_m + \Delta P_m^C) - f(P_m) \approx \lambda_1 \Delta P_m^C. \quad (3.20)$$

If the energy stored in the battery during C should match with the energy retrieved during PSM, then ΔP_m^C is equal to:

$$\Delta P_m^C = \frac{1}{\eta_g \eta^+} \Delta P_s^{PSM} = \frac{1}{\eta_{bat}} \Delta P_m^{PSM}. \quad (3.21)$$

Note that one can charge the battery also at a different power level and adapt the charging time. Nevertheless, this has no effect on the results shown hereafter, due to the piece-wise linear behavior of the engine map and the battery model. Deciding whether PSM is beneficial to apply boils down to a comparison between (3.18) and (3.20). Only if the fuel reduction

with PSM is larger than the fuel costs from C, it is profitable to apply PSM. This is expressed with the following condition:

$$\Delta f^{PSM} > \Delta f^C \Leftrightarrow \eta_{bat} > \frac{\lambda_1}{\lambda_3} \quad (3.22)$$

Apparently, the overall efficiency of the battery should be high enough to benefit from PSM. In a similar way, the ratio between λ_1 and λ_3 puts a lower boundary on the required battery efficiency, for a successful application of PSM.

Another aspect determined by the efficiency of the battery is the trade-off between applying MO or not. Here, assume that mode BL is active and that the required power P_m^{MO} from the ICE remains below P_{m2} . Switching off the engine (*i.e.*, $S = 0$) and changing to mode MO reduces the fuel consumption with:

$$\Delta f^{MO} \approx f_1 + \lambda_1 P_m^{MO}. \quad (3.23)$$

The power drawn from the battery during MO is equal to:

$$P_s^{MO} = -\frac{1}{\eta^-} P_b^{MO} = -\frac{\eta_g}{\eta^-} P_m^{MO}. \quad (3.24)$$

When the battery is charged afterwards, extra power will be delivered by the engine:

$$\Delta P_m^C = \frac{1}{\eta_g \eta^+} P_s^{MO} = \frac{1}{\eta_{bat}} P_m^{MO}. \quad (3.25)$$

By applying this battery charging in the area where λ_1 holds, the extra fuel use is equal to (3.20), with ΔP_m^C taken from (3.25). Now it is economically attractive to apply MO, as long as the fuel costs from (3.20) are lower than the fuel savings in (3.23). Graphically, both functions are shown in Fig. 3.5 and it can be seen that MO yields the highest profits for P_m close to zero. The intersection of both curves reveals the point from where MO should not be applied anymore. This threshold level P_m^* is calculated by putting (3.23) equal to (3.20):

$$\Delta f^{MO} = \Delta f^C \Rightarrow P_m^* = \frac{\eta_{bat}}{\lambda_1(1 - \eta_{bat})} f_1 \quad \text{and} \quad \eta_{bat} < 1. \quad (3.26)$$

Note that this design rule loses its validity when the ICE, the generator, or the electric machine often reach their power limitations. Moreover, the effect of regenerative braking is also not included in the analysis from above. Since regen-braking allows the electric machine to recuperate kinetic energy

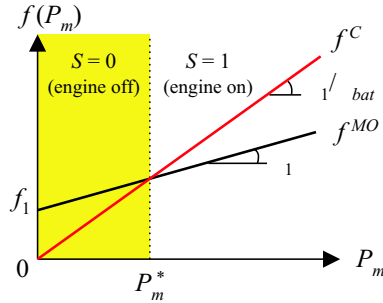


Figure 3.5: Visualization of fuel consumption for MO and C

during vehicle deceleration, the battery is charged without any fuel costs. It is clear that applying PSM or MO with energy from regenerative braking is always profitable, irrespective of the battery efficiency. As a result, the optimal threshold for switching the engine on will be slightly higher than P_m^* and depends on the profile of the driving cycle.

3.1.4 Optimal strategy

Problem definition

The main goal of the EM system is to improve the vehicle's fuel economy. This will be achieved by reducing the fuel costs for producing and distributing electric power. However, the reduction of particular tail-pipe emissions can be done in a similar way. Although the vehicle itself is a complex dynamical system, it turns out that only the actuated signals determine the momentary fuel consumption. Therefore, it is possible to formulate the fuel costs by means of algebraic relations, and the optimal EM strategy follows from a general optimization problem:

$$\min_x J(x) \quad \text{subject to} \quad G(x) \leq 0, \quad (3.27)$$

where $J(x)$ is the objective function and $G(x)$ expresses the constraints on decision variable x . The cost function J represents the cumulative fuel use of the ICE over an arbitrary driving cycle with time length t_e :

$$J(P_s, S) = \int_0^{t_e} F(P_s, S | P_d, P_L) dt, \quad (3.28)$$

where

$$F(P_s, S | P_d, P_L) = \begin{cases} 0 & \text{if } S = 0 \\ f_{e-line}(P_m) & \text{if } S = 1 \end{cases} \quad (3.29)$$

Note that the decision variable x covers two variables: the internal battery power P_s and the engine-running signal S . Furthermore, the individual models from the battery, the power net and the generator define a unique relation between P_m and P_s . For the situation that P_d and P_L are given, P_s can be calculated from P_m using the models from Section 3.1.1. All these models define a convex relation between their input and output signals, so the substitution in (3.29) also preserves convexity for F . This is an important property for calculating the minimum of (3.28) in an efficient way.

The operating range of the engine, the electric machine, and the battery is limited in power. Therefore, inequality constraints are introduced to limit the minimum and maximum powerflow through these components:

$$0 \leq P_m(t) \leq P_{mmax}(t) \quad \forall t \in [0, t_e] \quad (3.30)$$

$$P_{emmin}(t) \leq P_{em}(t) \leq P_{emmax}(t) \quad " \quad (3.31)$$

$$P_{bmin}(t) \leq P_b(t) \leq P_{bmax}(t) \quad " \quad (3.32)$$

Except for concentrating on the overall fuel consumption of the vehicle, the EM system has also the responsibility to guarantee a charge sustaining vehicle. A charge sustaining strategy claims that the battery satisfies a minimum SOE level at the end of the driving cycle. This is achieved by including an end-point constraint on the energy level of the battery:

$$E_s(t_e) \geq E_{sref} \Rightarrow E_s(0) + \int_0^{t_e} P_s(t)dt \geq E_{sref}, \quad (3.33)$$

where E_{sref} is an arbitrarily selected reference value that should be satisfied at $t = t_e$, *e.g.*, $E_{sref} = E_s(0)$.

Solution method

Suppose that the driving cycle of the vehicle is exactly known. In that case, it is possible to estimate an optimal power profile for the electric machine, which achieves minimum fuel consumption over the whole driving cycle. This optimal profile can be found with an optimization technique called Dynamic Programming (DP) [11]. First, a suitable cost function J

is selected that expresses the desired vehicle behavior. Next, the state- and input-variables are restricted to take a value on a finite grid. Furthermore, all model dynamics are translated into discrete time. Finally, the resulting optimization problem is numerically solved by evaluating all possible control sequences in a systematic way. The intermediate results are stored in a cost matrix \mathbf{R} that contains the minimum fuel costs found so far. In the end, the optimal control sequence can be derived from \mathbf{R} .

The selected cost function J for the DP algorithm equals the cumulative fuel consumption of the vehicle along the driving cycle:

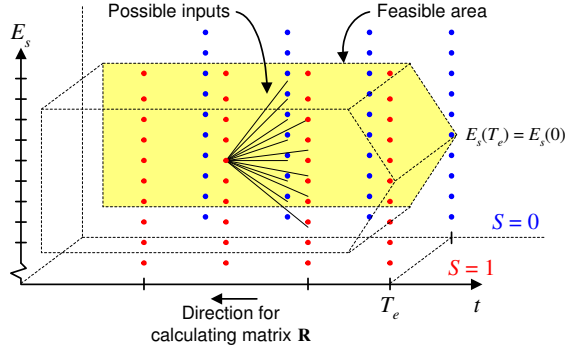
$$J = \int_0^{T_e} F(P_m(t), S(t) | P_d(t), P_L(t)) dt. \quad (3.34)$$

Except for this cost function, also constraints are present to limit the powerflow through components and to keep the energy in the battery within a suitable window. Furthermore, the energy in the battery at the end of the driving cycle should satisfy at least the energy at the start of the trip, so $E_s(T_e) \geq E_s(0)$. Two state-variables are selected. These are $E_s(t)$ and the status of the engine $S \in \{0, 1\}$. Although P_m will be the controlled variable, the selected input-variable is P_s . This is computationally attractive, because it allows corresponding grid-levels between state E_s and input P_s . A similar approach has been presented in [51].

After discretization of time, the cost matrix \mathbf{R} with state-entries (E_s, S, t) is created. This way, \mathbf{R} includes $2 \times N_E \times N_t$ grid points, using N_E discrete steps for E_s and N_t time steps for $t \in [0..T_e]$. In the end, \mathbf{R} represents a cost-to-go matrix, since each state represents the amount of fuel necessary to reach the end of the driving cycle, starting from the present state. A graphical representation for \mathbf{R} is shown in Fig. 3.6. The optimal control sequence is calculated afterwards, by searching for the path of minimal costs through \mathbf{R} .

3.1.5 On-line adaptive strategy

Finding the optimal solution for the problem defined in the previous section will be computationally demanding. Instead of solving the full optimization problem, one can also break down the problem into well defined sub-problems, each with limited complexity. The solution presented here reduces the complexity in two ways. First, the time horizon over the complete driving cycle is eliminated from the optimization problem. Second, the engine running-signal S takes only two values and for each value, a


 Figure 3.6: Projection of cost matrix \mathbf{R}

separate problem is formulated. It will be shown that this approach still can provide a similar solution as the optimal solution.

First, consider the situation with $S = 1$. This allows the S-HEV to operate in mode BL, PSM and C. Without the inequality constraints $G(x) \leq 0$, the optimization problem from (3.27) reduces to:

$$\min_{P_s} \int_0^{t_e} F(P_s | P_d, P_L) dt. \quad (3.35)$$

In case the final energy level of the battery has to be equal to the initial starting value $E_s(0)$, the inequality constraint from (3.33) changes into an equality constraint:

$$E_s(0) + \int_0^{t_e} P_s(t) dt = E_s(0) \quad \Rightarrow \quad \int_0^{t_e} P_s(t) dt = 0. \quad (3.36)$$

A new problem definition is formulated from (3.35) and with the equality constraint (3.36). For convenience, it is written in discrete time, although the sampling interval ΔT has been omitted:

$$\begin{aligned} \min_{P_s} \sum_{k=1}^{N_p} F(P_s(k) | P_d(k), P_L(k)), \\ \text{subject to} \quad \sum_{k=1}^{N_p} P_s(k) = 0. \end{aligned} \quad (3.37)$$

Finding a solution for this optimization problem can be done by incorporating the equality constraint into the Lagrangian function, using a Lagrange

multiplier λ . A similar approach has been followed by Guzzella in [34]. The following Lagrangian L is defined:

$$L(P_s(1), \dots, P_s(N_p), \lambda) = \sum_{k=1}^{N_p} F(P_s(k) | P_d(k), P_L(k)) - \lambda \sum_{k=1}^{N_p} P_s(k). \quad (3.38)$$

Physically, this new objective function makes sense, because it adds the energy exchange with the battery to the fuel consumption of the ICE. The quantity λ represents the corresponding fuel cost when energy is stored or taken from the battery. It is clear that there exists a strong relation between this quantity and the definition of λ as given in (3.14). The minimum value for $L(P_s(1), \dots, P_s(N_p), \lambda)$ satisfies the following $N_p + 1$ constraints:

$$\frac{\partial L(P_s(1), \dots, P_s(N_p), \lambda)}{\partial P_s(k)} = 0, \quad 1 \leq k \leq N_p, \quad (3.39)$$

$$\frac{\partial L(P_s(1), \dots, P_s(N_p), \lambda)}{\partial \lambda} = 0. \quad (3.40)$$

Without having an analytical description of $F(P_s | P_d, P_L)$, it is still possible to rewrite (3.39) and (3.40) into a more simple expression:

$$\frac{\partial F(P_s(k) | P_d(k), P_L(k))}{\partial P_s(k)} - \lambda = 0, \quad 1 \leq k \leq N_p, \quad (3.41)$$

$$\sum_{k=1}^{N_p} P_s(k) = 0. \quad (3.42)$$

Since $F(P_s | P_d, P_L)$ is a convex function, there exists one unique solution $(P_s^*(1), \dots, P_s^*(N_p), \lambda^*)$ to this set of $N_p + 1$ equations. Typically, the solution for λ^* is calculated with information about the entire driving cycle. This comes from (3.41), where $P_d(k)$ and $P_L(k)$ are assumed to be known at each time instant k . However, if λ^* is known, (3.41) and (3.42) are entirely decoupled. This means that calculating $P_s^*(k)$ can be done by solving (3.41) with information from P_d , P_L and λ^* only at time k . For a rigorous proof, the reader is referred to [81]. As a result, the optimal solution $P_s^*(k)$ from (3.37) is also found by minimizing the given criterion at each time instant k :

$$P_s^* = \arg \min_{P_s} \{F(P_s | P_d, P_L) - \lambda^* P_s\}. \quad (3.43)$$

The solution presented so far considers only the cost criterion in combination with one equality constraint. Returning back to the original problem, one has to guarantee that the inequality constraints from (3.30)-(3.32) are not violated. To that end, these constraints are combined into one new constraint on P_s , with the upper- and lower bound P_{smax} and P_{smin} , respectively. A feasible solution is obtained through saturation of P_s^* with these new boundaries:

$$P_s^{S1} = \text{sat} [P_s^*]_{P_{smin}^{P_{smax}}} , \quad (3.44)$$

where the saturation function $\text{sat} [x]_l^u$ is defined as:

$$\text{sat} [x]_l^u = \min(\max(x, l), u). \quad (3.45)$$

The corresponding fuel cost for the power setpoint P_s^{S1} is:

$$f^{S1} = F(P_s^{S1} | P_d, P_L) - \lambda^* P_s^{S1}. \quad (3.46)$$

It is important to notice that these extra constraints can be added without violating the optimality of the calculated solution. After all, the function $F(P_s | P_d, P_L)$ was assumed to be a convex function. By applying a saturation on P_s , this function still remains convex and hence, the optimal solution is uniquely defined.

It is clear that an optimal value for P_s will sometimes appear at its boundary. Therefore, the value for λ^* needs to be different for the situation that saturation is included. How to find an optimal value for λ^* for this new situation will be shown at the end of this section.

Now consider the situation with $S = 0$, so the engine is turned off and mode MO should be active. A necessary condition for MO is that the electric machine and the battery are able to supply the power request P_d and P_L . This condition is satisfied when the following inequalities hold:

$$-P_d \geq P_{emmin} \quad \wedge \quad \frac{-P_d}{\eta_{mm}} - P_L \geq P_{bmin}. \quad (3.47)$$

During braking phases, MO is also preferred but then the power through the electric machine is also limited. Moreover, for a correct driveability of the vehicle, the recuperation of free kinetic energy at the front wheels is restricted. Although the control of the front and rear wheel braking forces is beyond the scope of this thesis, it is important to realize that the EM system cannot recover all available kinetic energy solely at the front wheels. The parameters that determine the ideal braking force distribution

are, amongst others, the desired vehicle deceleration and the cargo weight. A good introduction to the braking force distribution in HEVs is given in [33]. Without loss of generality, this thesis assumes that the braking force at the front wheels is limited to 60%, whereas the rear wheels take care of the remaining part. Therefore, the power from the electric machine equals:

$$P_e^{MO} = \min\left(\frac{1}{\eta_{mm}} P_{em}^{MO}, \eta_{gm} P_{em}^{MO}\right), \quad (3.48)$$

with P_{em}^{MO} the drive train power during vehicle propulsion ($P_d \geq 0$), and only 60% returns during regenerative braking ($P_d < 0$):

$$P_{em}^{MO} = \text{sat}[-\max(0.60 \times P_d, P_d)]_{P_{em}^{min}}^{P_{em}^{max}}. \quad (3.49)$$

Similar to the electric machine, also the battery is limited in power. Incorporating these limitations yields the following net battery power:

$$P_s^{MO} = \min\left(\frac{1}{\eta^-} P_b^{MO}, \eta^+ P_b^{MO}\right), \quad (3.50)$$

$$\text{with } P_b^{MO} = \text{sat}[P_e^{MO} - P_L]_{P_b^{min}}^{P_b^{max}}. \quad (3.51)$$

The ICE is not running during MO, so the momentary fuel consumption is zero. However, the additional fuel costs for recharging the battery afterwards are estimated as follows:

$$f^{S0} = -\lambda^* P_s^{MO}. \quad (3.52)$$

To find out if MO is more beneficial than the other modes, a comparison between (3.46) and (3.52) is made. Selecting MO is preferred if the following condition holds:

$$f^{S0} < f^{S1} \quad (3.53)$$

The final control law for P_s is a combination of both situations. MO becomes active when both (3.47) and (3.53) are satisfied. Otherwise, discrimination between the modes BL, PSM and C is done in (3.43)-(3.44). Altogether, this yields the following EM strategy law for P_s :

$$P_s^{EM}(P_d, P_L, \lambda^*) = \begin{cases} P_s^{MO} & \text{if (3.47) } \wedge \text{ (3.53)} \\ P_s^{S1} & \text{elsewhere} \end{cases} \quad (3.54)$$

The actual power setpoint for the generator is calculated with the models given in (3.4) and (3.12).

3.1.6 On-line optimal strategy

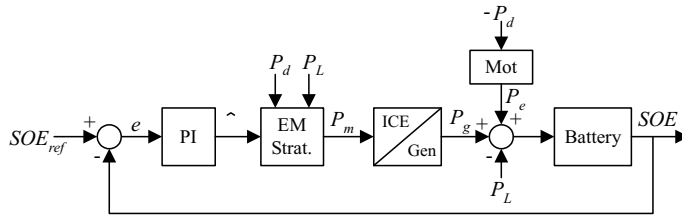
The control strategy presented above can achieve a similar result as the DP strategy, if a fixed value is selected for λ^* along the entire driving cycle. In fact, each driving cycle requires a different λ^* to achieve a preferred energy level in the battery at the end of the driving cycle. This λ^* corresponds to the situation where the energy need for MO and PSM is balanced with the energy from C. It is important to notice that MO and PSM take less energy from the battery for higher values of λ^* . On the other hand, C stores more energy in the battery when λ^* increases. As a result, there exists a unique solution for λ^* where the energy from C equals the energy from MO and PSM. Then it follows that the SOE at the beginning and end of the driving cycle is equivalent. This observation is also recognized by Delprat et al in [25]. By means of simulations, Chapter 4 shows that this strategy mimics the solution from DP, provided that there are no restrictions in the buffer size of the battery.

Adaptive Strategy

For calculating λ^* , accurate information about the vehicle power demand is required along the entire driving. This is inconvenient for on-line implementation because it requires, amongst others, an exact prediction of the vehicle speed including external disturbances such as wind or road inclination. Instead of focussing on how to obtain this prediction information, one could also rely on the driving behavior from the past. Assuming that the speed profile from the past provides a good representation of the future driving cycle, there are several methods to estimate an appropriate value $\hat{\lambda}$ for the optimal value λ^* .

The method that has been selected here, results in an adaptive strategy as presented in [51]. The basic idea is that the *SOE* of the battery indicates whether $\hat{\lambda}$ is estimated correctly or not. In case $\hat{\lambda}$ has been selected too small, the battery becomes depleted in the end. Conversely, when $\hat{\lambda}$ is selected too high, the battery becomes fully charged. From a control point of view, this corresponds to a levelling control problem where the *SOE* should be kept near a nominal value SOE_{ref} . A Proportional Integral (PI) controller with a rather small bandwidth fulfills this requirement. The block diagram is shown in Fig. 3.7, with $\hat{\lambda}$ equal to:

$$\hat{\lambda}(t) = \lambda_0 + K_P e(t) + K_I \int_0^t e(v) dv, \quad (3.55)$$

Figure 3.7: Feedback diagram for estimating $\hat{\lambda}$

with λ_0 an initial guess. For calculating the appropriate tuning parameters, the reader is referred to Appendix A. This appendix also provides an analysis on closed-loop stability, using Kharitonov's theorem.

3.2 Energy management for P-HEV

In a P-HEV configuration, both the ICE and the electric machine are connected to the drive train and can be used for vehicle propulsion. Compared to an S-HEV, these vehicles offer more freedom for the EM system. However, the mechanical connection between the ICE and the drive train does not allow the EM system to operate the ICE always on the e-line.

A P-HEV requires a suitable mechanical power split to connect the drive train to the ICE and to the electric machine. Depending on the size of the electric machine, different solutions are used, although all these vehicles can still use the same EM system. This section considers a vehicle implementation with an Integrated Starter/Generator (ISG) directly mounted on the crankshaft of the ICE. This construction is mostly seen in mild or medium HEVs, for example the Honda Civic Hybrid uses this mechanism with a 15 [kW] electric machine.

When the electric machine is smaller (typically less than 5 [kW]), it is more common to apply a belt-driven ISG. These vehicles are often referred to as micro HEV and the electric machine is assembled in a similar way as the belt-driven generator in traditional vehicles.

Finally, the full HEV utilizes an electric machine in the power range above 20 [kW]. This way, a full electric drive is supported, although the ICE might be necessary during heavy road load. These vehicles are typically equipped with an advanced power split device such as a planetary gear set. This advanced power split is also present in an S/P-HEV, and the EM

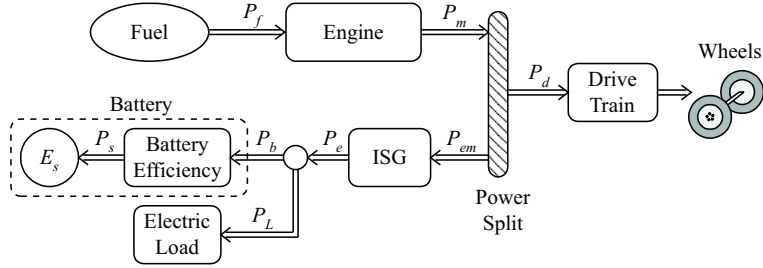


Figure 3.8: Vehicle topology (arrows indicate nominal powerflow)

system for these vehicles will be discussed in Section 3.3.

3.2.1 Vehicle model

In a P-HEV, both the ICE and the ISG can give tractive force to the wheels. Furthermore, the ISG will also be used as a generator to supply the electric loads. A schematic drawing of the vehicle configuration is shown in Fig. 3.8.

Drive train model

The power demand of the drive train P_d is calculated with the quasi-static backward-facing vehicle model from Section 2.1.2. P_d covers all the elements of the drive train, including the transmission and the clutch. The engine speed ω and the drive train torque τ_d are calculated back from the vehicle speed and denote the driver's power demand:

$$P_d = \omega \tau_d. \quad (3.56)$$

The power split device is assumed to have no energy losses and establishes the following power balance:

$$P_m = P_d + P_{em}. \quad (3.57)$$

Internal Combustion Engine

In an S-HEV, the EM system keeps the ICE permanently on the e-line but in a P-HEV, this is often not possible. The ICE is now mechanically connected to the drive train, so the engine speed matches with the wheel speed and

cannot be chosen freely. Nevertheless, it is still possible to express the corresponding fuel consumption as a function of engine power and speed. This map comes from the measured fuel map, although the crankshaft torque τ_m and the engine speed ω have been replaced by the engine power P_m :

$$fuelrate = f(\tau_m, \omega) = f(P_m | \omega) \quad [\text{g/s}]. \quad (3.58)$$

The notation with the conditional-operator $|$ emphasizes the dependency of $f(P_m)$ from ω . The fuel consumption becomes zero when the ICE is switched off and to start the ICE, no additional fuel use is considered. Furthermore, it is assumed that the drag torque of the ICE is negligible if it is switched off. Except for vehicle braking periods, this last simplification has no further consequences. This will become clear when discussing regenerative braking in Section 3.2.2.

Integrated Starter/Generator

The ISG is mounted on the crankshaft of the ICE and therefore, it is also coupled to the drive train of the vehicle. Since the ISG model uses power based signals, it is not possible to observe speed-dependent characteristics. The ISG operates similar to the electric machine in the S-HEV. It can operate in two modes: generator mode ($P_{em} \geq 0$) and motor mode ($P_{em} < 0$), and is described in (3.2) and (3.3).

Electric power net

The electric power net connects the ISG with the electric loads and the battery. No losses are assumed in the electrical wires, leaving the following description:

$$P_e = P_L + P_b. \quad (3.59)$$

Battery model

Similar as with the S-HEV, a battery model is used where the losses grow proportionally with the power during charging ($P_b > 0$) and discharging ($P_b < 0$). Furthermore, an integrator keeps track of the stored energy in the battery, see (3.12) and (3.13).

3.2.2 Strategy outline

Although the P-HEV moves the ICE through its entire operating range, it is still possible to draw a picture of the corresponding fuel consumption, with respect to engine power. To that end, the engine map shown in Fig. 3.2 is drawn again in Fig. 3.9, using separate curves for different engine speeds. Again, it turns out that a piece-wise linear relation exists between the engine power P_m and its fuel usage $f(P_m)$. Typically, the slope of these curves remains constant within each area and equals the following definition:

$$\lambda(P_m | \omega) = \frac{\partial f(P_m | \omega)}{\partial P_m} \quad [\text{g/J}]. \quad (3.60)$$

The quantity λ expresses the incremental fuel cost, as it indicates the additional fuel massflow to produce a small amount of mechanical power. In accordance with (3.15), the map can be approximated with a piece-wise affine function and $N_f = 2$:

$$f(P_m | \omega) \approx \begin{cases} 0 & \text{if } P_m < P_{m1} \\ f_1 + \lambda_1 P_m & \text{if } P_{m1} \leq P_m < P_{m2} \\ f_2 + \lambda_2 P_m & \text{if } P_m \geq P_{m2} \end{cases} \quad (3.61)$$

Note that all parameters f_j , λ_j and P_{mj} depend on ω .

The power towards the drive train and the power through the electric motor determine the operating point of the combustion engine. In particular, the situation where the engine power exactly matches the power demand for the drive train plus the electric load request is called Baseline (BL). By definition, BL implies that the battery is not used, so $P_b = 0$. In a P-HEV, there are three reasons why shifting the engine's operating point to a different location than BL is economically attractive:

1. Producing more power with the engine is valid as long as the additional fuel request remains small. These moments are characterized by a small value for λ_j .
2. Producing less power is favorable when the fuel use decreases significantly. This observation follows also from the actual value of λ_j .
3. The third reason for changing the engine operating point is initiated by the constant offset term f_1 . By turning off the ICE, the battery becomes the primary power source and although recharging requires additional fuel, this can still be economically attractive.

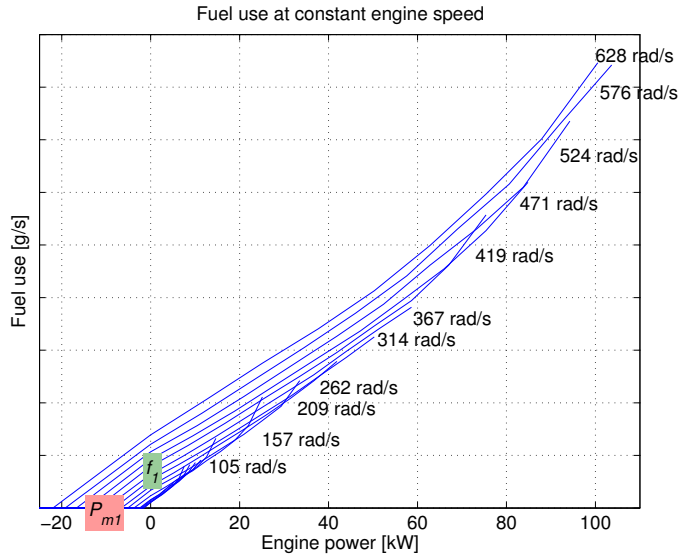


Figure 3.9: Fuel consumption matches piece-wise linear function

Altogether, the EM system relies on two engine characteristics: λ_j and f_1 . These characteristics can be exploited in different ways and therefore, separate modes are defined to address all situations. Except for BL, five additional modes are recognized: Motor only (MO), Motor assist (MA), Charging mode (C), Power supply management (PSM) and Regenerative braking (R). These modes are briefly explained below.

Motor only

During vehicle stand-still, it is allowed to turn off the engine. Without considering a penalty for engine restart, this directly reduces the fuel consumption by eliminating f_1 . Furthermore, the electric machine can provide tractive power to the wheels, so engine-off is also possible during vehicle launch.

Motor assist

In the situation of Motor assist (MA), the engine produces less mechanical power than requested by the drive train and the electric motor delivers the remaining part. MA should be applied at moments when the incremental

cost is relative high. Typically, this corresponds to the area where λ_2 in (3.61) becomes active.

Power supply management

Also PSM takes energy from the battery but here this energy is only used for the electric loads and not for vehicle propulsion. The electric machine now operates in generator mode, but it delivers only a fraction of the electric load request.

Regenerative braking

Regenerative braking (R) refers to the situation that the vehicle slows down and the electric machine recuperates free braking energy. The mechanical brakes are only activated if the generator size is insufficient to achieve the desired vehicle deceleration. In general, regenerative braking provides electric energy without extra fuel costs and should be applied if possible. Theoretically, R is limited to situations where $P_d \leq P_{m1}$ (and the engine has moved to its fuel cut-off point P_{m1} , see Fig. 3.9). For the moment, the simplification is made that mode R can be applied when $P_d < 0$. Hence, the engine drag torque is neglected here. This is a valid assumption for newly developed ICEs, which are typically designed for small friction losses during braking phases. For example the Honda Civic Hybrid can deactivate the cylinders of the ICE during deceleration to reduce the pumping losses [32].

Charging mode

In Charging mode (C), the electric machine produces extra power to charge the battery. Different than in R, this mode requires additional fuel consumption, so C is preferred when λ is small. According to (3.61), this will be in the area where λ_1 holds.

3.2.3 On-line adaptive strategy

To derive a suitable control strategy, the EM algorithm is formulated as an optimization problem. By applying a Lagrangian function with a basic optimization technique, the control algorithm becomes a causal EM strategy that does not rely anymore on prediction information and is suitable for on-line implementation.

Problem definition

Generally speaking, the control objective for the EM system in a P-HEV is similar to the control objective for the S-HEV. In both cases, the main goal is to improve the vehicle's fuel economy. Nevertheless, some differences exist for the control objective. This is due to the fact that the rotational speed of the wheels prescribes the speed of the engine ω . For the P-HEV, the control objective is given below:

$$\min_x J(x) \quad \text{subject to} \quad G(x) \leq 0, \quad (3.62)$$

with the cost function J equal to cumulative fuel use along a driving cycle with time length t_e , *i.e.*:

$$J(P_s, S) = \int_0^{t_e} F(P_s, S | P_d, P_L, \omega) dt, \quad (3.63)$$

where

$$F(P_s, S | P_d, P_L, \omega) = \begin{cases} 0 & \text{if } S = 0, \\ f(P_d + P_{em} | \omega) & \text{if } S = 1. \end{cases} \quad (3.64)$$

Again, the decision variable x covers two variables: the internal battery power P_s and the engine-running signal S . Furthermore, the ISG power P_{em} is defined in (3.2) and the relation with P_s follows from (3.59) and (3.12).

Similar to the S-HEV, the operating range of the engine, the electric machine, and the battery is limited in power. The required inequality constraints are repeated below:

$$P_{m \min}(t) \leq P_m(t) \leq P_{m \max}(t) \quad (3.65)$$

$$P_{em \min}(t) \leq P_{em}(t) \leq P_{em \max}(t) \quad (3.66)$$

$$P_{b \min}(t) \leq P_b(t) \leq P_{b \max}(t) \quad (3.67)$$

$$\forall t \in [0, t_e]$$

Also the P-HEV should be charge sustaining, so the energy in the battery at the end of the driving cycle should meet a reference value E_{sref} . This is achieved by the following end-point constraint:

$$E_s(t_e) = E_s(0) + \int_0^{t_e} P_s(t) dt \geq E_{sref}. \quad (3.68)$$

On-line solution method

A solution for the problem defined above is found by solving two sub-problems. The first sub-problem addresses the situation with $S = 1$ and covers the modes BL, MA, PSM and C. The second sub-problem focusses on the situation with $S = 0$ and takes care of the modes R and MO. First, consider the situation with $S = 1$. With a suitable value for λ^* (the optimal Lagrange multiplier, see Section 3.1.5), the optimal value for P_s is calculated in the following minimization:

$$P_s^* = \arg \min_{P_s} \{F(P_s | P_d, P_L, \omega) - \lambda^* P_s\}. \quad (3.69)$$

The solution found above takes only into account the end-point constraint from (3.68) and not the inequality constraints from (3.65)-(3.67). To guarantee that these constraints are not violated, they are combined into a new constraint on P_s , with the upper- and lower bound P_{smax} and P_{smin} , respectively. The saturation function $\text{sat}[\cdot]_l^u$ guarantees a feasible solution, without violating the convexity of the objective function:

$$P_s^{S1} = \text{sat} [P_s^*]_{P_{smin}}^{P_{smax}}. \quad (3.70)$$

The corresponding fuel cost for the power setpoint P_s^{S1} equals:

$$f^{S1} = F(P_s^{S1} | P_d, P_L, \omega) - \lambda^* P_s^{S1}. \quad (3.71)$$

Now consider the situation with $S = 0$, so the engine is turned off. The allowed operating modes are R and MO and each mode is handled separately. To apply R, the power request of the drive train needs to be negative, so $P_d < 0$. For driveability reasons, only 60% of the available kinetic energy can be recuperated at the front wheels (see Section 3.1.5 for an explanation). Furthermore, the power of the electric machine is limited in (3.66) and the battery power is restricted in (3.67). Therefore, the recuperated power with the electric machine P_{em}^R and the accepted battery power P_b^R during R become:

$$P_{em}^R = \text{sat} [-0.60 P_d]_0^{P_{emmax}}, \quad (3.72)$$

$$P_b^R = \text{sat} [\eta_{gm} P_{em}^R - P_L]_{P_{bmin}}^{P_{bmax}}. \quad (3.73)$$

The net battery power P_s^R follows from the inverse of (3.12):

$$P_s^R = \min(\eta^+ P_b^R, \frac{1}{\eta^-} P_b^R). \quad (3.74)$$

MO requires that the electric machine and the battery are capable to supply the power request P_d and P_L . This condition is satisfied when the following inequalities hold:

$$0 \leq P_d \leq -P_{em\ min} \quad \wedge \quad \frac{-P_d}{\eta_{mm}} - P_L > P_{b\ min} . \quad (3.75)$$

If MO is applied, the power drawn from the battery becomes:

$$P_s^{MO} = \frac{-P_d}{\eta_{mm}\eta^-} - \frac{P_L}{\eta^-}, \quad (3.76)$$

and the fuel costs for recharging the battery are estimated as:

$$f^{MO} = -\lambda^* P_s^{MO}. \quad (3.77)$$

To find out if MO is more beneficial than the other modes BL, MA, C or PSM, a comparison between (3.71) and (3.77) is made. Selecting MO is preferred when the following condition holds:

$$f^{MO} < f^{S1} \quad (3.78)$$

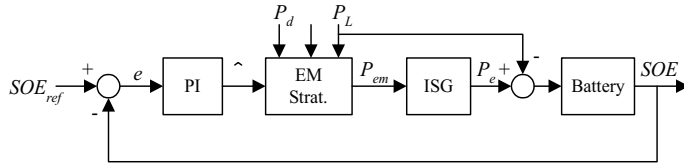
Altogether, the EM algorithm consists of one control law for P_s . This control law is constructed by combining the individual modes of operation as discussed above. R has the highest priority and will be applied if possible, *i.e.*, $P_d < 0$. Next, MO becomes active if (3.75) and (3.78) are satisfied. Discrimination between the other modes BL, MA, C and PSM is done automatically in (3.69)-(3.70). Finally, this leads to the following control law for P_s :

$$P_s^{EM}(P_d, P_L, \omega, \lambda^*) = \begin{cases} P_s^R & \text{if } P_d < 0 \\ P_s^{MO} & \text{if } (3.75) \wedge (3.78) \\ P_s^{S1} & \text{elsewhere} \end{cases} \quad (3.79)$$

The actual power setpoint for the ISG is calculated from (3.2), (3.59) and (3.12). The engine is turned off when the engine running signal S becomes zero, *i.e.*, during MO and R.

On-line implementation

The missing link towards an on-line strategy implementation is the method for calculating λ^* . Similar to the S-HEV, also the P-HEV needs a suitable value for λ^* to keep the battery sufficiently close to the reference value

Figure 3.10: Feedback estimation of $\hat{\lambda}$ in P-HEV

SOE_{ref} . As will be shown in Chapter 4, the solution with λ^* constant along the entire driving cycle resembles the optimal strategy from Dynamic Programming. Nevertheless, both concepts are non-causal, since they rely on knowledge from the future driving cycle.

Except for a constant value for λ^* , also the adaptive solution from Section 3.1.6 can be used to make an on-line estimation. Within a feedback loop, a PI-controller calculates $\hat{\lambda}$ according to the difference between the momentary SOE of the battery and SOE_{ref} , see Fig. 3.10. Simulation results in Chapter 4 illustrate how this adaptive solution achieves a fuel economy close to the result from the non-causal DP strategy.

3.3 Energy management for S/P-HEV

The most advanced vehicle topology considered in this thesis is the S/P-HEV. This vehicle configuration incorporates an advanced power split device for supplying power from the ICE and the electric machine towards the drive train. This enables both a series as well as a parallel interconnection between the ICE and the electric machine.

In many cases, the S/P-HEV employs an electronically-controlled CVT for the power split device. Also the Toyota Prius applies this power split device, and this S/P-HEV will be considered in this section. First, a short introduction to the CVT will be given. Next, the overall vehicle model will be discussed, followed by a suitable EM system.

3.3.1 Electronically-controlled CVT

The continuously variable transmission (CVT) is a viable solution for the integration of the internal combustion engine in the vehicle drive train. Traditionally, a CVT consists of a pure mechanical transmission with a hydraulic actuator system. Two shafts with a flexible radius are connected

through a pushbelt and by simultaneously changing the radii of both shafts, the preferred gear ratio is established. The actuator system controls the radii of the rotational shafts and monitors the clamping force of the belt to prevent slip. Unfortunately, hydraulic actuators consume relative much energy and this reduces the efficiency of the overall system. Therefore, researchers are currently investigating CVTs with an alternative actuator system. For example [80] presents the design of a CVT with an electromechanical actuator system. Moreover, in [12] it is shown that the clamping force in modern production CVTs is often higher than necessary to transfer the engine torque. Higher clamping forces result in additional losses and can reduce the endurance life of the belt. By using slip control technology, the CVT can be optimized for the best possible clamping force, combined with the highest transmission efficiency.

Instead of optimizing the actuator system of the CVT, it is also possible to change its transmission part. A method that turns out to be successful is the implementation of a planetary gear train in combination with an electric motor/generator pair. This so-called eCVT (electronically-controlled CVT) acts as a powersplit to run the internal combustion engine in its preferred operating range with assistance of one or more motor/generator pairs. Its commercial success is firstly demonstrated by Toyota with the introduction of the Prius in 1997. In the mean time, also other manufacturers have put vehicles with an eCVT into the market, e.g. the Ford Escape Hybrid or GM's Chevrolet Tahoe Hybrid. An excellent overview of the present status of the eCVT is given by Miller in [58].

3.3.2 Planetary gear train

A planetary gear train is characterized by the fact that it contains at least one gear that rotates about its own axis and simultaneously revolves about another axis. The central gear is called the sun and the gears around the sun are called planets. A schematic drawing of a planetary gear train is depicted in Fig. 3.11. In this gear train, all three planets are connected to the same arm, hereafter referred to as carrier. Furthermore, the planets are enclosed by an outer gear, which is denoted by the ring gear or annulus. Note that this ring gear is an internal gear, as its teeth are facing inward. Conversely, the sun gear and the planet gear have to be external gears, so that their teeth can mesh with each other. In literature, planetary gear trains are also referred to as epicyclic gear trains. This is because a point on the planet gears describes an epicycloid or an hypocycloid profile when

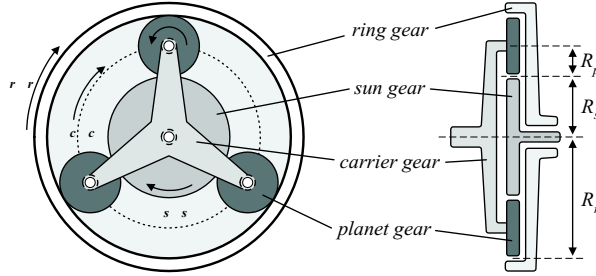


Figure 3.11: Description of planetary gear train

it rotates.

The kinematics of a planetary gear train define the relation between the rotational speeds of the ring gear ω_r , the sun gear ω_s and the carrier gear ω_c , see Fig. 3.11. Using the radii of the ring gear (R_r) and the sun gear (R_s), the rotational speed of the entire system is described by:

$$\omega_s R_s + \omega_r R_r = \omega_c (R_r + R_s). \quad (3.80)$$

The basic gear ratio of the planetary gear train is defined as:

$$Z = \frac{R_r}{R_s}. \quad (3.81)$$

Using this basic gear ratio, the kinematic description from (3.80) can be rewritten as:

$$\omega_s + \omega_r Z = \omega_c (Z + 1). \quad (3.82)$$

Now consider the side-view of the planetary gear train as shown in Fig. 3.11. It is clear that each gear must have a suitable dimension to obtain a feasible mechanical fit. Since the number of teeth is directly proportional to the diameter of the gear, the gears have to satisfy the following constraint:

$$N_s + 2N_p = N_r, \quad (3.83)$$

where N indicates the number of teeth.

In principle, the planetary gear train acts as a power split device. Assume that there are no inertias present and there is no energy dissipation within the system. Then the law of power conservation describes the static relation between all powers P applied to the system. Given the speed ω

and torque τ as defined in Fig. 3.11, the following relation emerges:

$$P_{sun} + P_c + P_r = 0, \quad (3.84)$$

$$\Leftrightarrow$$

$$\tau_s \omega_s + \tau_c \omega_c + \tau_r \omega_r = 0. \quad (3.85)$$

In addition, the torques acting on the sun, carrier and ring gear have to be balanced for the steady-state situation:

$$\tau_s + \tau_c + \tau_r = 0. \quad (3.86)$$

The relations (3.82), (3.85) and (3.86) provide a complete description of the planetary gear train. Nevertheless, for practical situations it is convenient to replace (3.85) and (3.86) with an alternative representation. A description with the basic gear ratio follows from substitution of (3.82) and (3.86) into (3.85). This yields two linear equations:

$$\tau_r = Z \tau_s, \quad (3.87)$$

$$\tau_c = -(Z + 1)\tau_s. \quad (3.88)$$

Note that these relations are also found by considering two special situations for (3.82) and (3.85): $\omega_c = 0$ and $\omega_r = 0$.

3.3.3 Vehicle model

In this thesis, the S/P-HEV model is derived from the Toyota Prius configuration. The eCVT in the Prius consists of a planetary gear train with two motor/generator pairs. The first motor/generator (MG1) is linked to the sun gear whereas the second motor/generator (MG2) is linked to the ring gear. Also the final drive is linked to the ring gear and transmits power to the front wheels. Finally, the ICE is connected to the carrier gear. A schematic diagram of the vehicle topology is depicted in Fig. 3.12.

Electric power net and battery

Both MG1 and MG2 are connected to the same power net, although the required power converters are not shown in the block diagram. The electric power net also connects to the battery and establishes the following power balance:

$$P_b + P_L = P_{e1} + P_{e2}. \quad (3.89)$$

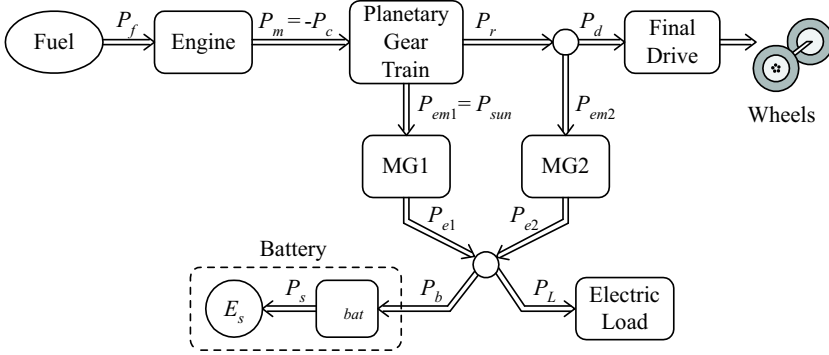


Figure 3.12: Power-based vehicle model for S/P-HEV

Similar to the S-HEV and the P-HEV, the battery model for the S/P-HEV incorporates an efficiency map with piece-wise linear losses. The parametric description for this loss-model is given in (2.13). By integrating P_s in (2.11), the battery calculates the stored energy E_s in the battery.

Final drive

The final drive transmits the propulsion power P_d to the front wheels. This power request is calculated from the backward vehicle model as presented in Section 2.1.2. The drive train and MG2 are both connected to the ring gear of the planetary gear train and for the power at the ring gear there holds:

$$P_r = P_d + P_{em2}, \quad (3.90)$$

Note that the planetary gear train acts as a variable transmission between the ICE and the final drive. Therefore, an additional gearbox is not required in the drive train of the vehicle. By selecting a fixed gear ratio $g_r = 1$, one can still apply (2.3) and (2.4) for calculating the mechanical power request in terms of ω and τ_d , respectively.

Internal Combustion Engine

Similar to the P-HEV, the model for the ICE is constructed from a static look-up table, expressing its momentary fuel consumption as a function of engine speed ω and torque τ_m , see (3.58). The ICE is connected to the carrier gear so $\omega = \omega_c$. Furthermore, the ICE delivers power to the

planetary gear train, and because this is in opposite direction as defined in (3.85), there holds $P_m = -P_c$ and $\tau_m = -\tau_c$. Since an S/P-HEV does not prescribe a unique relation between ω_d and ω , it is more convenient to work with engine torque rather than engine power to define the valid operating range. Finally, the ICE consumes no fuel when it is switched off and starting the ICE requires no additional fuel usage.

Motor/Generator

In the Toyota Prius, MG1 and MG2 have each their own functionality. Generally speaking, MG1 operates most of the time in generator mode and takes care of charging the battery. Only for starting the engine, MG1 is switched to motor mode. Compared to MG1, MG2 will frequently switch between motor and generator mode. For vehicle propulsion, MG2 operates in motor mode, whereas it switches to generator mode during periods of regenerative braking. A similar functionality will be used for the vehicle configuration that is considered here.

Both MG1 and MG2 have been modelled according to the description in (2.9), using a piece-wise linear efficiency map. Each machine can handle power in two directions: in motor mode the power is negative ($P_{em1} < 0$, $P_{em2} < 0$) and in generator mode the power is non-negative ($P_{em1} \geq 0$, $P_{em2} \geq 0$). This power is seen at the mechanical side of the electric machine and equals the product between torque τ_{em} and speed ω_{em} :

$$P_{em1} = \tau_{em1} \omega_{em1} \quad (3.91)$$

$$P_{em2} = \tau_{em2} \omega_{em2} \quad (3.92)$$

Note that the kinematic relations of the planetary gear train are not symmetric with respect to the sun-, carrier- and ring gear. Therefore, MG1 and MG2 have typically their own operating range for speed and torque.

3.3.4 On-line adaptive strategy

Strategy concept

The EM system coordinates the powerflow through MG1 and MG2, such that the ICE operates in a preferred working range. The vehicle speed determines the speed of the wheels, and since the final drive is connected to the ring gear and MG2, their rotational speed ω_r is also prescribed by the vehicle speed. For this reason, the control freedom for MG2 is limited to changes in torque τ_{em2} which affects the torque τ_r as seen by the ring gear.

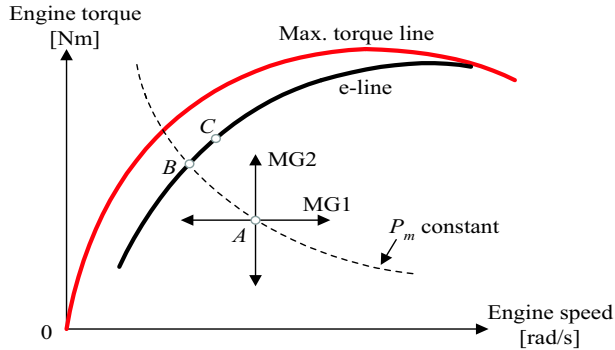


Figure 3.13: Shifting ICE operating point with MG1 and MG2

Now it is important to remember that the planetary gear train establishes a linear relation between the torque at the ring gear and the carrier gear, see (3.88). Since the ICE is connected to the carrier gear, a change in the power setpoint for MG2 affects primarily the engine torque and not its speed. Graphically, the influence of MG2 is visualized in Fig. 3.13.

On the other hand, MG1 is connected to the sun gear and also the amount of torque present at the sun gear is proportional to the ring gear, see (3.87). This means that τ_s is prescribed by τ_r and that the control freedom for MG1 boils down to changes in ω_s , *i.e.*, the speed of the sun gear. From (3.80) it follows that changing the speed of the sun changes also the speed of the carrier and hence, MG1 can be used to control the speed of the ICE, see Fig. 3.13. To explain all possible control actions from MG1 and MG2, three situations are examined:

1. No losses in MG1, MG2 and the battery

First, consider the ideal situation with no energy losses in MG1 and MG2 and assume that there are no limitations for their speed and torque range. In this case it is obvious to bring the ICE on the e-line by means of a suitable setpoint for MG1 and MG2. Notice that this approach often introduces a circulating power between MG1 and MG2, but this allows the ICE to provide the mechanical power with a minimum fuel use. Except for holding the ICE on the e-line, the electric machines offer even more freedom to the EM system. Taking advantage of this extra freedom should be done analogous to the EM system for an S-HEV. Since both vehicle configurations keep the ICE on the e-line, the same way of reasoning holds for switching the ICE on/off and how much power goes into or out of the

battery.

2. Losses in MG1 and MG2 but no battery use

The second situation does include losses in MG1 and MG2, but now the battery power P_b is kept permanently zero. Deciding whether it is still profitable to bring the ICE on the e-line depends directly on the losses in MG1 and MG2. If MG1 or MG2 suffers from a poor efficiency, then the operating point of the ICE will not move towards the e-line and the power through MG1 and MG2 remains often zero. On the other hand, the ICE moves towards the e-line when both MG1 and MG2 have an excellent efficiency. The extreme values are indicated in Fig. 3.13, where point A depicts the situation with zero efficiency, and point B refers to an efficiency of 100% for both MG1 and MG2. If there are small energy losses present, point B moves over the e-line towards point C . The additional power in C , compared to the power in B , compensates for the losses in MG1 and MG2.

3. Losses in MG1, MG2 and the battery

The third situation does include losses in MG1 and MG2 and it also allows usage of the battery. To get an indication about the fuel sensitivity of the ICE with respect to changes in the power demand from MG1 and MG2, one readily would like to consider the gradient of the fuel curves. However, MG1 corresponds primarily to the engine speed and MG2 relates to the engine torque, although both quantities determine the ICE power. Therefore, the gradient of the fuel curves should be considered in two ways. This is shown next.

MG2 has the ability to change the torque request from the ICE, and for a fixed engine speed a change in torque is directly proportional with engine power. Therefore, it makes sense to plot the fuel curves of the ICE with respect to power for a fixed engine speed, and consider the gradient of this map. In fact, this approach agrees with the EM strategy for a P-HEV, so the map depicted in Fig. 3.9 is also valid in this situation. Conversely, MG1 is used for changing the speed of the ICE and then the engine speed is proportional with power when the engine torque remains constant. Again, it is possible to draw the fuel curves with respect to power, but now each curve relates to a fixed torque level. The result is shown in Fig. 3.14.

The most important observation from Fig. 3.9 is that the fuel curves behave almost as a linear (affine) function. As a result, producing extra electric power with MG2 can be done along the entire operating range of the ICE with practically equal fuel costs. These costs are roughly estimated at 0.05 [g/kJ] for this particular ICE. On the other hand, the curves in Fig. 3.14 are far from linear and therefore, the fuel costs for producing

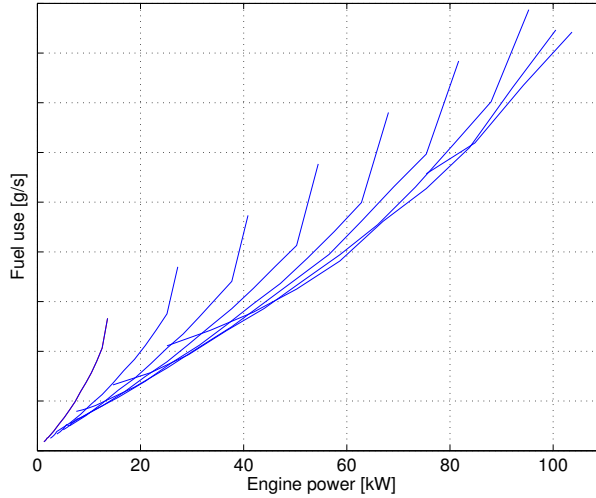


Figure 3.14: Fuel curves for different constant engine torque levels

power with MG1 will change with the operating point of the ICE. In the first place, the fuel curves increase significantly when they come close to their end-point value. This implies that raising the engine speed for extra mechanical power becomes less profitable when the ICE operates already near its maximum speed limit. A second trend is that the gradient of the curves reduces when the torque increases. More specifically, in the low torque range up to 100 [Nm], the slope of all curves is always above 0.05 [g/kJ]. Consequently, in this operating range the power delivered with MG1 requires more fuel than delivering this power with MG2. At higher torque levels, the slope of the curves is partially below 0.05 [g/kJ], so in this area it is more efficient to deliver power with MG1, instead of MG2.

It is important to realize that both observations are also justified by the shape of the e-line. Reconsider, for convenience, the e-line shown in Fig. 3.2, and recognize the vertical shape at low powers and the horizontal shape at high powers. Now recapitulate that the ICE delivers power with the highest efficiency when it operates on the e-line and producing extra power is preferably done by shifting the operating point over the e-line. In the lower power range, this is mainly achieved by increasing the engine torque, whereas at higher power levels, this primarily requires an increased engine speed. These observations resemble with the gradient of the fuel curves in Fig. 3.9 and Fig. 3.14.

In the end, both electric machines are connected to the same power net, so essentially there exists only one combined fuel cost for producing electric power. It turns out that focussing on the combined contribution from MG1 and MG2 with respect to the battery power is a very elegant way to estimate the actual fuel costs. This requires an optimization procedure to select the best combination for MG1 and MG2, which will be explained in the remainder of this section.

Problem definition for S/P-HEV

The control objective of the EM system for the S/P-HEV is chosen similar to the other vehicle configurations, namely maximize the fuel economy of the vehicle over an arbitrary driving cycle. Therefore, the EM system decides upon three control variables: the (mechanical) power demand P_{em1} and P_{em2} and the engine running signal $S \in \{0, 1\}$. Within the EM system, these variables control the energy level E_s in the battery, which is the only dynamical state that has to be considered. A formal definition of the control objective is given below:

$$\min_x J(x) \quad \text{subject to} \quad G(x) \leq 0, \quad (3.93)$$

with the cost function J equal to cumulative fuel use along a driving cycle with time length t_e , *i.e.*,

$$J(P_{em1}, P_{em2}, S) = \int_0^{t_e} F(P_{em1}, P_{em2}, S \mid \tau_d, \omega_d) dt, \quad (3.94)$$

where

$$F(P_{em1}, P_{em2}, S \mid \tau_d, \omega_d) = \begin{cases} 0 & \text{if } S = 0, \\ f(\tau_c, \omega_c) & \text{if } S = 1. \end{cases} \quad (3.95)$$

The decision variable x covers three variables: P_{em1} , P_{em2} and S . The ICE is connected to the carrier gear, so τ_c and ω_c correspond to the engine torque and speed, respectively. After selecting P_{em1} and P_{em2} , the signals τ_c and ω_c are calculated according to the steps indicated in Table 3.1.

In general, the ICE has a relative large fuel offset when it runs idle. Furthermore, the previous paragraph has learned that producing additional power requires almost equal fuel costs for every operating point of the ICE. Therefore, it will never be profitable to keep the engine running for charging the battery when the vehicle stands still. This means that $\omega_d = 0$ implies $S = 0$ and the calculations from Table 3.1 are well defined.

1. Given $P_d = \tau_d \omega_d$ and P_{em2} , the power requested from the ring gear P_r is calculated in (3.90).
 2. The torque acting on the ring gear is equal to: $\tau_r = P_r / \omega_d$.
 3. The torque seen at the sun gear (τ_s) and the carrier gear (τ_c) follow from (3.87) and (3.88).
 4. Since MG1 is connected to the sun gear and its power P_{em1} is known, the speed of the sun is also defined: $\omega_s = P_{em1} / \tau_s$.
 5. Finally, the carrier speed ω_c is calculated from (3.82) and equals the engine speed ω .
-

Table 3.1: Sequence of calculations to determine (τ_c, ω_c)

The inequality constraints in $G(x)$ include, amongst others, the physical limitations of the ICE, MG1, MG2 and the battery. Contrary to the S-HEV and the P-HEV, the S/P-HEV requires individual constraints to limit the speed and torque range of the ICE, whereas one constraint for the power from the ICE would be too conservative. Given the minimum and maximum torque line of the engine, it follows that this constraint is time dependent. A similar reasoning holds also for the engine speed, leading to the following constraints:

$$\omega_{min}(t) \leq \omega_c(t) \leq \omega_{max}(t) \quad (3.96)$$

$$\tau_{mmin}(t) \leq -\tau_c(t) \leq \tau_{mmax}(t) \quad (3.97)$$

$$\forall t \in [0, t_e]$$

The simulation models for MG1 and MG2 do not make a distinction between torque and speed and they only consider power. Also the battery model is power based and therefore, it is sufficient to apply here constraints in terms of power:

$$P_{em1min}(t) \leq P_{em1}(t) \leq P_{em1max}(t) \quad (3.98)$$

$$P_{em2min}(t) \leq P_{em2}(t) \leq P_{em2max}(t) \quad (3.99)$$

$$P_{bmin}(t) \leq P_b(t) \leq P_{bmax}(t) \quad (3.100)$$

$$\forall t \in [0, t_e]$$

The S/P-HEV needs to be charge sustaining and by means of a minimum required energy level E_{sref} in the battery this is established. There-

fore, the following end-point constraint is added to $G(x)$:

$$E_s(t_e) = E_s(0) + \int_0^{t_e} P_s(t) dt \geq E_{sref}. \quad (3.101)$$

On-line optimization strategy

Although the S/P-HEV offers significantly more freedom to the EM system, it is still possible to apply a similar optimization approach as used in the S-HEV and P-HEV. Again, the discrete variable S will be eliminated from the original problem by creating two sub-problems. Furthermore, it is assumed that a suitable value for the Lagrange multiplier λ^* is available, such that the optimal fuel cost for the production of electric power is known.

At first, the situation with $S = 1$ is considered, so the ICE is permanently on. For a given drive train torque τ_d and speed ω_d , the optimal power setpoints for MG1 and MG2 are calculated from the following minimization:

$$(P_{em1}^{S1}, P_{em2}^{S1}) = \arg \min_{\substack{(P_{em1}, P_{em2}) \\ \in \mathcal{Q}(\tau_d, \omega_d)}} \left\{ \begin{array}{l} F(P_{em1}, P_{em2} \mid \tau_d, \omega_d) \\ -\lambda^* P_s \end{array} \right\}, \quad (3.102)$$

where the set \mathcal{Q} covers only the feasible setpoints for MG1 and MG2 and satisfies the constraints in (3.97)-(3.100):

$$\begin{aligned} \mathcal{Q}(\tau_d, \omega_d) = \{ (P_{em1}, P_{em2}) \mid & P_{em1min} \leq P_{em1} \leq P_{em1max} \wedge \\ & P_{em2min} \leq P_{em2} \leq P_{em2max} \wedge \\ & P_{bmin} \leq P_{e1} + P_{e2} - P_L \leq P_{bmax} \wedge \\ & \tau_{min} \leq -\tau_c \leq \tau_{max} \wedge \\ & \omega_{min} \leq \omega_c \leq \omega_{max} \}. \end{aligned} \quad (3.103)$$

The signals τ_c and ω_c are calculated according to the steps indicated in Table 3.1. The model from MG1 and MG2 in (2.9) is used to calculate the electric power P_{e1} and P_{e2} , respectively. Finally, the net battery power P_s is calculated from the battery model (2.13).

Next, the same criterion is evaluated to estimate the expected fuel cost for this power setpoint $(P_{em1}^{S1}, P_{em2}^{S1})$:

$$f^{S1} = F(P_{em1}^{S1}, P_{em2}^{S1} \mid \tau_d, \omega_d) - \lambda^* P_s^{S1}, \quad (3.104)$$

where P_s^{S1} is defined by P_{em1}^{S1} , P_{em2}^{S1} and P_L in combination with the model for MG1, MG2 and the battery.

Now consider the situation with $S = 0$, so the engine is turned off. Depending on the direction of the powerflow through the drive train, two different modes are recognized: Motor only (MO) and Regenerative braking (R). An advantage of the planetary gear train is that it allows MG2 to recover all available kinetic energy during braking phases, without suffering from the drag torque losses in the ICE. This is possible as long as the sun gear with MG1 and/or the carrier gear with the ICE can rotate freely. On the other hand, when the carrier gear can rotate freely when engine is turned off, then MG1 cannot provide tractive force to the wheels. Consequently, this vehicle configuration has only MG2 available for R and MO. With respect to R, it is assumed that only 60% of the available kinetic power $P_d = \tau_d \omega_d < 0$ can be recuperated at the front wheels to meet the requirements for driveability. This decision is consistent with the other HEV configurations, see *e.g.*, Section 3.1.5. Furthermore, the maximum power for MG2 and the battery are defined in (3.99) and (3.100). This way, the power set-point P_{em2}^R for MG2 during R will be equal to:

$$P_{em2}^R = \text{sat} [-0.60 \times P_d]_0^{P_{em2}^{max}} . \quad (3.105)$$

$$(3.106)$$

The net battery power P_s^R follows from the inverse of (2.9) and (2.13):

$$P_b^R = \min(\eta_{gm2} P_{em2}^R, \frac{1}{\eta_{mm2}} P_{em2}^R) - P_L, \quad (3.107)$$

$$P_s^R = \min(\eta^+ P_b^R, \frac{1}{\eta^-} P_b^R). \quad (3.108)$$

MO requires that MG2 and the battery have sufficient power to supply the power request from the drive train and the electric load. This condition is covered by inequality constraints:

$$0 \leq P_d \leq -P_{em2}^{min} \quad \wedge \quad \frac{-P_d}{\eta_{mm2}} - P_L > P_{b}^{min} . \quad (3.109)$$

When applying MO, the power drawn from the battery equals:

$$P_s^{MO} = \frac{1}{\eta^-} \left(\frac{-P_d}{\eta_{mm2}} - P_L \right). \quad (3.110)$$

Now the expected fuel costs for recharging the battery are estimated as:

$$f^{MO} = -\lambda^* P_s^{MO}. \quad (3.111)$$

These estimated fuel costs are used to decide when to apply MO. By making a comparison between the fuel cost in (3.104) and (3.111), it follows that MO is preferred when the following inequality holds:

$$f^{MO} < f^{S1} \quad (3.112)$$

Finally, the EM system provides a control law for P_{em1} and P_{em2} . This control law is constructed from the individual modes as discussed above. R has the highest priority and will be applied if possible, *i.e.*, when $P_d < 0$. Next, MO will be active if (3.109) and (3.112) are satisfied. If these conditions are not satisfied, the strategy from (3.102) becomes active. Altogether, this leads to the following control law:

$$(P_{em1}, P_{em2}) = \begin{cases} (0, P_{em2}^R) & \text{if } P_d < 0 \\ (0, P_{em2}^{MO}) & \text{if (3.109) } \wedge \text{ (3.112)} \\ (P_{em1}^{S1}, P_{em2}^{S2}) & \text{elsewhere} \end{cases} \quad (3.113)$$

Furthermore, the engine is turned off when the engine running signal S becomes zero, so during R and MO.

Strategy implementation

An optimization algorithm will be required to perform the minimization procedure from (3.102) and calculate the power setpoint for MG1 and MG2 from (3.113). To that end, a dense grid has been selected for P_{em1} and P_{em2} , which covers the entire feasible operating range of MG1 and MG2. The advantage of using a grid in the optimization procedure, is that there are no requirements posed for convexity of the objective function. However, in case there does not exist a unique global minimum, the solution with the lowest battery activity is selected.

Similar to the S-HEV and P-HEV, also the EM strategy in (3.113) requires an on-line estimation for λ^* . The concept with a PI-controller in a feedback loop to estimate $\hat{\lambda}$ (see Section 3.1.6) is also valid for the S/P-HEV. The simulation results are shown in the next chapter.

3.4 Energy management including battery wear

The EM strategies from the preceding sections focussed primarily on minimizing the fuel consumption of the vehicle. To reach that goal, they frequently use the battery for temporarily storing electric energy. Unfortunately, this battery usage leads to extra battery wear and has negative

consequences for the available storage capacity of the battery, as well as a reduced life time. Therefore, it is desirable to include the costs for a replacement of the battery into the control objective of the EM strategy. A suitable method will be shown in this section.

Concerning the battery life time, manufactures can give a good approximation for the battery degradation process, when it is repeatedly charged and discharged in a predefined experiment. The most important operational conditions that affect the life time of a battery are the current profile and the temperature [75, 69]. The temperature T of the battery expresses two opposite effects. On the one hand, a higher temperature decreases the internal resistance of the battery, which lowers the energy losses during charging and discharging, and improves the cranking capability. Conversely, a higher temperature leads to more undesired chemical reactions in the battery, which can be irreversible and shorten its life time.

In addition to the temperature, also the current profile has a strong influence on the battery life time. In general, battery manufacturers define their aging tests in terms of Depth of Discharge (DOD). This quantity expresses the amount of net energy E_s removed from the battery as a percentage of the rated capacity $E_{s\,cap}$:

$$DOD = \frac{E_{s\,cap} - E_s}{E_{s\,cap}} \times 100 = 1 - SOE \quad [\%]. \quad (3.114)$$

During an aging test, a test cycle is repeatedly offered to the battery, which alternately discharges and charges the battery for a fixed DOD . Next, the cycle life $N_{life}(T, DOD)$ [-] of a battery is defined as the number of discharge cycles that the battery can handle, before its capacity falls below 80% of the initially rated capacity. This 20% capacity loss has been selected according to the standard regulations for the replacement of a VRLA battery in a stationary situation, see [1].

According to the definitions from above, the energy that can be drawn from the battery during its entire life time equals:

$$E_{life}(T, DOD) = N_{life}(T, DOD) \times \frac{DOD}{100} \times E_{s\,cap} \quad [\text{J}]. \quad (3.115)$$

This information is used to derive an appropriate weighting between the costs for battery degradation versus the achieved fuel benefits from the EM system. Therefore, the general objective function from the EM strategies in the preceding sections is repeated below:

$$J(P_s, S) = F(P_s, S | P_d, P_L, \omega) - \lambda^* P_s \quad [\text{g/s}]. \quad (3.116)$$

Now assume that the total costs for battery replacement are equal to \mathcal{R}_b [Euro]. Given the current fuel price \mathcal{F} [Euro/ ℓ], and the corresponding fuel density ρ_f [g/ ℓ], it becomes possible to rewrite the battery energy from (3.115) in terms of equivalent fuel cost:

$$\mu = \frac{\rho_f}{\mathcal{F}} \frac{\mathcal{R}_b}{E_{li\,fe}(T, DOD)} \quad [\text{g/J}]. \quad (3.117)$$

These equivalent fuel costs are added to the general control objective from (3.116). Since (3.115) considers only the energy from battery discharging, the battery can handle twice this energy if both charging and discharging is taken into account. An extra correction factor of 1/2 will compensate for this:

$$J'(P_s, S) = F(P_s, S | P_d, P_L, \omega) - \lambda^* P_s + \frac{1}{2} \mu |P_s| \quad [\text{g/s}]. \quad (3.118)$$

Although the derivative of this objective function is not well defined for $P_s = 0$, its minimum value can still be calculated, *e.g.*, by numerically evaluating $J'(P_s, S)$ on a dense grid.

Except for including battery wear in the objective function, the EM system requires also an update of the battery model. Although literature provides no detailed information about the energy efficiency of an aged battery in an HEV application, there are several indications that an older battery suffers from a higher internal resistance [29], and according to the measured battery current, it is very well possible to predict the increased internal resistance, see [69]. Furthermore, promising techniques are known from literature to estimate on-line the capacity of a battery [66]. Returning back to the battery model from the EM system, these effects require a regular update of the model parameters for the battery efficiency η_{bat} and its capacity $E_{s\,cap}$.

3.5 Conclusions

An on-line EM strategy has been developed for three vehicle configurations: the S-HEV, the P-HEV and the S/P-HEV. This strategy is derived from the optimal solution, but through an intelligent decision algorithm, there is no need for a global optimization nor a wish for prediction information. This allows for an easy vehicle implementation.

Contrary to existing EM strategies, the proposed EM system determines its

control actions primarily on the incremental fuel cost λ [g/J], rather than optimizing directly the engine efficiency η_{ice} [-].

The parameter λ indicates the extra fuel use of the ICE when a small amount of additional electric energy is produced. Although an EM system increases the overall efficiency of the vehicle, appropriate directions to reach this goal are hidden in η_{ice} through the fuel offset f_1 when the ICE runs idle. Conversely, λ directly provides the required information.

For each driving cycle, a fixed optimal solution λ^* exists. Based on the actual *SOE* of the battery, a PI-controlled feedback loop offers a valid approach to estimate this parameter on-line.

4

Simulation results

The previous chapter provided a general framework for energy management in three popular vehicle configurations: the series-, the parallel- and the series/parallel HEV. For each configuration, this chapter presents simulation results to illustrate the benefits in fuel economy. Moreover, it will be shown that the proposed EM concept has the ability to improve the vehicle fuel economy similar to an optimal strategy from Dynamic Programming (DP), but without exact knowledge about the future driving cycle and without complex calculations in the optimization algorithm.

Before reading this chapter, it is important to remember that this thesis does not answer questions about an optimal vehicle configuration, or finding a suitable component sizing. The reason is that these questions cannot be answered solely from an energy management perspective, but require other trade-offs, *e.g.*, functional requirements or driveability issues. At this point, the interested reader is referred to the work from Hofman et al. [35], whereas this chapter has selected its vehicle configurations based on experience.

The intention of this chapter is to provide insight into the benefits from an EM system, in terms of fuel economy, for a given vehicle configuration. First, details are given about the selected vehicles in Section 4.1. Next, Section 4.2 presents the corresponding simulation results and provides a detailed analyses for each strategy. Finally, the conclusions and recommendations can be found in Section 4.3.

	<i>S-HEV</i>	<i>P-HEV</i>	<i>S/P-HEV</i>
ICE (SI engine)	50 kW	100 kW	100 kW
MG1	Generator	ISG	MG1
$P_{em\ min}$	0 kW	-4.0 kW	-4.8 kW
$P_{em\ max}$	50 kW	6.25 kW	7.5 kW
η_{mm}	-	0.8	0.8
η_{gm}	0.9	0.8	0.8
MG2	MG2	-	MG2
$P_{em\ min}$	-50 kW	-	-12.0 kW
$P_{em\ max}$	50 kW	-	18.75 kW
η_{mm}	0.8	-	0.8
η_{gm}	0.8	-	0.8
Battery			
$P_{b\ min}$	-50 kW	-5 kW	-25 kW
$P_{b\ max}$	50 kW	5 kW	25 kW
η_{bat}	0.85	0.85	0.85
$E_{s\ cap}$	4.0 MJ	2.0 MJ	4.0 MJ
P_L	645 W	645 W	645 W

Table 4.1: Parameter settings for HEV configurations

4.1 Simulation environment

The simulation environment entails separate models for each vehicle configuration: S-HEV, P-HEV and S/P-HEV. The vehicle models are implemented according to the description given in Section 2.1. All three vehicle configurations make use of a similar backwards vehicle model when calculating the mechanical power request P_d . The parameter settings of this drive train model are listed in Table 2.1. The other vehicle components depend on the selected vehicle configuration and their parameter settings are summarized in Table 4.1. In terms of efficiency, there is a strong similarity between the components of different vehicles, whereas their sizes vary according to the selected vehicle configuration. The reasoning behind this component scaling will be clarified in the remainder of this section.

4.1.1 Description of S-HEV

In an S-HEV, no mechanical connection exists between the engine and the wheels. As a result, there is no need to apply an ICE that matches with the

maximum drive train power and it is possible to use a down-scaled version of the 2.0 [ℓ] SI engine from Chapter 2. After downsizing, the maximum engine power now satisfies 50 [kW] and according to this power constraint, also the generator can handle power up to 50 [kW], so $P_{em} \leq 50$ [kW]. The electric machine MG2 can operate in generator mode and motor mode with an equal power limit in both directions: $|P_{em}| \leq 50$ [kW]. For many other driving cycles, the size of this electric machine will be inadequate but for the NEDC it meets the requirements. The efficiency of the generator is selected $\eta_g = 0.9$ [-], and for MG2 it is equal to $\eta_{mm} = \eta_{gm} = 0.8$ [-].

Assume, for the moment, a nominal battery voltage of 200 [V] and a rated capacity of 11 [Ah]. Since the battery voltage decreases when it discharges, it is assumed that only 50 [%] of the rated [Ah] capacity is effectively available:

$$E_{cap} \approx 0.5 \times 3600 \times C_{bat} \times U_{bat}^{nom} = 0.5 \times 3600 \times 11 \times 200 = 4.0 \text{ [MJ]} \quad (4.1)$$

Hence, the battery capacity is $E_{cap} = 4.0$ [MJ] and its efficiency is selected $\eta_{bat} = 0.85$ [-]. From a practical point of view, this battery capacity might be too small to satisfy the necessary charge acceptance during regenerative braking periods. This follows from the fact that the charge acceptance is closely related to the size of the battery. However, the reason to keep the battery size limited in the simulation environment is that it reduces the state-space size, such that Dynamic Programming (DP) can be easily applied. To overcome the limited charge acceptance in the battery, one could connect an additional storage device to the powernet (*e.g.*, a super-capacitor [48, 59]), but these concepts are beyond the scope of this thesis. Finally, the auxiliary loads have a permanent power demand of $P_L = 645$ [W].

4.1.2 Description of P-HEV

The P-HEV configuration represents a mild-HEV with an integrated starter/generator (ISG). The clutch is located between the ISG and the transmission. The battery and the ISG can handle electric power up to 5 [kW]. Because the efficiency in motor mode and generator mode equals $\eta_{mm} = \eta_{gm} = 0.8$ [-], the mechanical power range is equal to $-4000 \leq P_{em} \leq 6250$ [W], see also Table 4.1. The effective battery capacity is assumed to be $E_{cap} = 2.0$ [MJ] and its efficiency is equal to $\eta_{bat} = 0.85$ [-]. These battery parameters represent a 36 [V] battery with a rated capacity of $C_{bat} = 30$ [Ah]. Similar to the S-HEV, only 50 [%] of the rated capacity is effectively

available in terms of energy:

$$E_{cap} \approx 0.5 \times 3600 \times C_{bat} \times U_{bat}^{nom} = 0.5 \times 3600 \times 30 \times 36 = 2.0 \text{ [MJ]} \quad (4.2)$$

4.1.3 Description of S/P-HEV

The electronically-controlled continuously variable transmission (eCVT) in the S/P-HEV makes use of a planetary gear train to connect the ICE with MG1, MG2 and the drive train. The basic gear ratio is selected equal to the Toyota Prius: $Z = 78/30$, see (3.81). There should be mentioned that this gear ratio has been selected as a preliminary value. Since the remaining components of the drive train are also different from the Toyota Prius, it is clear that this gear ratio can be further optimized.

The sizes of MG1 and MG2 are defined by their maximum power ratings at 6 [kW] and 15 [kW], respectively. These power limits correspond to the electric side of the machine, whereas the mechanical power limits are listed in Table 4.1. Both electric machines are relative small, compared to other S/P-HEVs that are currently available on the market. For example the Toyota Prius applies a 50 [kW] electric machine for MG2 in its 2003 model. Conceptually, there should be no difference for the required EM strategy with respect to the maximum power ratings for MG1 and MG2. The main reason to keep the size of MG1 and MG2 here limited, is from a computational point of view. A smaller power range for MG1 and MG2 reduces the set of possible input combinations and hence, the required calculation time for a full optimization with DP remains limited. The battery size is selected similar to the S-HEV. Also here it is possible that the rated battery size and charge acceptance are not feasible in practice.

4.2 Simulation results

4.2.1 Results S-HEV

The simulations for the S-HEV cover four different strategies from Section 3.1, indicated here with $S1...S4$. Simulation $S1$ refers to the baseline (BL) strategy, with the battery power permanently zero and the engine always running, so $P_b(t) = 0$ [W] and $S(t) = 1$ for $t \geq 0$. Note that this strategy utilizes a small fraction of the available energy from regenerative braking (R), since it supplies only the electric loads during braking phases and battery charging is not allowed. The second simulation $S2$ evaluates the DP strategy. In fact, this is an off-line simulation because the control

sequence calculated with DP is calculated off-line and stored in a look-up table. Simulation *S3* applies the adaptive strategy from (3.54), with λ^* taken constant along the entire driving cycle. Its value is determined by a bi-section search algorithm, such that $SOE(T_e) = SOE(0)$. The last simulation *S4* applies also the strategy from (3.54), but now the PI controller from (3.55) is used to estimate λ^* .

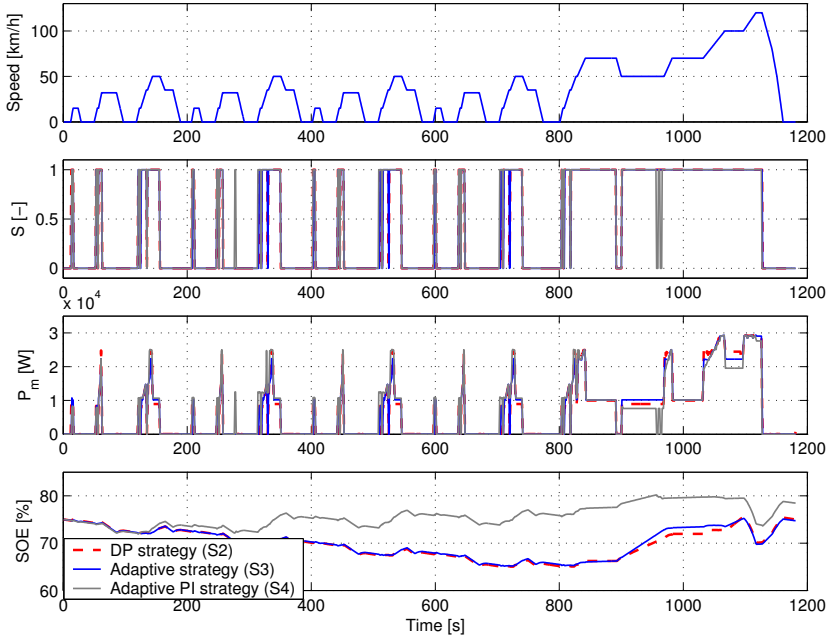
The control sequences for *S2*, *S3* and *S4* are shown in Fig. 4.1. From the *SOE* trajectory it is clear that *S2* and *S3* exhibit almost similar behavior. The plot with the engine power P_m indicates that there are two favorable power levels for the ICE. They are located at 10 [kW] and at 25 [kW]. The point at 10 [kW] is selected because the slope of the e-line incorporates a local non-convexity at this point. Although this is not clearly visible in Fig. 3.3, the e-line around 10 [kW] does not follow a straight line but its slope is slightly lower. This implies that the ICE can produce additional power here with relative less fuel usage. For this reason, it becomes profitable to bring the ICE often at 10 [kW], although the power request for propulsion is lower. This happens, amongst others, when the vehicle travels at 50 [km/h] whereas the extra power is stored in the battery.

The other operating point is determined by the sweet-spot¹ of the ICE. It turns out that the sweet-spot of the down-sized ICE is located at $P_m = 25.1$ [kW]. At moments when the driver requests more than 10 [kW] for vehicle propulsion, it becomes attractive to produce significantly more power with the ICE and store the surplus energy in the battery. In the mean time, the ICE runs in its sweet-spot.

The overall fuel consumption for each strategy is depicted in Table 4.2. Because simulation *S4* ends with significantly more energy in the battery, $SOE(T_e) = 81.4$ [%], the fuel consumption has been corrected for this with the average value of $\hat{\lambda}$, see *e.g.*, [73] for a similar approach. Furthermore, the tuning parameters for the PI-controller are still preliminary values. Finding their final values is a topic for further research, but from experience it is known that the initial guess yields already good results on the NEDC driving cycle. This is further explained in Appendix A.

Two important observations emerge from Table 4.2. First, simulation *S2* does not achieve the absolute lowest fuel consumption, although this would be expected from the DP algorithm. The reason is that *S2* has been calculated with a discrete grid of 200 [W] for all state- and input variables. To limit the required calculation time as well as memory usage,

¹The sweet-spot of an ICE refers to the operating point where it achieves the absolute highest fuel-efficiency η_{ice} in (2.2).

Figure 4.1: Simulation results for $S2$, $S3$ and $S4$

this grid density cannot be chosen infinitely small. This is different with $S3$ and $S4$. Although these strategies also apply a discrete grid for the input variable P_m , they can apply a very dense grid, without violating the required calculation time.

The second observation is that $S3$ and $S4$ achieve an almost similar fuel economy. Apparently, the sensitivity between the overall fuel usage and the selected EM strategy turns out to be rather limited. Referring back to Fig. 3.3, this comes not as a surprise. Because the e-line is very well approximated by a linear curve below 30 [kW], it is obvious that producing extra power can be done at many points, all requesting an almost equal fuel use.

4.2.2 Results P-HEV

For the P-HEV, five different EM-strategies are evaluated. All strategies start at $SOE = 75$ [%]. The first simulation ($S1$) applies only mode BL with the engine always running, so $P_b = 0$ [W] and $S = 1$. The second simulation

<i>Simulation No.</i>	<i>Absolute fuel use [g]</i>	<i>Relative fuel use [%]</i>
<i>S1</i> (Baseline)	582	100
<i>S2</i> (Dynamic Programming)	476	81.8
<i>S3</i> (On-line strategy, λ^* fixed)	472	81.1
<i>S4</i> (On-line strategy, PI-control)	474	81.4

Table 4.2: Fuel consumption of S-HEV on NEDC

(*S2*) evaluates a control strategy obtained from DP. By definition, DP provides an optimal strategy within the selected grid accuracy and serves here as a benchmark. The third simulation (*S3*) uses the EM-strategy from (3.79) with λ^* taken constant. Here, a careful selection of λ^* guarantees that the *SOE* at the end of the driving cycle equals 75 [%]. Simulation *S4* applies the same strategy as *S3*, but now $\hat{\lambda}$ is estimated with the PI controller from Section 3.1.6. Finally, the fifth simulation (*S5*) is a subset of *S3* and allows only three modes from (3.79): BL, R and MO. This strategy emphasizes the importance of mode R and MO in the overall performance.

For each strategy, the corresponding fuel consumption is shown in Table 4.3. *S4* has ended the simulation with a slightly different *SOE* level and the average value of $\hat{\lambda}$ is used to correct its fuel consumption. An important observation is that *S3* and *S4* achieve almost a similar improvement in fuel consumption, although *S4* does not rely on knowledge about the future driving cycle. The reason why *S3* performs slightly better than *S2* is because DP is restricted to the accuracy of the grid, whereas *S3* does not suffer from this limitation. Comparing *S5* to *S3*, it follows that two modes (R and MO) are responsible for 64 [%] of the total fuel profits. R produces electric energy when $\lambda = 0$ and MO eliminates the fuel offset f_1 . These are the two characteristics where an EM strategy always yields profits. The third characteristic relates to variations in λ , when the ICE changes to different operating points. Especially the opportunity to do more MO with energy from C provides the largest contribution in the remaining 36 [%] of the potential benefits. The added value of MA is limited to only a few percent, due to the small variations in the engine map for λ .

The control sequences for *S2*, *S3* and *S4* are shown in Fig. 4.2. From the *SOE* trajectory it is clear that *S2* and *S3* execute similar behavior. Because these strategies utilize (limited) a-priori knowledge from the driving cycle, they allow large deviations for *SOE* and still return to 75 [%] at the end of

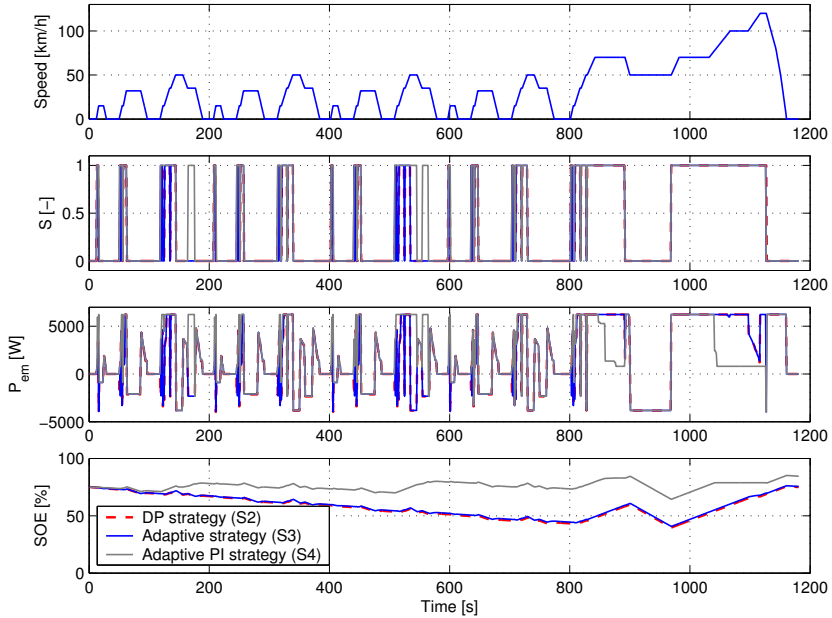
<i>Simulation No.</i>	<i>Absolute fuel use [g]</i>	<i>Relative fuel use [%]</i>
<i>S1</i> (Baseline)	577	100
<i>S2</i> (Dynamic Programming)	436	75.6
<i>S3</i> (On-line strategy, λ^* fixed)	435	75.4
<i>S4</i> (On-line strategy, PI-control)	441	76.4
<i>S5</i> (Only BL+R+MO, λ^* fixed)	486	84.2

Table 4.3: Fuel consumption of P-HEV on NEDC

the cycle. This is different for *S4*. By construction, this strategy keeps the *SOE* close to its reference value, but the main control actions from *S2* and *S3* are still visible. Another point of attention is the control setpoint P_{em} . Due to the piece-wise linear behavior of the engine map, desired control actions are often found in extremes, giving rise to non-smooth switching behavior.

A typical characteristic of the NEDC driving cycle is that it contains four identical city trips with a speed range up to 50 [km/h], and the cycle ends with an extra-urban part (*i.e.*, a short journey on the freeway), see the upper plot from Fig. 4.2. During the city part, the vehicle travels approximately 4.0 [km] in 780 [s]. Next, the extra-urban part covers almost 7.0 [km] and lasts 400 [s]. For both trajectories it is interesting to examine the added value of the EM system. Therefore, Table 4.4 shows the fuel consumption of *S1* and *S2*, with each part of the driving cycle in a separate column. These figures show that the *S2* simulation achieves an enormous fuel reduction on the city part, whereas extra fuel is needed on the extra-urban part. The fuel reduction during the city trip emerges mainly from the various idling periods, where the vehicle stands still and the ICE is turned off. Furthermore, the ISG uses energy from the battery to launch the vehicle, and the EM algorithm produces insufficient power during the city trips to compensate for this. As a result, battery charging takes place on the extra-urban part and consequently, *S2* consumes more fuel than *S1*.

In terms of fuel economy (*i.e.*, the fuel consumption per driven kilometer, [g/km]), a similar effect can be noticed, see the columns with fuel economy in Table 4.4. Typically, conventional vehicles achieve a better fuel economy during freeway driving than on city trips. This situation is also valid for *S1*. However, by applying an EM strategy it is very well possible that the vehicle achieves a better fuel economy during city traffic than on

Figure 4.2: Simulation results for $S2$, $S3$ and $S4$

the freeway. This is exemplified by $S2$. It is clear that this result depends on the content of the driving cycle, but it emphasizes the possible effects of an EM system on fuel economy.

4.2.3 Results S/P-HEV

The S/P-HEV model is evaluated for three EM strategies $S1$, $S2$, and $S3$. $S1$ implements an off-line control law calculated from DP. Simulation $S2$ makes use of the control strategy shown in (3.113) with a fixed value for λ^* . Finally, $S3$ applies the same control law as $S2$, but now it uses the PI-controller to estimate $\lambda^* = \hat{\lambda}$ online.

Unfortunately, none of these strategies represent a baseline configuration. The reason for this is that the ICE cannot provide tractive force to the wheels when the eCVT has no control algorithm. This makes it difficult to define a baseline strategy without an EM system incorporated. Moreover, car manufacturers are hesitated in giving details about their EM system. This complicates the implementation of a realistic baseline strategy in the simulation environment.

<i>Sim. No.</i>	<i>City part - 780 [s]</i>		<i>Extra-Urban part - 400 [s]</i>	
	<i>Absolute fuel use [g]</i>	<i>Fuel economy [g/km]</i>	<i>Absolute fuel use [g]</i>	<i>Fuel economy [g/km]</i>
<i>S1</i>	279	69.3	298	42.9
<i>S2</i>	119	29.5	318	45.7

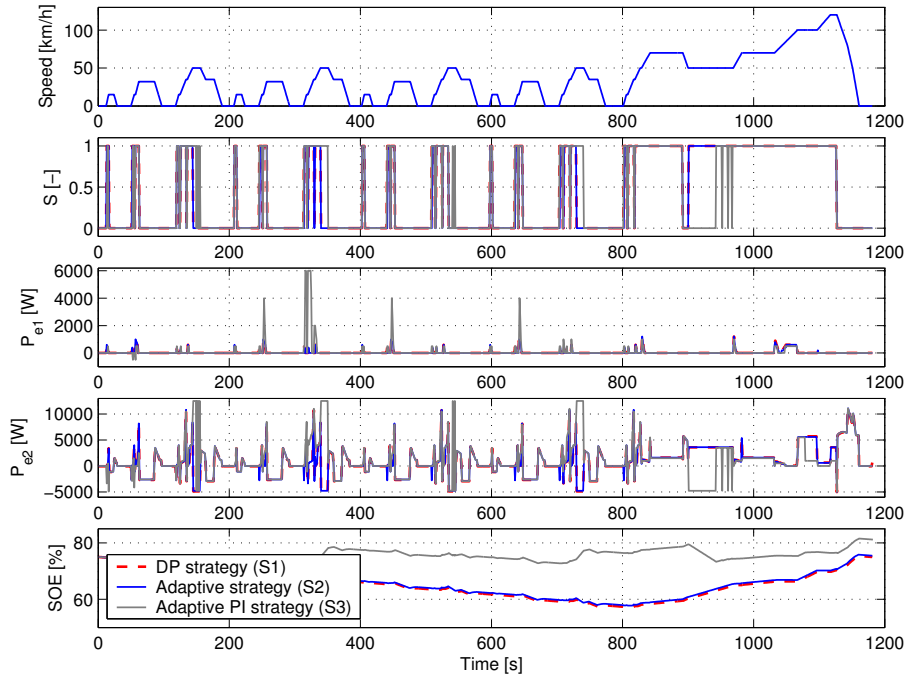
Table 4.4: Cycle dependent fuel economy of P-HEV

The signals of interest for all three simulations are shown in Fig. 4.3. It turns out that the power P_{e1} through MG1 is often zero and MG1 generates electric power only during vehicle acceleration. This is completely different for MG2. Here, P_{e2} is typically non-zero, except for the moments when the vehicle is not moving. One can see that MG2 applies regenerative braking during vehicle deceleration. Furthermore, when the vehicle travels through the city at a constant speed, MG2 provides the power request for the drive train and the ICE remains off.

Altogether, the control actions from MG1 and MG2 take care that the ICE operates very close to the e-line. This is elucidated in Fig. 4.4, which shows the operating points of the ICE during *S2*. From this figure, it can be concluded that the efficiency of MG1, MG2 and the battery are high enough to bring the ICE frequently on the e-line. On the other hand, the situations where the ICE is not running on the e-line are mainly determined by the power limitations of MG2. Furthermore, other simulations have learned that all operating points start moving towards the sweet-spot of the ICE, when the efficiency of MG1, MG2 and the battery increases. In the end, the size of MG1 and MG2 put a restriction on whether the ICE can reach its sweet-spot or not.

Similar as with the other HEV configurations, the *S2* strategy approximates very well the DP strategy *S1*. This follows from the *SOE* profile in Fig. 4.3, where both curves are close together. The corresponding fuel consumption is shown in Table 4.5, and again, the performance of the DP algorithm in *S1* is limited through its grid size of 150W. Especially for the S/P-HEV configuration it is not possible to run *S1* with a more dense grid. This is caused by the fact that the S/P-HEV incorporates three decision variables, whereas the S-HEV and P-HEV have only two degrees of freedom.

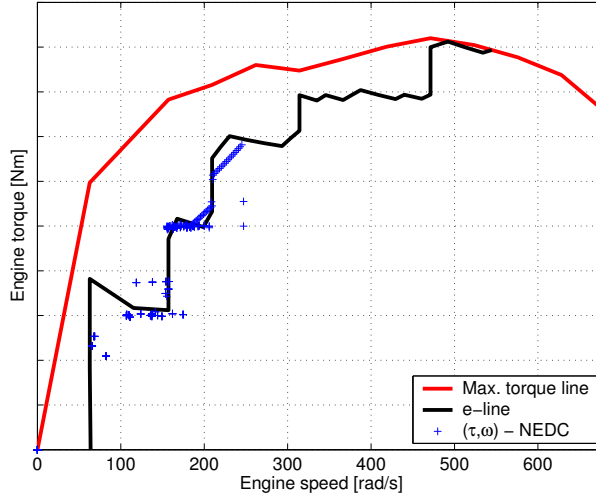
Finally, the small difference in fuel consumption between *S2* and *S3* indicates again that the S/P-HEV configuration works well with a PI-

Figure 4.3: Simulation results for $S1$, $S2$ and $S3$

controller for estimating $\hat{\lambda}$ online. Nevertheless, the parameters of the PI-controller are optimized for the NEDC driving cycle (see Appendix A), and a more careful analysis will be needed for other driving cycles.

4.3 Evaluation

The results presented in this chapter have been obtained from a simulation environment with a limited model complexity. Properties which are not included in the simulation environment are for example an additional fuel-penalty for engine cranking. Furthermore, the free energy from regenerative braking reduces in the P-HEV and S/P-HEV, due to friction losses in the ICE as well as in the transmission, whereas some of these losses are neglected in the simulation environment. In fact, one could eliminate these friction losses by installing an extra clutch in the drive train (see *e.g.*, [50]), but this is beyond the scope of this thesis. In addition, also the efficiency model for the battery and the electric machine can have more complexity

Figure 4.4: Operating points ICE for $S2$ simulation

<i>Simulation No.</i>	<i>Fuel use [g]</i>
$S1$ (Dynamic Programming)	405
$S2$ (On-line strategy, λ^* fixed)	403
$S3$ (On-line strategy, PI-control)	405

Table 4.5: Fuel consumption of S/P-HEV on NEDC

in reality. Therefore, it is not the intention of this chapter to state that the presented results match perfectly with results from a real vehicle. Nevertheless, it is reasonable to believe that the relative difference between alternative EM strategies remains equal in a real vehicle driving the NEDC driving cycle. As a result, the EM strategy with a PI-controller to estimate $\hat{\lambda}$ is an appealing concept, since it achieves a performance close to the optimum result without the explicit need for prediction information. Moreover, the required calculations have a low computational demand. This is a big advantage for vehicle implementation, where computational power is usually limited.

Also from a control perspective, it is possible to explain why the on-line strategy does not need prediction information and still achieves a performance close to the non-causal DP strategy. Therefore, the frequency spectrum of the power demand from the driving cycle should be considered

(see also Appendix A). Since the speed profile of the NEDC driving cycle changes frequently, there are regular variations in its power demand. The bandwidth of the on-line EM system with the PI-controller is selected small, such that many frequency components of the driving cycle appear outside the frequency range of the PI-controller. As a result, not much variations are seen in the estimated fuel cost $\hat{\lambda}$, provided that its initial value λ_0 is selected correctly. Ultimately, a fixed value $\hat{\lambda} = \lambda^*$ can be used which cuts down the bandwidth of the PI-controller to zero. This means that no frequency components of the driving cycle are filtered out by the PI-controller, and the EM strategy can benefit from them. For this situation it is shown that the on-line EM system resembles the DP strategy.

Nevertheless, a solution with zero bandwidth has no feedback mechanism and will not be feasible in practice. Due to uncertainties in the driving cycle and the vehicle model, it is impossible to calculate λ^* accurately in advance. As a result, the EM system suffers from drift in the actual *SOE* of the battery. Consequently, some feedback will always be necessary to apply corrections on-line, such that the *SOE* is kept within a preferred operating range. More details on this topic are given in Appendix A.

4.3.1 Conclusions

This chapter demonstrates the validity of the proposed EM system from Chapter 3. Although a-priori knowledge about the future driving cycle improves the overall performance, excellent results are also achieved without using prediction information.

The benefits in fuel consumption from an EM system are strongly related to three driving characteristics: engine stop/start, energy recovering during regenerative braking, and variations in the gradient of the fuel map for different operating areas of the ICE. These elements are fully exploited when the vehicle travels at various speeds. Consequently, an EM system is most effective during city trips and not on the freeway where the vehicle speed remains rather constant.

From the overall performance of an EM system, most of the profits are achieved by applying regenerative braking in combination with motor-only mode (approximately 64 [%]). The remaining benefits come from changing the operating point of the ICE. Here, charging of the battery is most profitable if the extra energy is used for additional motor-only mode. Using this energy for motor assist yields minor profits and contributes to only a few percent of the total EM potential.

4.3.2 Recommendations

The vehicle models used in this chapter have a limited model complexity and are not validated against experimental data. Further research should concentrate on the verification of the used models, to quantify the accuracy of the presented results.

The models of the battery and the electric machine rely on simple algebraic relations to express their energy losses. The accuracy of these relations can be improved by including functions with more complexity. As long as these functions contain only static relations and no dynamics, they can be directly incorporated in the presented EM system.

The present parameters for the PI-controller to estimate $\hat{\lambda}$ are tuned on the NEDC driving cycle. At this moment, it is unsure how these settings work in other driving situations. Therefore, further research is desired to select appropriate parameters under real-world driving conditions.

In all simulation results, the engine stop/start signal $S \in \{0, 1\}$ incorporates many switching moments, and the time interval that the ICE is running can be short. This is due to the fact that the ICE model does not penalize a restart of the engine. For driveability reasons, it is possible to include an additional fuel term for engine cranking in the objective function, such that the stop/start feature is used more carefully.

5

Energy management with electronic horizon

In the previous chapters, information about the future driving cycle has been excluded from the on-line strategies, such that a causal EM strategy emerged. Nevertheless, it is certainly valid to ask whether the on-line strategies are able to incorporate future road information into their decision process and when this is profitable. This will be the subject of the present chapter.

In terms of an electronic horizon (e-horizon), a preferred State of Energy (SOE) trajectory for the battery is calculated, according to the expected propulsion power needed in future road segments. Especially the digital road maps from a car navigation system can be helpful in providing the necessary information. It turns out that knowledge from the road ahead provides a positive contribution to the effectivity of an EM system, although the extra profits in fuel economy are limited. Driving cycles with a considerably different power demand on succeeding road segments have the highest potential to benefit from the e-horizon. Therefore, the simulations in this chapter are done for a different driving cycle than the NEDC.

5.1 Road information

From a car navigation system it is expected that it provides, amongst others, travelling directions for the driver. However, also the EM system can receive information from the navigation system. This is currently not used, but researchers are investigating several concepts on road information for EM strategies [4, 9, 13, 67]. However, none of these concepts recognize the

importance of scheduling energy through the battery among different road segments.

The database of a digital road map is organized through road segments and according to the geometry of the road, this corresponds to a graph of possible road trips. To date, the digital road map contains many characteristics of the road (*e.g.*, maximum speed, road category, position of traffic lights, etc.) and this information is available on each road segment. In addition to these road characteristics, more information from the road can be added to the map. This extra information should allow for a calculation of the expected power demand along each road segment, using technical information from the vehicle. The following types of road information characterization can be distinguished:

Statistic information

Road information by means of statistics provides a description of the amplitude distribution for the signals of interest (*e.g.*, the vehicle speed and its acceleration profile) for each road segment. To store this data, the amplitude range of each signal is divided into a set of intervals. For each road segment, a histogram is determined for the signals of interest. Because signals such as speed and acceleration can be correlated to each other, they are combined into one histogram.

All road information needs to be supplied at least once for each road segment. Next, it is possible to update the information of the road segments when the vehicle travels more regularly over the same trajectory. Nevertheless, publications about an EM system using statistic road information have not been found in literature.

Stochastic information

A road characterization in terms of stochastic information considers the frequency distribution of signals. With a statistic description, it is not relevant in which sequence the values of signals occur. A stochastic description describes the dependencies among the amplitudes at succeeding time instants.

An excellent technique to use stochastic signals within an EM system is Stochastic Dynamic Programming (SDP), see [11] volume two. An advantage of SDP is that all time-consuming calculations can be done off-line. By definition, SDP considers an objective function over an infinite time horizon, such that one static control law emerges, stored in a state-dependent look-up table, see [46, 54].

Deterministic information

A deterministic description of the future road profile describes the signals of interest over a certain time horizon at a pre-defined sampling frequency. These signals describe only one realization for driving a certain road segment. Due to all kinds of uncertainties, it is not realistic to expect that a measured realization will be exactly reproduced when the vehicle drives the same road segment again.

To benefit from this information, one can apply an EM system using Model Predictive Control (MPC), see *e.g.*, [7, 28, 42, 83]. Chapter 6 addresses this topic by presenting an MPC-based strategy. Dynamic Programming (DP) presented in Chapter 3 also relies on deterministic prediction information. In Chapter 4 it was assumed that this prediction is exactly valid along the entire driving cycle. Then, DP can be used as a bench-mark for other strategies.

A disadvantage of these methods is that they require a considerable amount of memory to store all information. To circumvent this problem, one can do a pattern recognition on the prediction signals using standard road classes. This leads to a road classification for each road segment. Methods that are commonly used here are clustering techniques and neural networks [3, 4, 53]. Since information is lost through this data reduction step, these techniques are not further investigated in this thesis.

5.2 Energy management with electronic horizon

The previous section discussed three alternatives to deal with road information. All these methods provide at least an indication for the vehicle propulsion power to travel a certain road segment. It will be shown that this information is sufficient to calculate an e-horizon. In the remainder of this section, it is assumed that the car navigation system provides the statistic information.

5.2.1 Statistic road information

As shown in Chapter 4, the proposed causal EM strategy with the PI-controller to estimate $\hat{\lambda}$ works fine for trips that require only small excursions of SOE around SOE_{ref} . This is true for the NEDC driving cycle, because of the frequent variations in its speed profile. However, road trips over a long distance can give rise to situations where larger deviations in

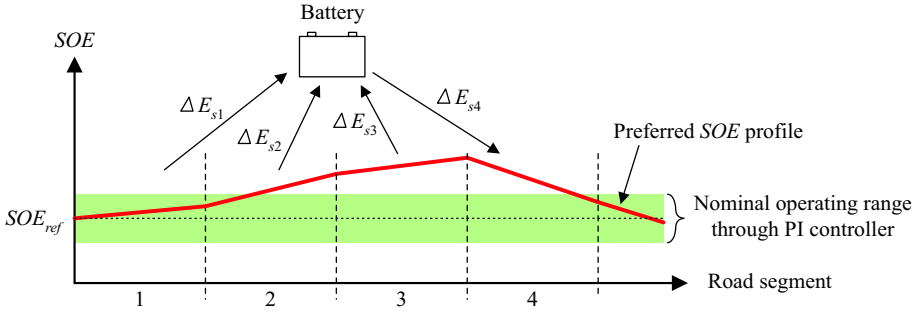


Figure 5.1: Energy exchange between road segments

SOE are desirable. This is because long road trips can have a monotonic power distribution over time, such that the EM system prefers a permanent charging or discharging from the battery over a long time interval. Furthermore, travelling over a long distance might ask from the battery to remain at a low or high SOE level, on a time scale within the bandwidth of the PI-controller.

Consider, for convenience, a driving cycle over a long distance and suppose that all the road segments are either cheap or expensive to produce electric power. This situation occurs, for example, on a trip through the mountains, where the road goes first downhill, followed by a climb uphill. Due to the order and the length of the road segments, it is profitable to charge the battery during the downhill part further from its nominal reference value (SOE_{ref}) than acceptable for the PI-controller. This way, more energy from the cheap road segments can be transferred to the expensive uphill part. This situation has been visualized in Fig. 5.1. If no modifications are done, the PI-controller forces the SOE of the battery into a small operating range around SOE_{ref} .

By using prediction information, it becomes possible to anticipate on upcoming events which are still far ahead. Moreover, with the assumption that the EM strategy from Chapter 3 works correctly for one single road segment, the statistic prediction in combination with the sequence of road segments provides sufficient information to calculate the e-horizon, and schedule the energy exchange with the battery. First, a method is given to describe the statistic road information.

Suppose that for each road segment $r \in \mathbb{N}$, a characteristic speed profile $v(k)$ has been measured with discrete sampling interval $k = 1 \dots N_r$. The

corresponding wheel torque $\tau_w(k)$ and speed $\omega_w(k)$ can be calculated with the aid of the backward vehicle model from Chapter 2. Next, the speed and torque range are divided into subintervals with size ε_ω [rad/s] and ε_τ [Nm], respectively. Each interval is denoted by a unique index number p and q :

$$\tau^p = \left\{ \tau \mid -\frac{1}{2} \varepsilon_\tau < p \varepsilon_\tau - \tau \leq \frac{1}{2} \varepsilon_\tau \right\} \quad (5.1)$$

$$\omega^q = \left\{ \omega \mid -\frac{1}{2} \varepsilon_\omega < q \varepsilon_\omega - \omega \leq \frac{1}{2} \varepsilon_\omega \right\} \quad (5.2)$$

Finally, a Probability Density Function (PDF) $\wp(\tau^p, \omega^q)$ captures the statistic properties of τ_w and speed ω_w for a single road segment r :

$$\wp^r(\tau^p, \omega^q) = \frac{1}{N_r} \sum_{k=1}^{N_r} (\tau_w(k) \in \tau^p \wedge \omega_w(k) \in \omega^q), \quad (5.3)$$

such that the following two properties hold:

$$(1) \quad \wp^r(\tau^p, \omega^q) \geq 0 \quad \forall p, \forall q, \quad (5.4)$$

$$(2) \quad \sum_{\forall p} \sum_{\forall q} \wp^r(\tau^p, \omega^q) = 1. \quad (5.5)$$

Depending on the actual vehicle configuration (*e.g.*, S-HEV, P-HEV or S/P-HEV) this PDF can be translated into a power demand for the drive train using the vehicle descriptions in Chapter 3. For convenience, this chapter only considers the S-HEV configuration for presenting simulation results.

According to the information in the PDF, it is possible to make an estimate about the fuel cost for producing additional power on each road segment. This is done in the following way. First, a random but reasonable driving cycle is constructed for each road segment with the same statistical properties as the corresponding PDF. It is clear that this driving cycle should have a feasible power demand for the vehicle under consideration. Next, the EM strategy from Section 3.1.5 is used to solve the EM problem for each road segment iteratively, using an increased value for λ^* . Each simulation starts with $SOE(0) = SOE_{ref} = 75\%$, to allow for sufficient freedom in the battery. By construction, a higher value for λ^* forces the EM system to produce more electric power and hence, the battery holds more energy at the end of the driving cycle. For similar reasons, also the fuel consumption increases when λ^* takes a higher value. An example for both functions is depicted in Fig. 5.2. For convenience, λ^* has been multiplied

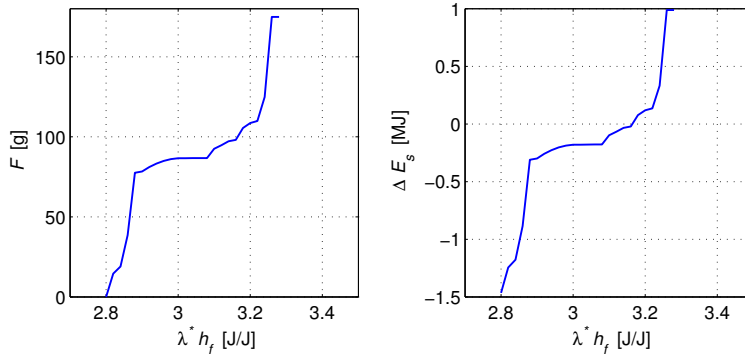


Figure 5.2: An example for function $F(\lambda^* h_f)$ and $\Delta E_s(\lambda^* h_f)$

with the lower heating value for fuel h_f [J/g], see Section 2.1. This yields a suitable scaling on the horizontal axis. In the given example, the fuel function $F(\lambda^* h_f)$ starts at zero, whereas the function $\Delta E_s(\lambda^* h_f)$ starts at $\Delta E_{s \min} = -1.5$ [MJ]. These points correspond to the situation where the EM system leaves the ICE permanently off and all energy required for vehicle propulsion is taken from the battery. For a given battery capacity $E_{s \text{ cap}} = 4.0$ [MJ], the *SOE* drops from 75% to 37.5% at the end of the road segment. On the other hand, charging is only possible from *SOE*=75% to 100%. This corresponds to $\Delta E_{s \max} = 1.0$ [MJ].

Instead of drawing two individual functions for F and ΔE_s , one can also draw the combined relation $F(\Delta E_s)$ in one graph. This is done in Fig. 5.3, and for simplicity, the dependency on λ^* has been omitted. Induced by the piece-wise linear losses in the battery model during charging and discharging, this curve shows a discontinuity at $\Delta E_s = 0$. Furthermore, slightly non-linear behavior is initiated by the extra losses in the ICE when it operates at higher power levels. Therefore it is reasonable to approximate this curve with a convex quadratic function:

$$F^r(\Delta E_s) \approx \gamma_2 (\Delta E_s)^2 + \gamma_1 \Delta E_s + \gamma_0 \quad [\text{g}] \quad \text{and} \quad \gamma_2 > 0. \quad (5.6)$$

This function $F^r(\Delta E_s)$ expresses the expected fuel use of the vehicle for road segment r and with a change ΔE_s in the battery energy. In the next section, this knowledge is used for scheduling energy among different road segments within the e-horizon.

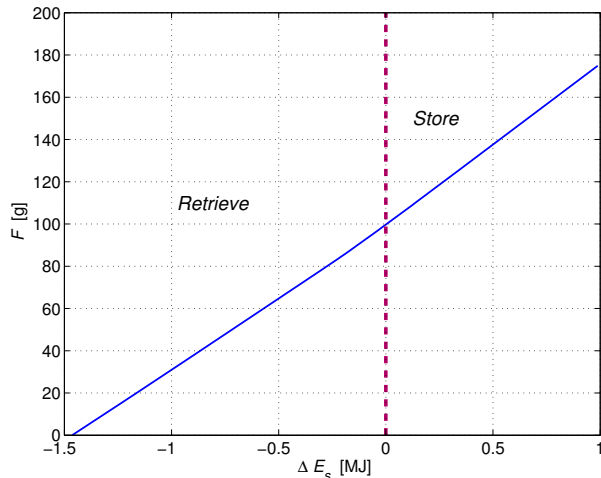


Figure 5.3: Fuel consumption F versus battery energy ΔE_s

5.2.2 Energy scheduling between road segments

The prediction information as expressed by $F^r(\Delta E_s)$ in (5.6), will assist the EM strategy to schedule energy from cheap road segments to expensive ones. To that end, an optimization problem is formulated within the Quadratic Programming (QP) framework. The objective function represents the fuel consumption over many road segments, whereas the decision variables denote the net energy exchange with the battery on each road segment. The solution of this optimization problem yields the *SOE* reference trajectory of the e-horizon.

Suppose that the driver has planned a trip with its navigation system over M road segments. This defines the length of the e-horizon. For each road segment $r = [1..M]$, the EM system receives the corresponding PDF $\wp^r(\tau^p, \omega^q)$ from the navigation system. Next, this information is translated into the fuel curves $F^r(\Delta E_{s,r})$ from (5.6). To calculate the fuel consumption over the entire e-horizon, the objective function adds the fuel use of the individual road segments:

$$J(\Delta E_s) = \sum_{r=1}^M F^r(\Delta E_{s,r}) = \sum_{r=1}^M \gamma_2^r (\Delta E_{s,r})^2 + \gamma_1^r \Delta E_{s,r} + \gamma_0^r \quad (5.7)$$

In addition to this objective function, the EM system takes into account

the following restrictions:

- At the end of the e-horizon, the energy in the battery should not be less than the initial value $E_{s,0}$.
- In each road segment, the maximum net energy change for the battery is bounded between $\Delta E_{s\min,r}$ and $\Delta E_{s\max,r}$.
- Within the e-horizon, the energy in the battery can move freely between $E_{s\min}$ and $E_{s\max}$.

Mathematically, this boils down to the following QP problem with inequality constraints:

$$\min_{\Delta E_s} J(\Delta E_s) \quad (5.8)$$

subject to:

$$\sum_{r=1}^M \Delta E_{s,r} \geq 0, \quad (5.9)$$

$$\Delta E_{s\min,r} \leq \Delta E_{s,r} \leq \Delta E_{s\max,r}, \quad 1 \leq r \leq M, \quad (5.10)$$

$$E_{s\min} \leq E_{s,0} + \sum_{j=1}^r \Delta E_{s,j} \leq E_{s\max}, \quad 1 \leq r \leq M. \quad (5.11)$$

For this convex problem, a QP-solver can be used to calculate the optimal solution $\Delta E_s^* = [\Delta E_{s,1}^* \dots \Delta E_{s,M}^*]$. It is noted that the structure of this optimization problem has a strong relation with the structure of the original EM strategy from Section 3.1.5. Consider, for convenience, the situation where the energy in the battery is equivalent at the start and end of the driving cycle. In that case, the inequality constraint (5.9) becomes an equality constraint and together with the objective function (5.8) it fits into the Lagrange formulation. Then, the solution strategy from Section 3.1.5 can be utilized.

After solving the QP-problem, the EM strategy (3.54) with the PI-controller (3.55) can benefit from this extra information in the following way. Given the initial battery energy $E_{s,0}$, the solution ΔE_s^* prescribes exactly how much energy should be charged or discharged during each road segment r . This is easily translated into a preferred SOE_{ref} level on each road transition:

$$E_{s,r} = E_{s,0} + \sum_{k=1}^r \Delta E_{s,k} \quad (5.12)$$

$$\Leftrightarrow SOE_{ref}^r = SOE(0) + \frac{1}{E_{s\ cap}} \sum_{k=1}^r \Delta E_{s,k}, \quad 1 \leq r \leq M. \quad (5.13)$$

Although information within a road segment is missing, an educated guess is to apply linear interpolation when predicting the *SOE* trajectory within a road segment. These trajectories complete the e-horizon.

The calculated *SOE_{ref}* trajectory from the e-horizon is used as an external reference signal for the PI-controller of the EM system, see Fig. 3.7. A similar observation is also made by Boucharel et al in [13]. This way, the e-horizon acts as an algorithm for path-planning, with its decisions taken on a long time scale described by the e-horizon. At a lower level, the original EM system considers a short time scale and takes care of the necessary energy in the battery. By means of the PI-controller, the EM system will smoothly follow *SOE_{ref}*, although it is still possible to deviate from the reference trajectory.

5.3 Simulation results

In Chapter 4, simulations have been done with the NEDC driving cycle. For this driving cycle, it was shown that the difference in fuel economy between the DP strategy and the causal on-line strategy is extremely small (using not only the S-HEV, but also the P-HEV and the S/P-HEV). This is mainly caused by the fact that the NEDC speed profile entails a rich variation for the mechanical power demand along the entire driving cycle.

To illustrate the added value of prediction information, this section presents the simulation results on a trip through the mountains. For convenience, an S-HEV will be used to present the simulation results. However, the P-HEV or S/P-HEV could be used just as well. This is because primarily the storage capacity of the battery determines the potential benefits from the e-horizon, and not the selected HEV configuration.

The trip through the mountains is deliberately separated into two phases. During the first phase, the vehicle travels uphill with a road slope of +3 degrees (*i.e.*, 5.2 [%]). The speed profile is during the first 585 [s] equivalent to the NEDC driving cycle, but through the road inclination, the required

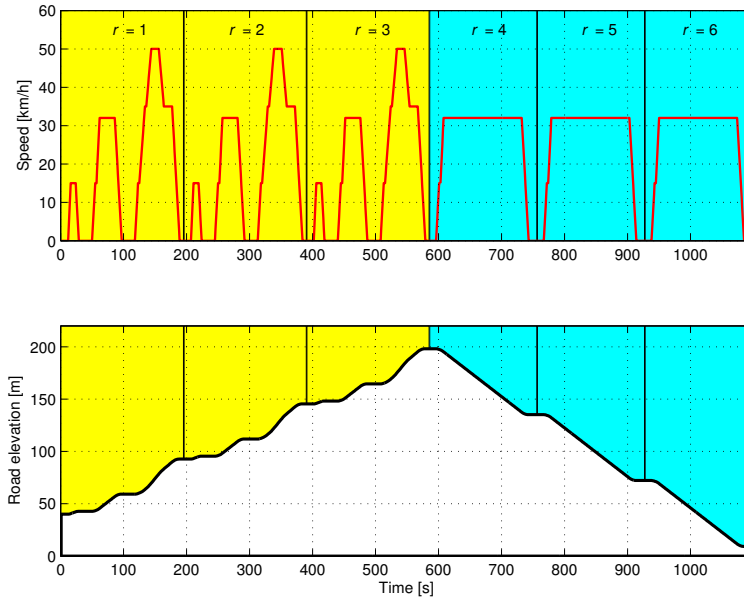


Figure 5.4: Alternative road trip up- and downhill

propulsion power is substantially higher. Next, the vehicle goes downhill with an almost constant speed of 32 [km/h] over 513 [s]. Here, the gradient of the road equals -3 degrees. The speed trajectory and the road inclination are shown in Fig. 5.4. Notice that the cycle contains three road segments uphill and three road segments downhill, so $M = 6$. The three segments uphill have an equal power distribution and also the three segments downhill have an equal distribution. Consequently, only two PDFs are required for the entire e-horizon: one for driving uphill ($r = 1..3$) and one for driving downhill ($r = 4..6$).

The driving cycle starts with the relative expensive road segments at the beginning of the trip, whereas the cheap road segments (with free energy from regenerative braking) appear only at the end of the cycle. Therefore, it is desirable to discharge the battery during the first part, whereas battery charging should be done in the second part of the trip.

<i>Simulation No.</i>	<i>Absolute fuel use [g]</i>	<i>Relative fuel use [%]</i>
<i>S1</i> (Baseline)	352	100
<i>S2</i> (Dynamic Programming)	272	77.3
<i>S3</i> (Adaptive EM, SOE_{ref} fixed)	276	78.4
<i>S4</i> (Adaptive EM, with e-horizon)	271	77.0

Table 5.1: Fuel consumption with different strategies

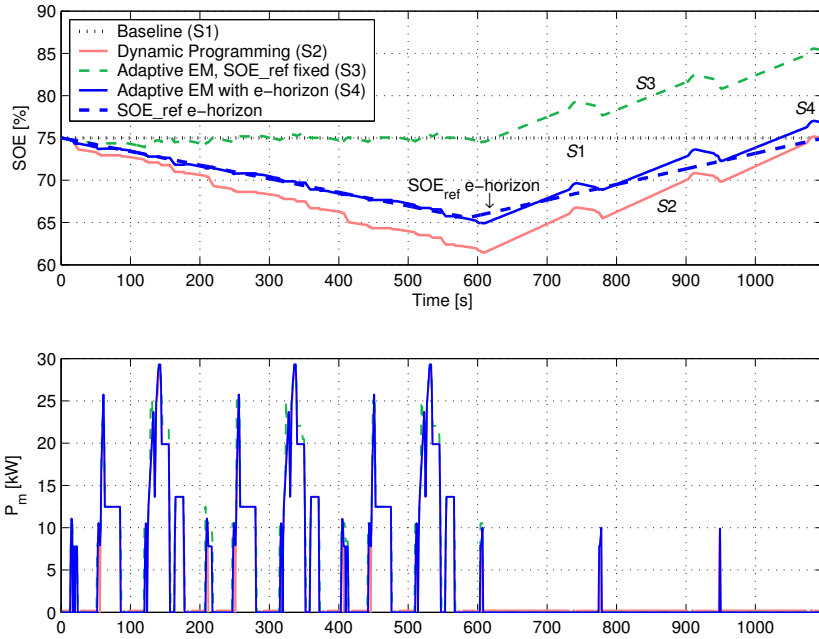
5.3.1 Strategy evaluation

Four EM strategies are evaluated for this driving cycle. The first simulation (*S1*) applies the baseline strategy, with the ICE always running and the battery power permanently zero. Dynamic Programming is used in simulation *S2* and this strategy provides an optimal control law within the accuracy of grid. Simulation *S3* uses the EM strategy from Section 3.1.5 with a PI-controller to estimate $\hat{\lambda}$, but without an e-horizon so the reference value is fixed at $SOE_{ref} = 75$ [%]. Finally, *S4* applies the same EM strategy from *S3*, but now the e-horizon has been added to update SOE_{ref} .

To gain insight into the maximum benefits from road prediction, *S4* applies an e-horizon where the content of the PDF for each road segment matches accurately with the actual driven cycle. This is achieved by using the actual speed profile of the vehicle and the slope of the road to calculate the corresponding PDF for each road segment. Furthermore, the intervals in the PDF are chosen small: $\varepsilon_\omega = 2$ [rad/s] and $\varepsilon_\tau = 4$ [Nm].

Table 5.1 summarizes the fuel consumption for all strategies. This table also indicates the relative fuel consumption with respect to the baseline strategy. Because *S3* and *S4* end the driving cycle at a different SOE level, their fuel consumption has been corrected for this. The corresponding SOE trajectories along the driving cycle are shown in Fig. 5.5a. This figure also includes the SOE_{ref} trajectory from the e-horizon. Furthermore, Fig. 5.5b visualizes the power delivered by the ICE. This plot shows that the ICE is usually switched on in the uphill phase, whereas it remains off during downhill.

Considering the results from *S3* and *S4*, there can be concluded that for this particular driving cycle, the extra fuel reduction achieved by the e-horizon is only 1.4 [%]. This result emphasizes that even for a carefully selected driving cycle, the extra fuel profits from the e-horizon are small. Moreover, *S3* still achieves a performance close to the optimal solution from

Figure 5.5: *SOE* trajectories and engine power for different strategies

S2, but without prediction information.

The difference between *S3* and *S4* originates from the fact that *S4* recovers more energy from regenerative braking than *S3*. This is explained as follows. During the uphill part, *S3* uses the ICE with the generator to provide immediately the electric power request. However, through the e-horizon *S4* knows that cheap energy from regenerative braking comes available at the end of the driving cycle. Therefore, it discharges the battery with the amount of energy that can be recharged in the downhill part. In this second part, the *SOE* for *S4* increases from 65 to 77 [%]. In Fig. 5.5a, one can see that also *S3* benefits from the free energy from regenerative braking. Through a suitable gain for the PI-controller, the *SOE* is allowed to increase significantly and store the energy from braking periods. During the downhill phase, the *SOE* for *S3* increases up to 85 [%]. This is an increase of approximately 10 [%], but *S4* recovered 2 [%] more. According to the battery capacity $E_{s\text{cap}} = 4.0$ [MJ], the additional energy stored by *S4* is:

$$\Delta E_s = \frac{0.02}{100} \times E_{s\text{cap}} = 80 \text{ [kJ]} \quad (5.14)$$

The average costs for producing electric power with $S4$ equals $\tilde{\lambda} h_f \approx 3.0$ [J/J]. Using the chemical energy content of fuel $h_f = 44.5$ [kJ], the corresponding fuel usage for ΔE_s is calculated:

$$\Delta F = \tilde{\lambda} \Delta E_s = \frac{3.0}{44.5 \cdot 10^3} \times 80 \cdot 10^3 = 5.4 \text{ [g]} \quad (5.15)$$

In Table 5.1, the absolute difference in fuel consumption between $S3$ and $S4$ is 5 [g], and this confirms the statement that the difference between $S4$ and $S5$ originates primarily from regen-braking energy.

With help of the e-horizon, the on-line EM system $S4$ achieves a slightly better fuel economy than the DP strategy in $S2$. Nevertheless, the e-horizon in this particular example includes no uncertainties about the future power demand of the vehicle. Therefore, it is not realistic to assume that this performance can be reached in a real-world driving situation. Further research should include the effects of uncertainties in the e-horizon. Theoretically it is even possible that the e-horizon leads to a performance degradation.

5.3.2 Discussion

The simulation results presented above needed a specific driving cycle with an accurate prediction for the e-horizon, to enforce a small improvement in fuel economy between $S3$ and $S4$. Nevertheless, other driving cycles are likely to exist that offer more profits for the e-horizon. The exact conditions that contribute to more profits from the e-horizon will not be given in this chapter, but will be a topic for further research. As a starting point, Appendix A examines the following properties:

1. The frequency spectrum $\Phi_d(\omega)$ from the vehicle power demand;
2. The closed-loop bandwidth ω_B [rad/s] of the EM strategy with the PI-controller.

If $\Phi_d(\omega) = 0$ for $\omega < \omega_B$, then the frequency spectrum of the vehicle power demand falls completely outside the bandwidth of the closed-loop EM strategy. This means that the PI-controller does not interfere with any frequency component from the driving cycle, so the EM system without e-horizon benefits already from all driving characteristics and adding an e-horizon offers no additional fuel profits.

In case $\Phi_d(\omega) \neq 0$ for $\omega < \omega_B$, slow varying frequency components from the driving cycle are present that cause drift in the SOE of the battery. Without the e-horizon, this drift is suppressed by the PI-controller and the

battery is forced to SOE_{ref} . This means that the EM system does not take into account the slow varying behavior of the driving cycle. By updating SOE_{ref} according to the e-horizon, the EM-strategy anticipates on these slow-varying signals with the possibility to improve its performance.

Nevertheless, also for this last situation, the profits from the e-horizon will be ultimately bounded. This is due to the storage capacity of the battery. Think for example of a similar driving cycle as used in the simulation results. If this trip is extended with a longer period uphill and a longer period downhill, the extra profits from $S4$ compared to $S3$ will further increase. However, there will be a point where the e-horizon exploits the entire storage capacity of the battery. Beyond that point, the benefits from the e-horizon can only improve marginally.

5.4 Conclusions

This chapter presents a novel approach to incorporate road information from the future driving cycle into the causal EM strategies from Chapter 3. It is shown how information from future road segments can be translated into an e-horizon. The e-horizon provides a planning for the energy exchange with the battery among future road segments. This information is used to adjust the reference value SOE_{ref} for the on-line EM strategy.

It turns out that adding the e-horizon to the EM strategy yields limited extra profits in fuel economy. The major contributions for fuel profits come from regenerative braking and engine stop/start. These situations are already utilized by the causal EM strategy from Chapter 3, without prediction information. Hence, relatively few profits from an e-horizon are to be expected.

6

Case-study: Conventional vehicles

The research presented in the previous chapters focussed on Energy Management (EM) for Hybrid Electric Vehicles (HEVs). Since these vehicles consume a significant amount of electric energy, the potential benefits from an EM strategy are high. Nevertheless, the electric power demand in traditional road vehicles increases rapidly and to supply all electric loads efficiently, an energy management (EM) is an interesting concept.

As a case-study, the EM strategies developed in this chapter focus on vehicles with a conventional drive train. By exploiting the storage capacity of the battery, the production and distribution of electric power is rescheduled to more economic operating points of the internal combustion engine (ICE). In addition, this chapter explores the advantages of electric loads with a flexible power demand. Based on optimization techniques, an optimal off-line strategy as well as a causal on-line strategy are presented. Simulations illustrate the benefits of the EM strategies in terms of fuel economy. The on-line strategy has also been implemented in a series-production vehicle. Real-world experiments on a roller dynamometer test-bench point out the correctness of the strategy but also reveal additional fuel benefits because of unexpected side-effects from the engine control unit and the driver. Profits in fuel economy are measured up to 2.6%, requesting only minimal changes to the vehicle hardware.

The content of this chapter has been accepted for publication in [43]. Earlier publications of the proposed EM strategies appeared in [42], whereas preliminary results from the vehicle experiments are presented in [44].

6.1 Introduction

Reducing fuel consumption has always been a major challenge to the automotive industry. Whereas first marketing aspects gave rise to innovative research, nowadays also environmental regulations force the industry to look for alternative solutions. Historically, the research concentrated on improvements for the mechanical side of the vehicle. However, due to the growing electric power demand, the electric power supply cannot be neglected anymore [62, 27]. Moreover, the introduction of Hybrid Electric Vehicles (HEV), where the propulsion power can also be delivered by an electric machine, contributes to even higher electric power demands. As indicated in [76], Energy Management (EM) becomes more and more important for the electric power net, such that the fuel request and the corresponding emissions remain limited.

In general, it is expected that EM should be applied only in combination with an HEV. However, a traditional vehicle with a conventional drivetrain and a belt-driven alternator also offers freedom for EM. Conceptually, the topology of a parallel HEV looks similar to a traditional vehicle, although the power through the alternator is limited to one direction. Moreover, the size of the electric machine in an HEV is much larger as it provides tractive force to the wheels.

In combination with a suitable battery pack, the additional investments for an HEV are currently rated between \$3,000 and \$7,000, see [68]. This initiated the question what EM can offer in a traditional vehicle, without the need for additional investments in vehicle hardware. With primarily changes in vehicle software, the return on investment is really high. Nevertheless, the absolute fuel profits will be limited, because the mechanical power demand is far more dominant than the electric power request in a traditional vehicle.

An EM strategy uses the storage capacity of the battery when the power from the alternator does not match with the power request of the electric loads. This concept has two disadvantages: first, temporarily storing energy always brings additional losses and second, the storage device wears out faster. To overcome both problems, this chapter also considers electric loads with a flexible power demand. This way, the power request from the loads can be adapted to the generated power. Loads with a flexible power demand are characterized by the fact that they accept, up to a certain level, more or less power, without serious performance degradation for the driver. Especially heating and cooling functions are suited for this purpose,

as shown in [5].

With only minor changes to the vehicle, it is possible to implement an EM strategy that takes into account two degrees of freedom: the power from the alternator and the power to the electric loads. The power to the battery is controlled indirectly. For convenience, the alternator power control problem will be called Power Supply Management (PSM), whereas PSM extended with additional freedom for the electric loads is captured by Power Distribution Management (PDM). Earlier publications on PSM and PDM appeared in [51] and [42], respectively.

Over the years, much research is carried out in the field of EM. Especially the EM strategies for an HEV (see, *e.g.*, [86] for an extended overview) address similar concepts that are also used in this work. A technique that has been applied by many researchers is Dynamic programming (DP) [11]. This optimization technique provides an optimal control law for EM within the accuracy of the discretized state-space. However, the future driving cycle must be exactly known. Due to the computational demand, an on-line strategy is generally not implementable, but the results are used as a benchmark for other strategies, see [55]. Moreover, PDM uses a two-dimensional state-space and due to the preferred accuracy, also the required memory resources are readily to explode.

One can also obtain an optimal control law using alternative optimization techniques such as Linear Programming (LP) and Quadratic Programming (QP). Here the work of Tate and Boyd [78] is an excellent starting point and provides a well defined LP-problem. Compared to DP, the LP and QP method avoid excessive memory usage or extreme calculation times while handling a multi-dimension state-space. Furthermore, these methods are easily incorporated into a Model Predictive Control framework [17]. This way, the added value of additional prediction information can be analyzed using a prediction horizon with variable length. For the research presented here, there has been decided to apply the QP-method as a benchmark for other strategies.

It turns out that an EM strategy becomes very conservative if only limited prediction information is available and the strategy has to guarantee a preferred energy level in the battery at the end of the prediction horizon. To overcome this problem, EM strategies are developed that introduce an equivalent fuel cost for the energy exchange with the battery, see *e.g.* [65, 73]. The EM strategy developed in this chapter follows a similar reasoning, but differs from existing strategies through the equivalent fuel cost parameter that incorporates both a mathematical and a physical

explanation. A practical solution is presented to determine this parameter on-line in the vehicle. Furthermore, the EM strategy can handle loads with a flexible power demand and it includes a tuning mechanism to prevent battery wear. The strategy has been analyzed in a simulation environment and validation is done with vehicle experiments on a roller-dynamometer.

This chapter is organized as follows. Section 6.2 presents the vehicle model that is used for strategy development. A formal control problem is given in Section 6.3. By means of Quadratic Programming, Section 6.4 presents an optimal off-line control law and Section 6.5 derives an on-line strategy. The simulation environment and the vehicle implementation is explained in Section 6.6. An overview of the results is presented in Section 6.7. Finally, the strategies are evaluated in Section 6.8 and the conclusions are given in Section 6.9.

6.2 Vehicle control model

The PSM and PDM strategy make use of a power-based vehicle model, see Fig. 6.1. In this model, the internal combustion engine (ICE) and the alternator rely on quasi-static maps. Because the EM system does not interfere with the vehicle dynamics, these models are sufficiently accurate.

The drivetrain model calculates the mechanical power request P_d [W] as well as the engine speed ω [rad/s] from the speed profile of the driving cycle. The ICE converts fuel into mechanical power P_m . This power goes to the drivetrain for vehicle propulsion (P_d) and a small portion goes to the alternator (P_g). The alternator is connected to the powernet, so electric power P_e can go directly to the electric loads (P_L) or it can be stored in the battery (P_b). The battery model consists of an efficiency map followed by an integrator to keep track of the energy level E_s in the battery. The PSM strategy allows freedom in P_e whereas the PDM strategy allows freedom in both P_e and P_L .

The engine model is described by a non-linear static map which specifies the relation between the fuel massflow \dot{m} , engine power P_m , and engine speed ω :

$$\dot{m} = f(P_m | \omega) \text{ [g/s]}, \quad \text{where} \quad P_m = P_d + P_g. \quad (6.1)$$

The notation with the conditional-operator $|$ is introduced to emphasize the difference between the design variable P_m and the time-varying parameter ω . In literature, fuel maps are often presented as a function of engine torque and engine speed. However, the engine torque can be derived from

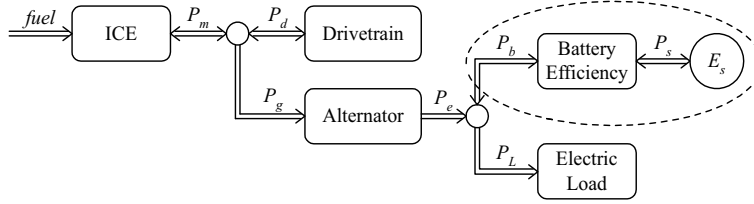


Figure 6.1: Overview of powerflow signals in the vehicle

the engine power if the engine speed is known, so these maps represent identical information.

Using a similar approach, the alternator model is captured by a non-linear static map, expressing the mechanical power P_g as a function of the electric power P_e :

$$P_g = g(P_e | \omega) \text{ [W]}, \quad \text{where} \quad P_e = P_L + P_b. \quad (6.2)$$

Obtaining an accurate model of the battery is part of ongoing research. In this chapter, the battery model consists of two blocks. The first block introduces the energy losses between the power P_b at the battery terminals and the net stored/retrieved power P_s :

$$P_b = \eta(P_s) \text{ [W]}. \quad (6.3)$$

For simplicity, the losses in the battery depend only on the actual battery power, but it is very well possible to extend this model with additional parameters such as the actual energy level in the battery or its temperature. More details about the function $\eta(P_s)$ will be given in Section 6.4. The second block in the battery model keeps track of the energy level E_s by means of a simple integrator:

$$E_s(t) = E_s(0) + \int_0^t P_s(\tau) d\tau \text{ [J]}. \quad (6.4)$$

Furthermore, it is assumed that the energy capacity E_{cap} of the battery is fixed. Consequently, the relative energy level in the battery can be denoted by the quantity State of Energy (SOE):

$$SOE(t) = \frac{E_s(t)}{E_{cap}} \cdot 100\%. \quad (6.5)$$

6.3 Problem definition

The control objective of the EM system is to improve the vehicle's fuel economy, although the reduction of particular tail-pipe emissions is done in a similar way. The primary energy source in the vehicle is the ICE whereas the storage capacity of the battery offers freedom to schedule the driver's power request over time. Furthermore, the flexible electric loads offer additional freedom to maximize the fuel economy. For developing an EM strategy with optimal performance, the control problem is formulated as an optimization problem:

$$\min_x J(x) \quad \text{subject to} \quad G(x) \leq 0. \quad (6.6)$$

The cost function J is selected such that it represents the vehicle's fuel use over an arbitrary driving cycle with time length t_e :

$$J(P_s, P_L) = \int_0^{t_e} F(P_s, P_L | P_d, \omega) dt, \quad (6.7)$$

where

$$F(P_s, P_L | P_d, \omega) = f(P_d + g(P_e | \omega) | \omega), \quad (6.8)$$

and P_e defined in (6.2). Note that the decision variable x covers two variables: the internal battery power P_s and the power to the electric loads P_L . The corresponding control variable P_e is calculated afterwards using (6.2) and (6.3).

Constraints on the decision variables are due to physical limitations of components as well as the requirement to have a charge sustaining vehicle. The operating range of the engine, the alternator, and the battery is limited in power, so inequality constraints are introduced on the minimum and maximum powerflow of these components:

$$P_{m \min}(t) \leq P_m(t) \leq P_{m \max}(t) \quad (6.9)$$

$$P_{e \min}(t) \leq P_e(t) \leq P_{e \max}(t) \quad (6.10)$$

$$P_{b \min}(t) \leq P_b(t) \leq P_{b \max}(t) \quad (6.11)$$

$$\forall t \in [0, t_e]$$

A charge sustaining strategy claims that the battery satisfies a minimum SOE level at the end of the driving cycle. This can be achieved by including an end-point constraint on the energy level of the battery:

$$E_s(t_e) = E_s(0) + \int_0^{t_e} P_s(t) dt \geq E_{s \text{ref}}, \quad (6.12)$$

where E_{sref} is an arbitrarily selected reference value that should be satisfied at $t = t_e$ e.g., $E_{sref} = E_s(0)$.

Finally, constraints on P_L are used to characterize the energy and power demand of the electric loads. It is assumed that all individual loads can be aggregated and this results in a separate power and energy constraint:

$$P_{Lmin}(t) \leq P_L(t) \leq P_{Lmax}(t) \quad \forall t \in [0, t_e] \quad (6.13)$$

$$\int_0^t P_L(\tau) d\tau \geq E_{Lmin}(t) \quad \forall t \in [0, t_e] \quad (6.14)$$

6.4 Quadratic programming

Finding the optimal solution for the problem defined in the previous section will be computationally demanding. To come to a solution close to the global optimal solution, the original problem is approximated with a Quadratic Programming (QP) problem. Such a QP-structure is characterized by a quadratic cost function, subject to linear constraints:

$$\min_x \frac{1}{2} x^\top H x + h^\top x \quad \text{subject to} \quad A x \leq b. \quad (6.15)$$

6.4.1 Model reduction

To derive a quadratic description for the cost function (6.7), the models of the individual components need to be reduced. For the engine map, a (piece-wise) linear approximation will be used:

$$\dot{m} = f(P_m | \omega) \approx \alpha_1 P_m + \alpha_0. \quad (6.16)$$

The parameters α_1 and α_0 are state dependent (P_d , ω) and are selected such that they represent a local fit of the fuel map in the area $P_m = [P_d, P_d + P_{gmax}]$. In practical situations, the fuel map of an engine is obtained by measuring its fuel consumption at a finite number of grid points. These grid points cover the entire operating area of the engine. Compared to the power range of the alternator, this is a relative coarse grid and therefore it is acceptable to approximate the fuel consumption by a local linear fit.

The efficiency of a conventional alternator varies according to its operating point between 40% and 80%. Similar to the ICE, these large variations are due to friction losses and they have a dominant effect when the alternator generates no electric power. Nevertheless, measurement data shows that the mechanical input power increases almost proportional with the

output power. Only at higher power levels these losses increase more than proportional. For that reason, the alternator map is approximated by a quadratic fit:

$$P_g(P_e | \omega) \approx \gamma_2 P_e^2 + \gamma_1 P_e + \gamma_0. \quad (6.17)$$

The parameters γ_2 , γ_1 and γ_0 are speed dependent. They approximate the alternator map over its entire power range $P_e = [P_{e \min}, P_{e \max}]$ at a certain engine speed ω .

According to impedance spectra measurements of a lead-acid battery [16], it is known that the losses in the battery increase for higher power flows. Moreover, the impedance changes when charging or discharging the battery. Consequently, there has been decided to use a battery model incorporating linear and quadratic losses:

$$P_b(P_s) \approx \beta P_s^2 + \max(\eta^- P_s, P_s/\eta^+). \quad (6.18)$$

In Fig. 6.2 the contribution of each individual term is shown. The parameter $\beta > 0$ represents the quadratic losses whereas $0 < \eta^+ < 1$ and $0 < \eta^- < 1$ indicate the piece-wise linear losses for charging and discharging, respectively. In this work, these parameters are estimated from experimental data. However, they can also serve as a tuning parameter to limit the actual battery usage of the EM strategy. That is, incorporating more losses in the battery model than actually present in reality, will discourage the EM strategy to use the battery as an energy storage buffer. Because battery usage is strongly related to battery wear, the parameters β , η^+ and η^- turn out to be a trade-off between battery wear versus performance from EM.

6.4.2 QP formulation

The battery model described in (6.18) cannot be directly included in the QP-framework of (6.15). Fortunately, the restrictions on β , η^+ and η^- guarantee that (6.18) is always a convex function. As shown in [22], it is possible to reformulate the expression $\max(\eta^- P_s, P_s/\eta^+)$ with an auxiliary variable P_a :

$$\min_{P_a} P_a \quad \text{subject to} \quad \begin{cases} P_a \geq P_s \eta^- \\ P_a \geq P_s / \eta^+ \end{cases} \quad (6.19)$$

Now the substitution of (6.17)-(6.19) into (6.16) results in a 4th-order expression between fuel use and battery power P_s . Because a quadratic relation is needed for a QP-structure, a second order Taylor approximation

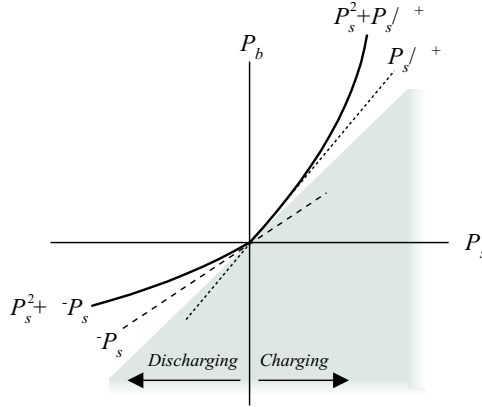


Figure 6.2: Parameters in battery efficiency model

has been applied, leaving out the higher order terms. To that end, the decision variable P_L has been changed into the zero-mean variable ΔP_L , representing the deviation from the average load power \bar{P}_L :

$$P_L := \bar{P}_L + \Delta P_L. \quad (6.20)$$

The cost criterion in (6.7) is rewritten in discrete time with sampling interval ΔT over N_p periods:

$$J = \sum_{k=1}^{N_p} F(P_s(k), \Delta P_L(k), P_a(k)) \Delta T. \quad (6.21)$$

The decision variable $x = [P_s \ \Delta P_L \ P_a]^\top \in \mathbb{R}^{3N_p}$ covers all periods $k = 1, \dots, N_p$ and yields the following description for H and h in (6.15):

$$H = \text{diag}[H(1), \dots, H(N_p)], \quad (6.22)$$

$$h = [h(1), \dots, h(N_p)]^\top, \quad (6.23)$$

with

$$H(k) = \begin{bmatrix} 2\alpha_1\gamma_1\beta + 4\alpha_1\gamma_2\beta\bar{P}_L & 0 & 0 \\ 0 & 2\alpha_1\gamma_2 & 2\alpha_1\gamma_2 \\ 0 & 2\alpha_1\gamma_2 & 2\alpha_1\gamma_2 \end{bmatrix} \quad (6.24)$$

and

$$h(k) = \begin{bmatrix} 0 \\ \alpha_1\gamma_1 + 2\alpha_1\gamma_2\bar{P}_L \\ \alpha_1\gamma_1 + 2\alpha_1\gamma_2\bar{P}_L \end{bmatrix} \quad (6.25)$$

All constraints given in (6.9)-(6.14) have to be written as linear constraints on the decision variables. Due to the losses in the battery model, the relation between P_b and P_s is non-linear, see (6.18). Therefore, one cannot use a linear combination of P_s and ΔP_L to replace the constraint on P_e . To circumvent this problem, the energy losses in the battery model are neglected during constraint handling, so P_b is assumed to be equal to P_s at this point. Now it is possible to write (6.9) as a linear constraint on P_s and ΔP_L by using the inverse of (6.17) and selecting the correct solution. Also (6.10) appears as a linear constraint whereas the implementation of (6.11) is trivial. Note that these new constraints allow slightly more freedom than the original problem, but differences are very limited. Finally, the three constraints are aggregated into one constraint for each period $k = 1, \dots, N_p$:

$$P_{e\ min}^* \leq P_s + \bar{P}_L + \Delta P_L \leq P_{e\ max}^*. \quad (6.26)$$

The end-point constraint in (6.12) on the energy level in the battery becomes in discrete time:

$$E_s(0) + \sum_{k=1}^{N_p} P_s(k) \Delta T \geq E_{s\ ref}. \quad (6.27)$$

The requirements on the power and energy to the loads are written in terms of $\bar{P}_L + \Delta P_L$. For the constraint in (6.13) this is rather straight forward and for each period $k = 1, \dots, N_p$ there holds:

$$P_{L\ min} \leq \bar{P}_L + \Delta P_L \leq P_{L\ max}. \quad (6.28)$$

The energy constraint from (6.14) needs to be evaluated in all periods $k = 1, \dots, N_p$, resulting in N_p constraints:

$$\sum_{i=1}^k (\bar{P}_L + \Delta P_L) \Delta T \geq E_{L\ min}(k), \quad k = 1, \dots, N_p. \quad (6.29)$$

Altogether, a driving cycle with N_p periods leads to $3N_p$ decision variables and $6N_p + 1$ constraints in the QP-structure from (6.15).

6.4.3 Model predictive control

The optimization problem formulated above requires that the entire driving cycle is known in advance. In real-world driving situations, this will be practically impossible. However, the idea that the vehicle speed can be

predicted in the near future is certainly realistic. With only minor changes, it is possible to put the QP-problem into a Model Predictive Control (MPC) framework, see [7] and [83]. Instead of performing the optimization in (6.15) over the entire driving cycle, it will be limited to a prediction horizon of N_p periods. Only the first value of the resulting control sequence is implemented, whereas the calculations are repeated each time instant with updated state and prediction information.

The implementation of this MPC strategy in a simulation environment learns that a reduced prediction horizon for (6.21) and (6.27) puts a serious limitation on its performance, see Section 6.7. Especially the end-point constraint (6.27) forces the strategy to keep the battery close to E_{sref} , such that it resembles the baseline (BL) situation, *i.e.*, $P_s = 0$. This end-point constraint is only a method to guarantee a charge sustaining solution. The next section presents an alternative solution by reformulating this constraint.

6.5 On-line strategy

This section presents a causal EM strategy, which is again derived from the original problem definition. It does not rely on prediction information through a relaxation of the end-point constraint from (6.27).

6.5.1 Strategy analysis

First consider the problem definition from (6.6) without the inequality constraints $G(x) \leq 0$. In the situation of PSM, the electric load cycle is predefined and the optimization problem reduces to one decision variable P_s :

$$\min_{P_s} \int_0^{t_e} F(P_s | P_d, P_L, \omega) dt. \quad (6.30)$$

Now assume that at the end of the trip the energy in the battery matches its initial starting value. This way, the end-point constraint changes into an equality constraint:

$$E_s(0) + \int_0^{t_e} P_s(t) dt = E_s(0) \Rightarrow \int_0^{t_e} P_s(t) dt = 0. \quad (6.31)$$

A new problem definition is formulated for the minimization of (6.30) in combination with the equality constraint (6.31). For convenience, it is

written in discrete time but the sampling interval ΔT has been omitted:

$$\begin{aligned} \min_{P_s} \sum_{k=1}^{N_p} F(P_s(k) | P_d(k), P_L(k), \omega(k)), \\ \text{subject to } \sum_{k=1}^{N_p} P_s(k) = 0. \end{aligned} \quad (6.32)$$

Finding a solution for this optimization problem can be done by incorporating the equality constraint into the Lagrangian function, using a Lagrange multiplier λ . A similar approach has also been followed by Guzzella in [34], but can be found already in [81]. The following Lagrangian L is defined:

$$\begin{aligned} L(P_s(1), \dots, P_s(N_p), \lambda) = \\ \sum_{k=1}^{N_p} F(P_s(k) | P_d(k), P_L(k), \omega(k)) - \lambda \sum_{k=1}^{N_p} P_s(k). \end{aligned} \quad (6.33)$$

Physically, this new objective function makes sense because it weighs the energy change of the battery with the actual fuel consumption of the engine. The quantity λ [g/J] represents the incremental fuel cost when energy is stored or taken from the battery. The minimum value for $L(P_s(1), \dots, P_s(N_p), \lambda)$ is found by putting the derivatives equal to zero:

$$\frac{\partial L(P_s(1), \dots, P_s(N_p), \lambda)}{\partial P_s(k)} = 0, \quad 1 \leq k \leq N_p, \quad (6.34)$$

$$\frac{\partial L(P_s(1), \dots, P_s(N_p), \lambda)}{\partial \lambda} = 0. \quad (6.35)$$

In case $F(P_s | P_d, P_L, \omega)$ is a strictly convex function, there exists a unique solution $(P_s^*(1), \dots, P_s^*(N_p), \lambda^*)$ for this set of $N_p + 1$ equations. Typically, the solution of λ^* is calculated with information about the entire driving cycle. However, if λ^* is known, the sequence $P_s^*(k)$, $k = 1, \dots, N_p$, can also be calculated by an optimization at the present moment k :

$$P_s^*(k) = \arg \min_{P_s} \{F(P_s | P_d, P_L, \omega) - \lambda^* P_s\}. \quad (6.36)$$

So far, all calculations are done with decision variable P_s , but the control variable is the alternator power P_e . Therefore, a description for the battery losses in (6.3) is required. For convenience, the description from (6.18) is taken with only linear losses present, so $\beta = 0$ and the overall battery

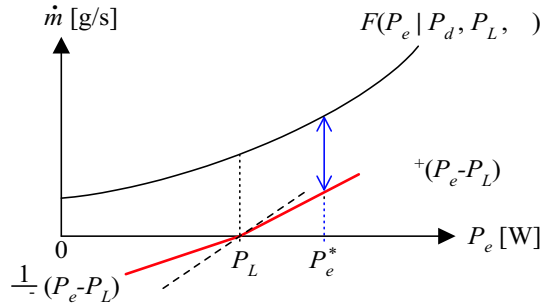


Figure 6.3: Objective function with minimum distance at P_e^*

efficiency equals $\eta_{bat} = \eta^- \eta^+ \leq 1$. The inverse battery model satisfies the following description:

$$P_s = \eta^{-1}(P_b) = \min\left(\frac{1}{\eta^-} P_b, \eta^+ P_b\right). \quad (6.37)$$

Using (6.37), the minimization from (6.36) is rewritten with P_e as optimization variable:

$$P_e^*(k) = \arg \min_{P_e} \{F(P_e | P_d, P_L, \omega) - \lambda^* \eta^{-1}(P_e - P_L)\}. \quad (6.38)$$

This last minimization procedure is illustrated in Fig. 6.3. The optimal value for P_e^* follows from the point where the distance between the curves $F(P_e | P_d, P_L, \omega)$ and $\lambda^* \eta^{-1}(P_e - P_L)$ is minimal. There are three locations where the minimum can appear: $P_e < P_L$, $P_e = P_L$ or $P_e > P_L$. The situation with $P_e = P_L$ becomes more favorable if the battery losses increase. In case $P_e < P_L$ or $P_e > P_L$, the exact setpoint for the alternator power is described by P_e^- and P_e^+ , respectively:

$$P_e^- = \arg \min_{P_e} \{F(P_e | P_d, P_L, \omega) - \lambda^* \frac{1}{\eta^-} (P_e - P_L)\} \quad (6.39)$$

$$P_e^+ = \arg \min_{P_e} \{F(P_e | P_d, P_L, \omega) - \lambda^* \eta^+ (P_e - P_L)\} \quad (6.40)$$

Altogether, the corresponding battery power is described by the following control law:

$$P_b = \max[P_e^+ - P_L, 0] - \max[P_L - P_e^-, 0]. \quad (6.41)$$

In this framework it is easy to include the power limitations of the alternator. Given the maximum alternator power $P_{e\max}$, the battery power is restricted to $P_{e\max} - P_L$, so (6.41) is extended to:

$$P_b = \max[\min[P_e^+ - P_L, P_{e\max} - P_L], 0] - \max[P_L - P_e^-, P_L - P_{e\max}, 0]. \quad (6.42)$$

Finally, the situation with PDM is considered, where the power to the electric load offers additional freedom. Similar to the required energy in the battery at the end of the driving cycle, also the loads require a certain amount of energy at the end of the trip. Taking a similar reasoning as shown previously, the load power is calculated as:

$$P_L^* = \arg \min_{P_L} \{F(P_e^* | P_d, P_L, \omega) - \lambda^* \eta^{-1}(P_e^* - P_L)\}. \quad (6.43)$$

The minimum and maximum power to the loads is restricted by (6.13). Incorporating these constraints leads to the following setpoint for P_L :

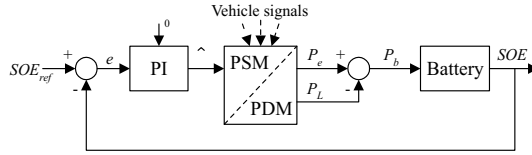
$$P_L = \max[P_{L\min}, \min[P_L^*, P_{L\max}]]. \quad (6.44)$$

6.5.2 Optimal performance

This on-line control strategy achieves the highest fuel benefits if λ^* is calculated correctly. Moreover, each driving cycle requires a different λ^* to obtain a preferred energy level E_{sref} at the end of the driving cycle. Notice that charging is done more frequently for higher values of λ^* . On the other hand, discharging the battery is less preferred when λ^* increases. As a result, there exists a unique solution for λ^* where the energy exchange with the battery is balanced and the SOE at the beginning and end of the driving cycle are equivalent.

6.5.3 Adaptive strategy

Instead of focussing on how to calculate λ^* off-line, one could also make an on-line estimation $\hat{\lambda}$. The method that has been selected here, results in an adaptive strategy as presented in [51]. Although different approaches are known from literature (*e.g.*, zone control, see [83]), this method enables the on-line EM strategy to achieve a performance close to the optimal MPC strategy from Section 6.4. The basic idea is that the SOE of the battery indicates whether $\hat{\lambda}$ is estimated correctly or not. In case $\hat{\lambda}$ has been selected too small, the battery becomes depleted in the end. Conversely, when $\hat{\lambda}$

Figure 6.4: Feedback diagram for estimating $\hat{\lambda}$

is selected too high, the battery becomes fully charged. From a control point of view, this corresponds to a levelling control problem where the SOE should be kept near a nominal value SOE_{ref} . A Proportional Integral (PI) controller with a rather small bandwidth fulfills this requirement. The block diagram is shown in Fig. 6.4, with $\hat{\lambda}$ equal to:

$$\hat{\lambda}(t) = \lambda_0 + K_P e(t) + K_I \int_0^t e(\tau) d\tau, \quad (6.45)$$

with λ_0 an initial guess.

6.6 Experimental validation

6.6.1 Simulation environment

For analyzing the EM-strategies, a simulation environment has been developed that describes the Ford Mondeo vehicle. This is a midsize series-production vehicle with a 2.0l gasoline engine and a 5-speed manual transmission. The simulation model is built around a dynamic forward-facing drivetrain model, including a dynamic model for the driver. A detailed description of this simulation model is given in Section 2.2.

6.6.2 Vehicle implementation

The strategy has been implemented in the Mondeo vehicle using a MicroAutoBox from dSPACE. The alternator has been modified such that its output voltage is not fixed but follows a voltage setpoint. A VRLA battery with a capacity of 60Ah replaces the original 12V battery.

During the vehicle tests, special attention is given to the interaction between the Engine Control Unit (ECU) and the alternator. In the original vehicle configuration, the alternator sends a status-signal to the ECU about its present electric load. Given this information, the ECU adds a

feedforward signal to the engine fuelling system, such that it anticipates on quick changes in the alternator power. However, this feedforward compensation leads to extra fuel injection during regenerative braking. Therefore, a by-pass of the alternator signal is done when the EM-strategy is implemented in the vehicle. Unfortunately, the original baseline configuration still applies the feedforward signal during the vehicle tests.

It turns out that also the original configuration benefits from this alternator by-pass in terms of fuel economy. To make a fair comparison in the simulation environment, the feedforward signal is never implemented here.

6.6.3 Evaluated strategies

The standard driving cycle for vehicle homologation in Europe is the New European Driving Cycle (NEDC). This cycle exactly prescribes the vehicle speed and the gearshifts for a trip over 1180 seconds. Based on this driving cycle, four different EM strategies are evaluated: BL (baseline), BL+250W, PSM and PDM. The BL configuration refers to the original vehicle configuration with a fixed alternator voltage at 13.7V, but with a different electric load. In line with the official NEDC regulations, configuration BL corresponds to the native engine load, which is approximately 220W. Unfortunately, this load is always present, and to validate the concept of PDM, more flexibility in the power demand is desired. This is achieved with an external electric load connected to the powernet. For the configuration BL+250W, this extra load adds 250W to the native engine load along the entire driving cycle. With PDM, this load follows the setpoints from the EM strategy, whereas the average load remains 250W through adapting the restrictions on P_L in (6.13):

$$P_{Lmin}(t) = \begin{cases} 0 & \text{if } E_L(t) \geq 250t \\ 250 & \text{if } E_L(t) < 250t \end{cases} \quad (6.46)$$

$$\begin{aligned} & \text{with } E_L(t) = \int_0^t P_L(\tau)d\tau, \\ P_{Lmax}(t) & = 500. \end{aligned} \quad (6.47)$$

In the simulation environment, both the off-line and the on-line strategies are evaluated for PSM and PDM. The simulation with the off-line MPC strategy is done in two steps. First, the signals P_d and ω are recorded during a pilot simulation with configuration BL. Next, these signals are used as prediction information in a second simulation with the MPC strategy. Afterwards, there has been verified that differences between the first and

<i>Simulation environment (hot engine)</i>	
BL	$\Leftrightarrow \left\{ \begin{array}{l} \text{PSM MPC} \\ \text{PSM On-line} \end{array} \right.$
BL + 250W	$\Leftrightarrow \left\{ \begin{array}{l} \text{PDM MPC} \\ \text{PDM On-line} \end{array} \right.$
<i>Roller-dynamometer experiments</i>	
BL (cold)	\Leftrightarrow PSM On-line (cold)
BL (hot)	\Leftrightarrow PSM On-line (hot)
BL + 250W (hot)	\Leftrightarrow PDM On-line (hot)

Table 6.1: Overview of evaluated strategies

second simulation for P_d and ω are sufficiently small. Otherwise, a further iteration would be required. The real-world experiments are only executed with the on-line strategy from section 6.5 and these experiments are done with a cold and hot engine start. In the simulation environment this is not possible because the engine model is only valid for a hot engine.

Table 6.1 provides a brief overview of all strategies that are considered in the next section. The MPC strategy calculates its control law by solving (6.15) with the cost criterion (6.21) and constraints (6.26)-(6.29). The control law for the on-line PSM strategy is given in (6.42), using (6.39)-(6.40), and the on-line PDM strategy applies (6.42)-(6.44). Note that by construction, PDM always incorporates the PSM strategy, so the results from PDM already include the fuel benefits from PSM. On the other hand, the PSM strategy is evaluated without PDM and the value of P_L is predefined by the driving cycle.

6.7 Strategy results

6.7.1 Influence of prediction horizon

The influence of the prediction horizon is evaluated with the QP method from Section 6.4 in an MPC-framework. Fig. 6.5a shows the reduction in fuel consumption whereas Fig. 6.5b visualizes the total amount of energy stored in the battery. Both the PSM and PDM strategy are simulated for receding horizons of increasing lengths, $N_p = 1 \dots 1181$ and $\Delta T = 1$ [s]. When the prediction horizon reaches the end of the driving cycle, the control

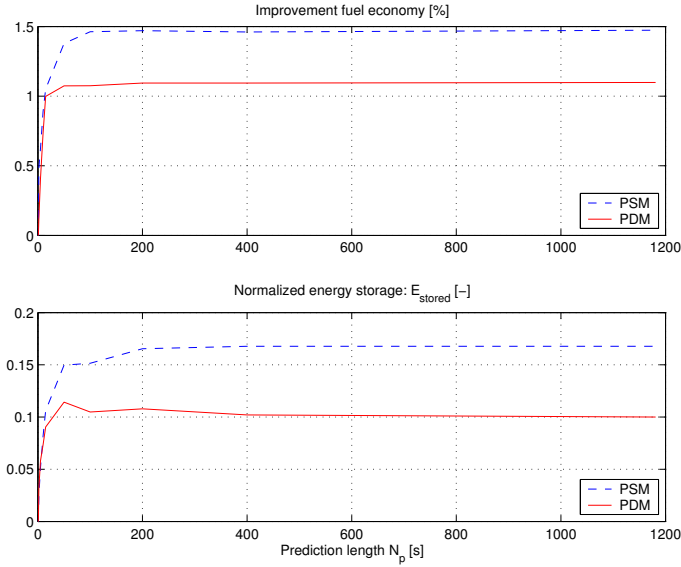


Figure 6.5: Influence of prediction horizon: (a) fuel use and (b) battery use

law is not updated anymore and all remaining control actions are directly taken from that time instant. The results for battery wear in Fig. 6.5b are normalized with respect to E_{cap} :

$$E_{stored} = \frac{\int_0^{t_e} \max(P_b(t), 0) dt}{E_{cap}} \quad [-]. \quad (6.48)$$

The first observation from Fig. 6.5a is that the achieved fuel reduction with PSM and PDM is ultimately bounded. Moreover, the fuel benefits increase rapidly until $N_p = 100$ and remain almost constant for a higher prediction length. This behavior can be explained as follows. The end-point constraint in (6.27) becomes very dominant for short predictions. That is, the EM strategy acts conservatively when N_p is small, because it has to guarantee the preferred energy level E_{sref} in the battery at the end of the prediction horizon. Moreover, the vehicle speed determines the operating point of the ICE and consequently also the incremental fuel cost λ . As shown in [23], the frequency spectrum of λ gives insight into the minimum length of the prediction horizon, so the speed profile of the NEDC is closely related to the required prediction length.

Strategy	SOE_0 [%]	P_L [W]	Fuel mass [g/km]	SOE^* [%]	Fuel eco [%]
BL	100	245	59.61	100.0	-
PSM MPC	75	195	58.70	74.6	1.5
PSM On-line	75	195	58.73	75.1	1.5
BL + 250W	100	475	61.09	100.0	-
PDM MPC	75	465	60.42	75.0	1.1
PDM On-line	75	465	60.42	75.1	1.1

Table 6.2: Overview of simulation results (hot-engine start)

To obtain a performance close to the optimal situation, an accurate speed prediction of at least $N_p \Delta T = 100$ [s] is required, but due to uncertainties these predictions are not readily available. As a result, a different EM concept is preferred that does not rely on lengthy predictions, but still achieves a similar performance. This is achieved with the on-line strategy, by relaxing the end-point constraint.

Finally, one can extend the information in Fig. 6.5 with an extra parameter for the efficiency of the battery model (6.3). By including extra losses in the battery model, the EM strategy tends to follow the baseline strategy and hence, E_{stored} decreases. Given the cycle life of the battery, it is up to the designer to optimize the trade-off between fuel benefits and battery wear.

6.7.2 Results from experimental validation

An overview of the simulation results and the results from the roller-dynamometer experiments is given in Tables 6.2 and 6.3, respectively. Each strategy has been tested at least two times on the roller-dynamometer, and Table 6.3 presents average results. The columns in these tables cover the following information:

- **SOE₀**: Initial SOE of the battery. Each baseline strategy starts with a completely charged battery, so $SOE_0=100\%$. The PSM and PDM strategies start at $SOE_0 = SOE_{ref}=75\%$.
- **P_L**: This column expresses the average measured electric load profile along the NEDC. The electric load request from the vehicle experiments has also been used in the simulation environment.

Strategy	SOE_0 [%]	P_L [W]	CO_2 [g/km]	SOE^* [%]	Fuel eco [%]
BL hot	100	242.7	183.6	100.0	-
PSM hot	75	192.7	179.2	74.7	2.4
BL+250W hot	100	472.7	188.0	100.0	-
PDM hot	75	465.8	185.4	75.2	1.4
BL cold	100	232.8	201.0	100.0	-
PSM cold	75	205.1	195.8	74.7	2.6

Table 6.3: Overview of roller-dynamometer experiments

- **Fuel mass and CO_2** : Knowledge about the vehicle's fuel economy is shown in these columns. The engine map in the simulation environment denotes the actual fuel massflow of the engine, so the simulation model directly provides the fuel consumption along the driving cycle. This is different with the vehicle experiments, where the tailpipe emissions are measured instead of the injected fuel massflow. A good representation for the vehicle's fuel consumption is the tailpipe Carbon Dioxide (CO_2) emission. The measured CO_2 emissions are shown in grams per kilometer and the relative reduction in CO_2 emissions will be used to calculate the benefits in fuel economy, see the last column.
- **SOE^*** : The final SOE level reached at the end of the driving cycle is indicated in this column.
- **Fuel eco**: The improvement in fuel economy for a particular strategy is calculated here. The values are calculated without taking differences between SOE_0 and SOE^* into account.

The signals of interest from one vehicle measurement (using the PSM strategy) are shown in Fig. 6.6 over the last 600 [s] of the NEDC driving cycle. In this figure, the following information is shown: the speed of the vehicle, the position of the accelerator pedal, the alternator power and the SOE of the battery. This figure also includes the corresponding signals from the simulation model. The accelerator pedal reveals that the human driver spends considerable more effort to follow the desired speed profile than the simulation model. The EM strategy makes use of the pedal positions to estimate the driver's power demand and the corresponding engine operating point. This explains why fluctuations in the accelerator pedal show up as variations in the alternator power setpoint during the vehicle measurements. Although the switching profile of the alternator power is much richer in the

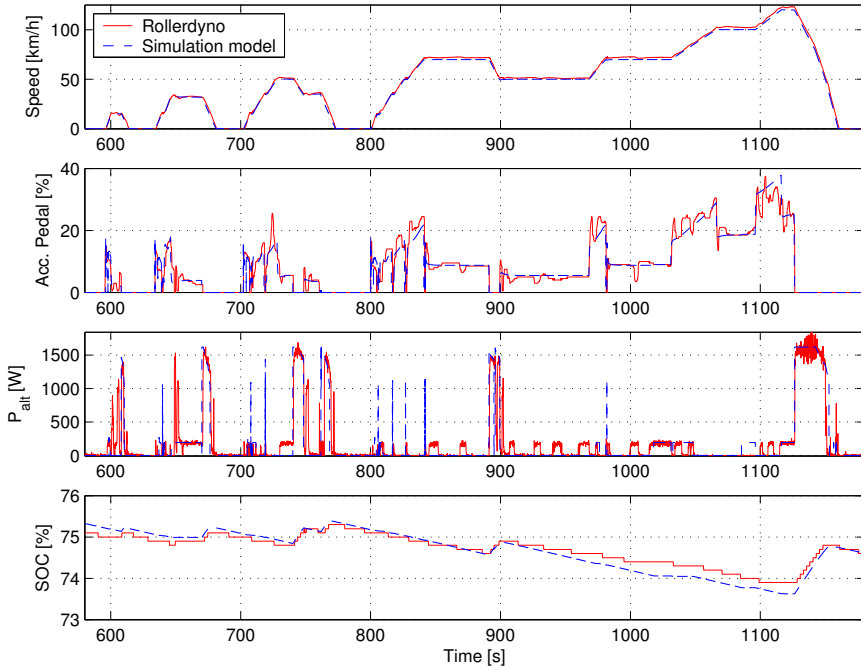


Figure 6.6: Control actions with PSM strategy (hot-engine start)

vehicle tests, its average behavior is similar to the simulation model. This follows from the SOE curves which remain close to each other.

6.8 Evaluation & Discussion

The results in Table 6.2 and 6.3 provide, among other things, insight in the improvement in fuel economy. All strategies achieve an improvement between 1.1% and 2.6%, whereas SOE^* is close to SOE_0 . The following three observations are contrary to the expectations and will be clarified in this section. First, the vehicle experiments achieve a better performance than expected from simulations. In simulations, PSM and PDM achieve a fuel reduction of 1.5% and 1.1%, respectively. This is significantly lower than in the vehicle experiments where the profits for PSM vary between 2.6% and 2.4% (cold and hot engine) and PDM achieves a fuel reduction of 1.4%. Second, the simulation results reveal that the off-line and on-line strategies achieve equal performance, although no predictions are used for the on-line

strategy. Finally, the last observation is that the profits with PDM are lower than with PSM, whereas higher profits are logically expected.

Differences between simulations and experiments

There are mainly two elements that explain why the vehicle experiments achieve a better fuel economy than indicated by the simulation environment: a) the behavior of the driver and b) the missing feedforward signal from the alternator to the ECU.

a) The PI-controlled driver model follows the desired speed profile perfectly and the accelerator pedal changes smoothly, see Fig. 6.6. Because the accelerator pedal is related to the engine operating point by means of the ECU, also less variation is recognized in the operation point of the engine. These variations are a necessity for an EM strategy and hence, the simulation model offers less opportunities for EM. For validation, the real-world driver has been emulated in the simulation model including its overshoot. Depending on the tuning-parameters of the driver model, the cumulative fuel use changes around $\pm 0.1\%$. Although this effect is relative small, it confirms that there is a correlation.

b) As discussed in Section 6.6, the feedforward signal from the alternator to the ECU is not present in the simulation environment. Only the vehicle tests with the baseline strategy use this signal. Additional simulations have been done with a baseline strategy that does include this feedforward signal. Depending on the bandwidth of the PI-controlled driver, an extra fuel consumption is seen. An accurate driver with a high bandwidth experiences only minor influence from the feedforward signal and the fuel consumption of the baseline strategy increases around 0.5%. On the other hand, a driver with a low bandwidth is not able to counteract the feedforward signal at undesired moments (*e.g.*, during vehicle deceleration). Here, the baseline strategy requires extra fuel up to 1.0%. More general, one can draw the conclusion that ignoring the alternator feedforward signal during deceleration phases is not only profitable for the EM strategy, but also for the baseline strategy as well.

Another side effect of increasing the alternator power when there is no feedforward signal present, is that the vehicle decelerates up to a certain extend. This can be compensated by the human driver, but especially during braking phases, this extra braking force is often preferred. The vehicle experiments point out that a vehicle with the EM strategy travels at a lower engine speed during the deceleration phases. Although the differences are rather small, the average engine speed over the entire driving cycle reduces

approximately 6 [rpm]. Simulations with this reduced engine speed indicate an extra fuel benefit of 0.3%.

Due to accuracy limitations of the roller-dynamometer, an adequate model is currently missing for the driver and the ECU. Nevertheless, it appears that a particular driver/vehicle combination offers additional opportunities to improve the fuel economy. Further research is needed to obtain appropriate models for the driver and the ECU.

Similar performance with off-line and on-line strategies

Theoretically, the MPC strategy achieves a better fuel economy than the on-line strategy, because it relies on exact prediction information from the future driving cycle, whereas the on-line strategy does not use this a priori knowledge. In practical situations, however, the computational power is limited and the off-line strategy uses a discrete sampling period of $\Delta T = 1$ [s]. On the other hand, the on-line strategy has a low computational demand and its sampling interval has been selected equal to $\Delta T = 0.01$ [s]. This way, the on-line strategy is able to anticipate on quick events and achieves a performance close to the MPC strategy. Note that the extra fuel benefits will be small in the simulation environment, due to the moderate driver behavior. However, during vehicle experiments, this higher sampling frequency becomes relevant because of more intensive driver behavior.

Lower profits with PDM than with PSM

Conceptually, PDM offers more freedom for energy management than PSM, because PDM controls two design variables (the alternator power and the electric load demand) whereas PSM is restricted to only one variable (the alternator power). Therefore, it is expected that PDM achieves a better fuel economy. However, the increased electric load demand that has been selected for PDM dominates the results of the experiments. Due to the extra load of 250W, the alternator reaches more often its power limitations, leading to less freedom for the PDM strategy. Furthermore, also the baseline strategy recovers a fraction of the free kinetic energy during vehicle deceleration and this fraction becomes larger when the electric load increases. This observation is extensively discussed in [49]. Consequently, the advantage of PDM with respect to the baseline becomes less visible if the electric load increases.

<i>Model property</i>	<i>FE change [%]</i>
PI-controlled driver	0.1
Alternator feedforward signal	0.5 - 1.0
Reduced engine speed	0.3

Table 6.4: Model uncertainties and influence on fuel economy (FE)

Discussion

The explanations given above indicate that there are many aspects that influence the actual fuel economy of the vehicle, although they are not the real intention of EM. Different from the MPC strategy, the on-line strategies do not enforce a fixed energy level E_{sref} for the battery at the end of the driving cycle. Nevertheless, they are able to finish the driving cycle close to E_{sref} by means of the PI-controller, leaving more freedom for EM. From other simulations it is known that the differences between SOE_0 and SOE^* as indicated in Table 6.3 have less than 0.1% effect on the fuel economy. As a result, no correction methods are used when calculating the absolute benefit in fuel economy.

An overview of all the side-effects that contribute to an improved fuel economy for the vehicle measurements is shown in Table 6.4. The cumulative uncertainty from these side-effects is of similar size as the improvement in fuel economy shown by PSM or PDM in the simulation environment. Adding these uncertainties to the simulation results is sufficient to close the gap with the roller-dynamometer experiments. Nevertheless, this large uncertainty indicates that the implementation of an EM strategy in the vehicle should be done with care, to obtain an improvement in fuel economy.

So far, no attention has been paid to the vehicle experiments with a cold engine start. Before the EM strategies were tested, vehicles experiments are done with the baseline strategy and a cold engine start. According to the measured relation between fuel use and engine coolant temperature, the assumption was made that temperature only influences the fuel offset f_1 , rather than the slope λ of the fuel curves. Considering the objective function in Fig. 6.3, it becomes clear that the location of P_e^* is only affected by the slope from F and not by its offset f_1 . Hence, the EM strategy required no modifications for a cold engine start and the PSM and PDM algorithms do not take the temperature of the ICE into account.

Remarkably, the results from Table 6.3 show that driving the NEDC with a cold engine start offers more potential for EM than starting this trip

with a hot engine. This means that the influence from the ICE temperature is not well understood. In future work, temperature aspects have to be considered for further refinement of the EM strategy.

6.9 Conclusions

EM strategies are developed for the electric powernet in a conventional vehicle. As a benchmark, an off-line strategy has been defined that solves a QP optimization problem in an MPC framework. Besides this strategy, also a causal on-line strategy has been developed that does not rely on prediction information. Additional freedom for EM is obtained by introducing electric loads with a flexible power demand. Furthermore, all strategies have the opportunity to include extra losses in the battery model. This allows the designer to make a trade-off between battery wear and fuel economy.

To obtain a performance that is close to the optimal solution, the off-line MPC strategy requires a prediction horizon of more than 100 [s], for a typical driving cycle. On the other hand, the on-line causal strategy achieves a similar performance without using any prediction information. This strategy is directly suitable for implementation in a vehicle.

The causal EM strategy has been implemented in a Ford Mondeo vehicle. A roller-dynamometer test-bench has been used to validate the control actions of the strategy. The tailpipe emissions are measured to obtain insight in the achieved profits in fuel economy. From the vehicle experiments can be concluded that EM has a positive effect on the vehicle's fuel economy up to 2.6%. This result is better than expected from simulations. Although the main contribution comes from the EM strategy itself, also other effects are responsible for the achieved profits. In particular the behavior of the human driver as well as the communication between the alternator and the ECU are dominant. These effects are not included in the results from the simulation environment.

A further refinement of the EM strategies requires additional vehicle experiments, gaining more in-depth knowledge of the driver and the vehicle and how the EM strategy interacts with them. The present roller-dynamometer experiments learn that typical vehicle aspects (*e.g.*, a cold engine start) require more understanding, in order to utilize the full potential of EM.

7

Conclusions & Recommendations

This chapter provides first an overview of general observations that originate from the research described in this thesis. Next, Section 7.2 summarizes the main conclusions from the preceding chapters. Finally, recommendations for further research are given in Section 7.3.

7.1 General observations

In literature, many solutions have been proposed for an energy management (EM) system for the electric power net in road vehicles. Basic assumptions are accurate knowledge of the future driving cycle and precise information about the technical characteristics of the vehicle drive train as well as components connected to the power net.

In practice, however, the first assumption cannot be satisfied. Up to now, no methods exist, neither navigation systems, advanced estimators nor sensor systems, which can predict accurately the future power demand for propulsion and the electric loads. Furthermore, also the second assumption turns out to be not realistic. Despite advanced production techniques, small deviations exist between components of different vehicles and during normal operation, these components suffer from wear and their characteristics depend on many different physical variables. But even when both assumptions are satisfied, the required computer resources for solving a full optimization over a reasonable trajectory, *e.g.*, with Dynamic Programming (DP), are prohibitive for an on-line EM strategy.

In this thesis, the assumption of having an accurate prediction has been dropped. A causal EM strategy is proposed which can easily be computed

on-line. Furthermore, the EM strategy applies to vehicles with a conventional drive train, as well as hybrid electric vehicles (HEVs). More specifically, the following HEV configurations are supported by the proposed EM strategy: the series, the parallel and the series/parallel HEV.

In all vehicle configurations under consideration, a battery is connected to the power net to store electric energy. This battery offers freedom to the EM system to schedule the production and the distribution of electric power on the power net. In this thesis, the primary goal of the EM system is to maximize the energy efficiency of the vehicle, such that its primary energy demand (*i.e.*, fuel) is as low as possible for an arbitrary driving cycle. In a similar way, this EM system can also be tuned to minimize exhaust emissions.

7.2 Conclusions

An EM strategy utilizes basically three characteristics for improving the vehicle fuel economy:

1. The **slope of the fuel map** as function of power. Depending on the operating point of the internal combustion engine (ICE), the slope of the fuel map changes to some extent. This leads to different fuel costs when the ICE produces extra power. An EM system schedules the production of additional (electric) power at those operating points where the fuel map exhibits its minimum slope.
2. The **offset of the fuel map** as function of engine speed. When the ICE runs idle, it produces no net mechanical power but it still consumes fuel to overcome its friction losses. These fuel costs can be eliminated by turning off the ICE if the vehicle is not moving. An HEV is equipped with an electric motor, and this motor can be used for vehicle propulsion whereas the ICE can still remain off. The losses in the electric motor and the battery, compared to the losses in the ICE, determine when this motor-only mode is profitable.
3. Independent of the two ICE characteristics given above, **regeneration of free kinetic energy** during braking periods is always an attractive option and should be applied in any EM system when the fuel benefits are higher than the extra cost for battery wear. Depending on the maximum power limits of the electric motor in combination

with the charge acceptance of the battery, the EM system captures (parts of) the available energy in the battery. The battery efficiency puts another restriction on the net profits from regenerative braking.

Differences in fuel economy between the solutions of the (non-causal) DP strategy and the proposed on-line (causal) strategy are extremely small on the NEDC driving cycle:

- **There is no need for a complex optimization algorithm in an EM system.**

Generally speaking, an EM strategy obtains the majority of its fuel benefits from engine stop/start and from regenerative braking. These modes are easily recognized in the vehicle, even by a heuristic strategy. An EM strategy that applies these two methods, and if it uses the free energy from regenerative braking for motor only mode, requires no complex optimization whereas most fuel profits are covered. There is only one option left for further improvement: motor assist in combination with battery charging. In these modes, the operating point of the ICE is shifted to a lower and higher power level, respectively. However, the fuel curves of the considered Spark Ignition (SI) engine exhibit nearly linear behavior with respect to engine power, so the variations in the incremental fuel cost λ are limited and the extra fuel profits are small.

- **A priori knowledge from the speed profile of the NEDC driving cycle yields little profits.**

In Chapter 4, the DP strategy has accurate knowledge about the future driving cycle, which allows for deep battery discharging and still it returns to the SOE reference value (SOE_{ref}) at the end of the trip. This is different for the on-line EM system, which receives no prediction information and the Proportional Integral (PI) controller keeps the SOE close to SOE_{ref} . Nevertheless, both strategies achieve almost similar performance in terms of fuel economy. This is because the NEDC driving cycle contains sufficient variations in its speed profile.

To operate properly, the on-line EM system requires knowledge about the incremental fuel cost during the future driving cycle. The PI-controller estimates this future incremental cost $\hat{\lambda}$ from the difference between the actual SOE and SOE_{ref} . Through a correct tuning of the PI-controller, the closed-loop bandwidth of the EM system

becomes sufficiently small, such that most frequency components of the driving cycle appear outside the bandwidth of the system. Hence, decisions from the EM strategy will not affect the estimated cost $\hat{\lambda}$, unless the SOE drifts away from SOE_{ref} .

With sufficient accurate knowledge about the future driving cycle, one can omit the PI-controller and calculate a constant value λ^* for $\hat{\lambda}$, such that the on-line strategy mimics the control actions from DP, provided that there are no limitations for the storage capacity of the battery. With a fixed λ^* , all frequency components of the driving cycle are taken into account by the EM system. Nevertheless, using no feedback is not a practical solution, since model uncertainties are not considered by the EM system. Furthermore, no feedback means that the initial value for $\hat{\lambda}$ should be correct. A careful selection can only be done, if accurate information about the future driving cycle is available, so causality will be lost.

- **Minor fuel profits from the e-horizon.**

Knowledge about the future driving cycle becomes important when many frequency components from the driver's power demand fall in the bandwidth of the PI-controller. In those situations, the PI-controller suppresses possible SOE variations, which could be used by the EM.

To overcome this drawback, an e-horizon can be used to incorporate road predictions into the EM system. The e-horizon schedules energy between cheap and expensive road segments, by calculating a preferred SOE trajectory for the battery for the next coming road segments. Chapter 5 demonstrates that this approach is valid for typical driving cycles, but the extra profits in fuel economy remain limited.

The on-line EM strategy has been validated in a vehicle with a conventional drive train.

By means of vehicle experiments on a roller-dynamometer test bench, profits in fuel economy are measured up to 2.6%. Essentially, only software changes are required to implement the EM system, so the return on investment is really high. Since these fuel profits are higher than expected from simulations, it is clear that some important vehicle characteristics are still excluded from the simulation environment. It turns out that the behav-

ior of the driver and the dynamics of the engine control unit are not well defined in the simulation model.

7.3 Recommendations

The research described in this thesis focussed on developing an EM system for a given vehicle configuration. Questions about selecting a suitable vehicle topology as well as sizing of components are not addressed in this work. By construction, these aspects influence the overall fuel economy of the vehicle. It is clear that these aspects should be included in further research.

The simulations in Chapter 4 make use of a model that has not been validated against experimental data. To improve the reliability of the simulation results, it is desirable to have measurement data for all HEV configurations (including data from individual components) and determine the validity of the simulation model.

Especially the battery model needs to be extended with information about battery wear. Due to the presence of the EM system, the battery is intensively used and this normally leads to a faster battery degradation. However, literature provides no detailed knowledge about this degradation proces. For the EM system, it is important to know how battery wear can be prevented. Moreover, the question should be answered whether battery aging leads to a loss in battery capacity only, or that it also affects the energy losses during charging or discharging. This latter effect definitely requires a periodic update of the battery model, to guarantee that the decisions of the EM system are still optimal. If knowledge about battery wear is available, the extra costs for replacement of the battery can be explicitly added as an extra term in the optimization criterium, or implicitly through the losses in the battery model.

Except for the battery model, also the fuel map of the ICE takes a dominant position in the decision proces of the EM system. Depending on the information in this map, the EM system decides whether it is beneficial to produce electric energy or not. Up till now, a static map is used to calculate the corresponding fuel consumption. Although this method is commonly used, exact conditions when this approach is valid are currently missing. Moreover, the fuel characteristics might also change when the ICE becomes older, or is somewhere between two periodic service intervals. Therefore, it is recommended to investigate the possibility for on-line identification of the relevant characteristics of the fuel map. Also the influence from the

engine control unit should be taken into account.

So far, a frequent engine stop/start is not penalized by the EM strategies, but for driveability reasons this will be an important issue. A valid approach is to include extra energy losses for engine cranking in the model. This way, engine stop/start becomes less attractive. Note that this method is also proposed to make a trade-off between battery usage versus profits in fuel economy. If the designer includes extra losses in the efficiency model of the battery, the EM system prefers less battery activity.

The tuning parameters from the PI-controller in the EM system are selected according to insight and experience, but an analytical method for selecting these parameters is missing. Further analysis is suggested on the actual bandwidth of the EM system, and its dependency on typical driving cycle characteristics (see Appendix A). This analysis should also address topics such as the frequency spectrum of real-world driving cycles, as well as the impact of a limited battery capacity on the tuning parameters. In the direction of frequency analysis for driving cycles, a start has been made in [23].

Appendix A

Bandwidth of energy management strategy

The EM system from Chapter 3 uses a Proportional Integral (PI) controller to regulate the State of Energy (SOE) of the battery towards a reference value SOE_{ref} . This appendix provides the basic results for robust stability and tuning of this control loop. It will show how the PI-controller influences the overall performance of the EM system and how to select a suitable closed-loop bandwidth.

For simplicity, this appendix focusses on the S-HEV vehicle model as described in Section 3.1. Nevertheless, a similar analysis can be done for the P-HEV and S/P-HEV configuration.

A.1 Closed-loop stability

The control objective of the EM strategy from Chapter 3.1 focusses on minimizing the vehicle fuel consumption. Its control law is calculated by minimizing an objective function $J(P_s, S)$ [g/s]. This function depends on the net battery power P_s [W] and the engine running signal S [-]. Depending on the engine running signal $S \in [0, 1]$, two modes are recognized. The first mode considers the situation that the EM strategy selects $S = 1$, so the ICE is running. The corresponding objective function is repeated below, see also (3.43):

$$J(P_s) = F(P_s | P_d, P_L) - \lambda P_s \quad [\text{g/s}] \quad (\text{A.1})$$

Assume for the moment that the model of the electric machine, the generator and the battery do not suffer from energy losses, so there holds $\eta_{mm} = \eta_{gm} = \eta_g = \eta_{bat} = 1$ [-] in (3.2), (3.5) and (3.12). For this situation, (A.1) can be approximated by a quadratic polynomial function, which

originates from the slope of the engine map:

$$\begin{aligned}
 J'(P_s) &= F(P_s | P_d, P_L) - \lambda P_s \\
 &= f_{e-line}(P_s + P_d + P_L) - \lambda P_s \\
 &\approx \gamma_2(P_s + P_d + P_L)^2 + \gamma_1(P_s + P_d + P_L) + \gamma_0 - \lambda P_s \\
 &= cP_s^2 + bP_s + a - \lambda P_s
 \end{aligned} \tag{A.2}$$

with

$$\begin{aligned}
 c &= \gamma_2, \\
 b &= 2\gamma_2(P_d + P_L) + \gamma_1, \\
 a &= \gamma_2(P_d^2 + P_L^2 + 2P_dP_L) + \gamma_1(P_d + P_L) + \gamma_0.
 \end{aligned}$$

The EM strategy will find the minimum of (A.2) by forcing the derivative to zero:

$$\frac{\partial}{\partial P_s} J'(P_s) = 2cP_s + b - \lambda = 0 \tag{A.3}$$

$$\Rightarrow P_s^1 = \frac{\lambda - b}{2c} \tag{A.4}$$

Next, consider the other situation, where the EM strategy decides to leave the ICE off, so $S = 0$. In that case, the battery power P_s^0 is exclusively defined by the mechanical power demand P_d and the electric load power P_L :

$$P_s^0 = -P_d - P_L. \tag{A.5}$$

Altogether, the control scheme of the EM strategy is elucidated in Fig. A.1. It turns out that the feedback loop is only closed for $S = 1$. In that situation, the EM strategy acts as a gain $H_{EM}(s) = 1/(2c)$, with an external signal b present on its input. The parameters c and b are prescribed by the driving cycle under consideration. The situation $S = 0$ disconnects the feedback-loop, but this situation is not taken into account for the closed-loop stability analysis, since P_d and P_L are exogenous inputs.

The block diagram in Fig. A.1 also incorporates the PI-controller for estimating $\hat{\lambda}$ [g/J]. The transfer function of this controller is given by:

$$H_C(s) = k \left(1 + \frac{1}{\tau s} \right) = k \frac{\tau s + 1}{\tau s}, \tag{A.6}$$

with the time constant τ [s/rad] and gain k [g/J]. Furthermore, the battery is represented by an integrator with a scaling factor $E_{s\ cap}$ [J] for the battery

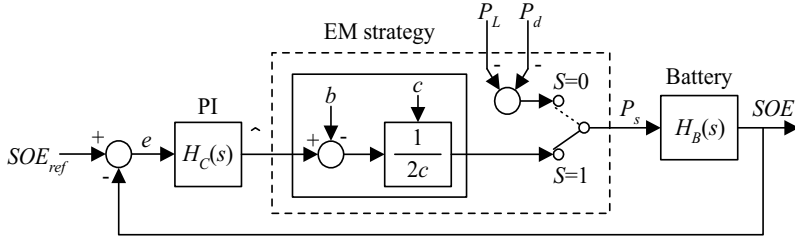


Figure A.1: EM strategy with feedback loop

capacity:

$$H_B(s) = \frac{1}{E_{s\text{cap}} s}. \quad (\text{A.7})$$

If $S = 1$, the transfer function from SOE_{ref} to SOE coincides with the complementary sensitivity function $T(s)$, known from classical control theory [30]:

$$\begin{aligned} T(s) &= \frac{H_C(s)H_{EM}(s)H_B(s)}{1 + H_C(s)H_{EM}(s)H_B(s)} = \frac{k \frac{\tau s + 1}{\tau s} \frac{1}{2c} \frac{1}{E_{s\text{cap}} s}}{1 + k \frac{\tau s + 1}{\tau s} \frac{1}{2c} \frac{1}{E_{s\text{cap}} s}} \\ &= \frac{k(\tau s + 1)}{2c\tau E_{s\text{cap}} s^2 + k\tau s + k} \end{aligned} \quad (\text{A.8})$$

The locations of the poles of $T(s)$ are given by:

$$s = \frac{-k\tau \pm \sqrt{k^2\tau^2 - 8kc\tau E_{s\text{cap}}}}{4c\tau E_{s\text{cap}}} \quad (\text{A.9})$$

Then it follows that if parameter c [g s/J²] is known from the driving cycle, stability and a preferred bandwidth is established with τ and k . *E.g.*, for a critically damped system (two poles that coincide on the real-axis), the gain k must be equal to:

$$k^2\tau^2 = 8kc\tau E_{s\text{cap}} \Rightarrow k = \frac{8cE_{s\text{cap}}}{\tau}. \quad (\text{A.10})$$

Furthermore, the frequency $s = j\omega^*$ from where $|T(j\omega^*)|$ starts decreasing asymptotically, is defined here as the closed-loop bandwidth. It is calculated through the substitution of (A.10) into (A.9):

$$\omega^* = \left| \frac{-k\tau \pm \sqrt{0}}{4c\tau E_{s\text{cap}}} \right| = \frac{2}{\tau} \quad [\text{rad/s}]. \quad (\text{A.11})$$

However, parameter c is not constant, but changes over time as prescribed by the driving cycle, with $0 < c^- \leq c \leq c^+$. If k and τ are fixed, this introduces an uncertainty in the location of the closed-loop poles and also changes the actual bandwidth of the system. Note that one can also adapt k and τ to keep the bandwidth fixed, but this solution is not considered here.

A.1.1 Kharitonov theorem

The stability of $T(s)$ with k and τ fixed will be analyzed according to Kharitonov's theorem¹. The characteristic polynomial $\chi(s, q)$ from (A.8) is considered:

$$\chi(s, q) = q_2 s^2 + q_1 s + q_0, \quad (\text{A.12})$$

with the uncertainty parameter $q \in Q \subseteq \mathbb{R}^3$ defined as:

$$2c^- \tau E_{s \text{ cap}} \leq q_2 \leq 2c^+ \tau E_{s \text{ cap}}, \quad (\text{A.13})$$

$$q_1 = k\tau, \quad (\text{A.14})$$

$$q_0 = k. \quad (\text{A.15})$$

A polynomial $\chi(s)$ with fixed parameters is *stable* if all its roots lie in the open left half plane. Furthermore, the family of polynomials $\chi(s, q)$ is said to be *robustly stable* if all polynomials are stable, with $q \in Q$.

Kharitonov's theorem states that each member of the family of polynomials

$$\chi(s, q) = q_n s^n + \dots + q_1 s + q_0, \quad (\text{A.16})$$

$$\text{with } q_i^- \leq q_i \leq q_i^+, \quad i = 0, 1, \dots, n, \quad (\text{A.17})$$

is stable if and only if each of the four Kharitonov polynomials

$$k_1(s) = q_0^+ + q_1^+ s + q_2^- s^2 + q_3^- s^3 + q_4^+ s^4 + q_5^+ s^5 + \dots, \quad (\text{A.18})$$

$$k_2(s) = q_0^- + q_1^- s + q_2^+ s^2 + q_3^+ s^3 + q_4^- s^4 + q_5^- s^5 + \dots, \quad (\text{A.19})$$

$$k_3(s) = q_0^- + q_1^+ s + q_2^+ s^2 + q_3^- s^3 + q_4^- s^4 + q_5^+ s^5 + \dots, \quad (\text{A.20})$$

$$k_4(s) = q_0^+ + q_1^- s + q_2^- s^2 + q_3^+ s^3 + q_4^+ s^4 + q_5^- s^5 + \dots, \quad (\text{A.21})$$

are stable.

The polynomial (A.12) includes only one uncertainty q_3 . Therefore, it is sufficient to consider only the roots of $k_1(s)$ and $k_2(s)$ for robust stability, whereas the roots from $k_3(s)$ and $k_4(s)$ are redundant.

¹For an excellent survey on Kharitonov's theorem, the reader is referred to [8].

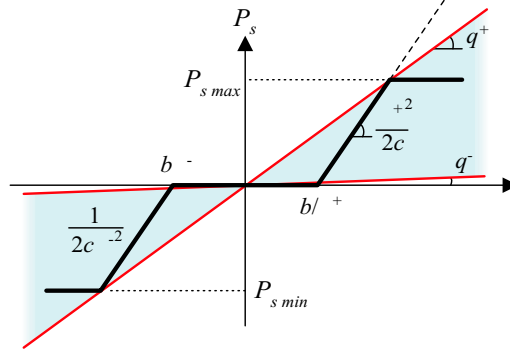
For the S-HEV, the following vehicle parameters are found: $c^- = 1.0 \times 10^{-12}$ [gs/J²], $c^+ = 4.0 \times 10^{-9}$ [gs/J²] and $E_{scap} = 4.0 \times 10^6$ [J]. The parameters of the PI-controller are selected $k = 2.40 \times 10^{-5}$ [g/J] and $\tau = 85$ [s/rad], but more details about these settings are given in Section A.2. Given these parameter settings, the calculated roots for both $k_1(s)$ and $k_2(s)$ have negative real parts. Hence, there can be concluded that the characteristic polynomial (A.12) is robustly stable. This result implies also that the closed-loop system (A.8) is stable for all possible parameter variations $c^- \leq c \leq c^+$.

A.1.2 Model components with losses

Up till now, the analysis considered only the situation without losses in the model of the battery and the electric machine. Nevertheless, a similar reasoning can be used when these losses are included. This is shown below, by reconsidering (A.1) with the losses in the battery equal to $\eta_{bat} < 1$. From the battery model (3.12), it follows that $J'(P_s)$ in (A.2) changes into:

$$\begin{aligned}
 J''(P_s) &= F(P_s | P_d, P_L) - \lambda P_s \\
 &= f_{e-line}(P_b + P_d + P_L) - \lambda P_s \\
 &= f_{e-line}(\max(\eta^- P_s, \frac{1}{\eta^+} P_s) + P_d + P_L) - \lambda P_s \\
 &\approx \gamma_2(\max(\eta^- P_s, \frac{1}{\eta^+} P_s) + P_d + P_L)^2 \\
 &\quad + \gamma_1(\max(\eta^- P_s, \frac{1}{\eta^+} P_s) + P_d + P_L) + \gamma_0 - \lambda P_s \\
 &= \gamma_2 \max((\eta^- P_s)^2, (\frac{1}{\eta^+} P_s)^2) \\
 &\quad + (2\gamma_2(P_d + P_L) + \gamma_1) \max(\eta^- P_s, \frac{1}{\eta^+} P_s) \\
 &\quad + \gamma_2(P_d^2 + P_L^2 + 2P_d P_L) + \gamma_1(P_d + P_L) + \gamma_0 - \lambda P_s \\
 &= c \max((\eta^- P_s)^2, (\frac{1}{\eta^+} P_s)^2) + b \max(\eta^- P_s, \frac{1}{\eta^+} P_s) \\
 &\quad + a - \lambda P_s \tag{A.22}
 \end{aligned}$$

Contrary to the objective function from (A.2), the derivative of (A.22) has a discontinuity at $P_s = 0$. As a result, the EM system finds the mini-


 Figure A.2: Relation between λ and P_s

imum of $J''(P_s)$ in three different ways, depending on the value of λ :

$$P_s = \begin{cases} \frac{\lambda - b\eta^-}{2c\eta^{-2}} & \text{if } \lambda \leq b\eta^- \\ 0 & \text{if } b\eta^- < \lambda < \frac{b}{\eta^+} \\ \frac{(\lambda - \frac{b}{\eta^+})\eta^{+2}}{2c} & \text{if } \lambda \geq \frac{b}{\eta^+} \end{cases} \quad (\text{A.23})$$

This function has been visualized in Fig. A.2. Similar to the situation without the energy losses, the power limitations of the battery and the electric machine introduces saturation of P_s between $P_{s\min}$ and $P_{s\max}$. Also the driving cycle introduces an uncertainty for parameter c , but the relation between λ and P_s can still be characterized with a static gain $q^- \leq q \leq q^+$. The boundaries of q are elucidated in Fig. A.2, with the shaded areas. The shape of this uncertainty region resembles with the situation where no losses were present, except for the situation $q^- = 0$. For that situation, the roots of the Kharitonov polynomials appear on the imaginary axis. Strictly speaking, this means that the closed-loop system is not robustly stable and to guarantee robust stability, $q^- > 0$ is needed.

A.2 Closed-loop bandwidth

Guaranteed stability as shown in the previous section is a necessary, but not a sufficient condition for a good performance of the EM system. It turns out that the bandwidth of the closed-loop system determines how well the EM strategy can improve the fuel economy of the vehicle. Directions how to select a suitable bandwidth are given in this section.

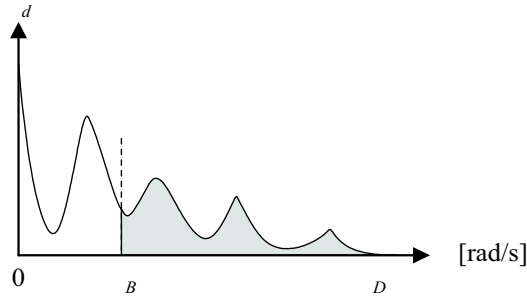


Figure A.3: Spectrum of driving cycle and bandwidth of EM system

In many control problems, a large bandwidth is desirable to establish a good tracking performance. This is different for the EM system, where a relative small bandwidth is preferred for the PI-controller to update the parameter $\hat{\lambda}$ (which expresses the expected costs for producing electric power in the future). The ideal bandwidth will be a compromise between a slow adaptation of $\hat{\lambda}$ to update for uncertainties in the driving cycle, versus a fast response when the battery's SOE threatens to drift away from the preferred reference value SOE_{ref} .

A.2.1 Power spectrum

To explain the decision process when selecting a suitable bandwidth, the spectrum from the driving cycle will be considered. This spectrum $\Phi_d(\omega)$ is calculated from the power demand $P_d + P_L$ using the Fourier transform:

$$\Phi_d(\omega) = \int_{-\infty}^{\infty} (P_d(t) + P_L(t)) e^{-j\omega t} dt. \quad (\text{A.24})$$

Each driving cycle has a unique spectrum $\Phi_d(\omega)$ with frequencies up to $\omega \leq \omega_D$, *i.e.*, $\Phi_d(\omega) = 0$ for $\omega > \omega_D$. Now assume that the bandwidth of the EM system equals $\omega_B < \omega_D$. Then ω_B divides the spectrum $\Phi_d(\omega)$ into two areas. This is elucidated in Fig. A.3. For each area, the following observations are made:

$$0 \leq \omega \leq \omega_B$$

For this frequency range, the power demand of the driving cycle changes rather slowly. These variations are recognized by the PI-controller as possible drift of the battery, and by adapting $\hat{\lambda}$, the

PI-controller actively counteracts these variations and keeps the battery near SOE_{ref} .

There are two reasons why this control mechanism for updating $\hat{\lambda}$ is desirable. First, it prevents battery depletion or overcharging when the driving cycle contains lengthy periods where the EM strategy continuously charges or discharges the battery. Second, a slow update of the parameter $\hat{\lambda}$ is required, since uncertainties in the future power demand, as well as inaccuracies in the vehicle model make it impossible to calculate $\hat{\lambda}$ off-line in advance.

On the other hand, the actions from the PI-controller are not always profitable for the performance of the EM system. Since the PI-controller adapts $\hat{\lambda}$ to counteract the SOE variations, all frequency components $\omega < \omega_B$ in $\Phi_d(\omega)$ are suppressed by the PI-controller and the SOE is forced to SOE_{ref} in this frequency range. Without using an electronic horizon (see Chapter 5) SOE_{ref} is a fixed value, so here the de facto EM strategy coincides with the baseline situation and the battery is never charged or discharged. Hence, in the frequency range where the PI-controller is active, economic profits are sacrificed to satisfy a charge sustaining strategy.

$\omega > \omega_B$

The profits from the EM system are covered in this frequency range. Since all frequencies above ω_B fall outside the scope of the PI controller, the parameter $\hat{\lambda}$ will not be updated and remains constant for this frequency range. The EM strategy can calculate P_s , without interference with the PI-controller. Therefore, charging and discharging of the battery is possible to obtain fuel profits with the EM strategy.

It follows that the EM strategy achieves maximum profits in fuel economy when ω_B is selected as low as possible, *i.e.*, $\omega_B = 0$. However, this solution is practically not feasible, since $\hat{\lambda}$ will not be updated anymore and its initial guess needs to be accurate. A suitable solution will be a compromise between a small bandwidth for a high performance, versus a larger bandwidth to guarantee a charge sustaining strategy. These observations are summarized in Table A.1.

A.2.2 Example NEDC driving cycle

The spectrum of the NEDC driving cycle is shown in Fig. A.4. The amplitude has been normalized, such that there holds: $\Phi(0) = 1$. The NEDC

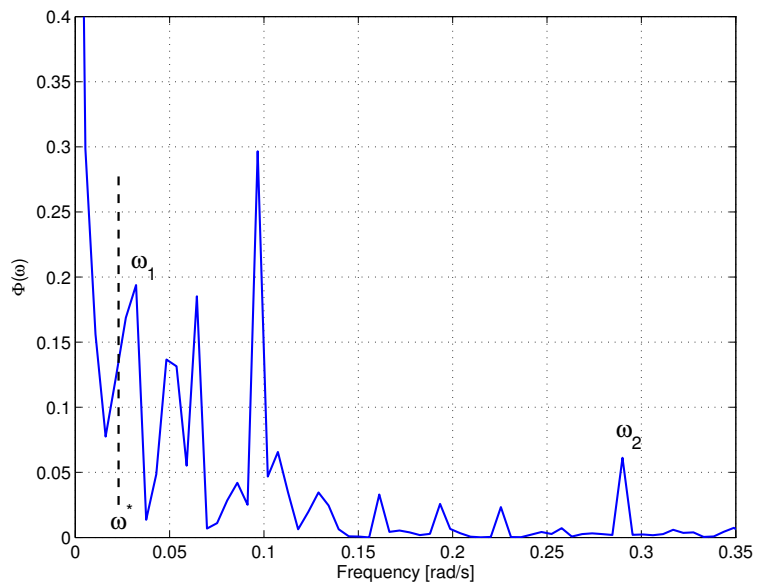


Figure A.4: Spectrum of P_d for NEDC driving cycle

Bibliography

- [1] IEEE Std. 1188-2005: Recommended Practice for Maintenance, Testing, and Replacement of Valve-Regulated Lead-Acid (VRLA) Batteries for Stationary Applications.
- [2] R.W. Allen, T.J. Rosenthal, and J.R. Hogue. Modeling and simulation of driver/vehicle interaction. In *SAE International Congress & Exposition*, Detroit, MI, USA, February 1996. SAE 960177.
- [3] I. Alvarez, J. Fontanilles, J. Mestre, and R. Große. An embedded time-series prediction strategy based on ANN for vehicle status definition for energy, power & load management. In *Proc. of the FISITA World Automotive Conf.*, Barcelona, Spain, May 2004.
- [4] I. Arsie, M. Graziosi, C. Pianese, G. Rizzo, and M. Sorrentino. Optimization of supervisory control strategy for parallel hybrid vehicle with provisional load estimate. In *Proc. of the 7th Int. Symp. on Advanced Vehicle Control (AVEC)*, Arnhem, The Netherlands, August 2004.
- [5] M. Åsbogård, F. Edström, J. Bringhed, M. Larsson, and J. Hellgren. Evaluating potential of vehicle auxiliary system coordination using optimal control. In *Proc. of the 7th Int. Symp. on Advanced Vehicle Control (AVEC)*, Arnhem, The Netherlands, August 2004.
- [6] J.H. Aylor, A. Thieme, and B.W. Johnson. A battery state-of-charge indicator for electric wheelchairs. *IEEE Trans. on Industrial Electronics*, 39(5):398–409, October 1992.
- [7] M. Back, M. Simons, F. Kirschaum, and V. Krebs. Predictive control of drivetrains. In *Proc. of the IFAC 15th Triennial World Congress*, Barcelona, Spain, 2002.
- [8] B.R. Barmish and H.I. Kang. A survey of extreme point results for robustness of control systems. *Automatica*, 29(1):13–35, January 1993.
- [9] S. Barsali, C. Miulli, and A. Possenti. A control strategy to minimize fuel consumption of series hybrid electric vehicles. *IEEE Trans. on Energy Conversion*, 19(1):187–195, March 2004.
- [10] B.M. Baumann, G. Washington, B.C. Glenn, and G. Rizzoni. Mechatronic design and control of hybrid electric vehicles. *IEEE/ASME Trans. on Mechatronics*, 5(1):58–72, March 2000.
- [11] D.P. Bertsekas. *Dynamic Programming and Optimal Control*. Athena Scientific, Belmont, MA, 2nd edition, 2000.
- [12] B. Bonsel, T.W.G.L. Klaassen, R.J. Pulles, S.W.H. Simons, M. Steinbuch, and P.A. Veenhuizen. Performance optimisation of the push-belt CVT by variator slip control. *International Journal of Vehicle Design*, 39(3):232–256, 2005.
- [13] P. Boucharel, M. Sans, M. Fadel, and J. Faucher. Hybrid vehicle efficiency optimization on a planned trip. In *Proc. of the FISITA World Automotive Conf.*, Helsinki, Finland, June 2002.

- [14] A. Brahma, Y. Guezennec, and G. Rizzoni. Optimal energy management in series hybrid electric vehicles. In *Proc. of the American Control Conf.*, pages 60–64, Chicago, IL, June 2000.
- [15] E.A. Bretz. By-Wire cars turn the corner. *IEEE Spectrum*, 38(4):68–73, April 2001.
- [16] S. Buller, M. Thele, E. Karden, and R. W. de Doncker. Impedance-based non-linear dynamic battery modeling for automotive applications. *J. of Power Sources*, 113(2):422–430, January 2003.
- [17] E.F. Camacho and C. Bordons. *Model Predictive Control*. Springer-Verlag, London, 2nd edition, 2004.
- [18] B.M. Castaing, J.S. Cowart, and W.K. Cheng. Fuel metering effects on hydrocarbon emissions and engine stability during cranking and start-up in a port fuel injected spark ignition engine. In *Int. Fall Fuels and Lubricants Meeting and Exposition*, Baltimore, Maryland, October 2000. SAE Paper 2000-01-2836.
- [19] J.-S. Chen and M. Salman. Learning energy management strategy for hybrid electric vehicles. In *Proc. of the IEEE Vehicle Power and Propulsion Conference (VPPC)*, Chicago, IL, September 2005.
- [20] S.R. Cikanek and K.E. Bailey. Regenerative braking system for a hybrid electric vehicle. In *Proc. of the American Control Conf.*, volume 4, pages 3129–3134, Anchorage, AK, May 2002.
- [21] Toyota Motor Corporation. Toyota hybrid system THSII. Technical report, May 2003. On-line available: <http://www.toyota.co.jp>.
- [22] B. de Jager. Predictive storage control for a class of power conversion systems. In *Proc. of the European Control Conf.*, Cambridge, UK, September 2003.
- [23] B. de Jager. Choosing the horizon in predictive storage control. In *Proc. of the American Control Conf.*, Boston, MI, June 2004.
- [24] A. Delaille, M. Perrin, F. Huet, and L. Hernout. Study of the “coup de fouet” of lead-acid cells as a function of their state-of-charge and state-of-health. *J. of Power Sources*, 158(2):1019–1028, August 2006.
- [25] S. Delprat, J. Lauber, T.M. Guerra, and J. Rimaux. Control of a parallel hybrid powertrain: Optimal control. *IEEE Trans. on Vehicular Technology*, 53(3):872–881, May 2004.
- [26] M. Desbois-Renaudin, R. Trigui, and J. Scordia. Hybrid powertrain sizing and potential consumption gains. In *Proc. of the IEEE VTS Symposium on Vehicular Power And Propulsion*, Paris, France, October 2004.
- [27] K. Ehlers, H.D. Hartmann, and E. Meissner. 42V - An indication for changing requirements on the vehicle electrical system. *J. of Power Sources*, 95:43–57, 2001.
- [28] M. Eifert. Fuel consumption reduction with a starter-alternator using an MPC-based optimisation. In *Proc. of the European Control Conf.*, Cambridge, UK, September 2003.
- [29] M. Fernández, F. Trinidad, J. Valenciano, and A. Sánchez. Optimization of the cycle life performance of VRLA batteries, working under high rate, partial state of charge (HRPSOC) conditions. *J. of Power Sources*, 158(2):1149–1165, August 2006.
- [30] G.F. Franklin, J.D. Powell, and A. Emami-Naeini. *Feedback control of dynamic systems*. Amsterdam : Addison-Wesley, 1994.

- [31] J. Fredriksson, O. Johansson, P. Stridh, M. Wall, and M. Åsbogård. Model-based energy management control for a parallel hybrid electric vehicle. In *Proc. of the 7th Int. Symp. on Advanced Vehicle Control (AVEC)*, Arnhem, The Netherlands, August 2004.
- [32] K. Fuchibe. Development of IMA system for the 2006 Civic Hybrid. In *Proc. of the EVS 22 - Electric Vehicle Symposium*, pages 486–491, Yokohama, Japan, October 2006.
- [33] Y. Gao and M. Ehsani. Electronic braking system of EV and HEV - Integration of regenerative braking, automatic braking force control and ABS. In *Proc. of the SAE Future Transportation Technology Conf.*, Costa Mesa, CA, August 2001. SAE Paper 2001-01-2478.
- [34] L. Guzzella and A. Sciarretta. *Vehicle Propulsion Systems - Introduction to Modeling and Optimization*. Springer-Verlag, Berlin Heidelberg, 2005.
- [35] T. Hofman, D. Hoekstra, R.M. van Druten, and M. Steinbuch. Optimal design of energy accumulator systems for hybrid vehicle powertrains. In *Proc. of the IEEE Vehicle Power and Propulsion Conference*, pages 73–77, Chicago, IL, September 2005.
- [36] T. Hofman and R. van Druten. Energy analysis of hybrid vehicle powertrains. In *Proc. of the IEEE Int. Symp. on Vehicular Power and Propulsion*, Paris, France, October 2004.
- [37] V.H. Johnson, K.B. Wipke, and D.J. Rausen. HEV control strategy for real-time optimization of fuel economy and emissions. In *Proc. of the Future Car Congress*, Washington, DC, April 2000. SAE Paper 2000-01-1543.
- [38] A. Jossen. Fundamentals of battery dynamics. *J. of Power Sources*, 154(2):530–538, March 2006.
- [39] E. Karden, D. Kok, E. Spijker, L. Gaedt, and D. Kees. Micro-HEVs as a step toward improved fuel economy and emissions. In *Proc. of the 5th International Advanced Automotive Battery and Ultracapacitor Conference (AABC-O5)*, Honolulu, Hawaii, June 2005.
- [40] J.G. Kassakian, J.M. Miller, and N. Traub. Automotive electronics power up. *IEEE Spectrum*, 37(5):34–39, May 2000.
- [41] J. Kessels, M. Koot, W. Hendrix, R. Ellenbroek, M. Heemels, M. Pesgens, M. Steinbuch, and P. van den Bosch. Vehicle modeling for energy management strategies. In *Proc. of the 7th Int. Symp. on Advanced Vehicle Control (AVEC)*, Arnhem, The Netherlands, August 2004.
- [42] J.T.B.A. Kessels, M. Koot, B. de Jager, and P.J.J. van den Bosch. Energy management for vehicle power net with flexible electric load demand. In *Proc. of the 2005 IEEE Conf. on Control Applications*, pages 1504–1509, Toronto, Canada, August 2005.
- [43] J.T.B.A. Kessels, M. Koot, B. de Jager, P.P.J. van den Bosch, N.P.I. Aneke, and D.B. Kok. Energy management for the electric powernet in vehicles with a conventional drivetrain. *IEEE Trans. on Control Systems Technology*, 2007. Accepted for publication.

Bibliography

- [44] J.T.B.A. Kessels, M.W.T. Koot, W.H.A. Hendrix, P.P.J. van den Bosch, N.P.I. Aneke, and H. Jung. Experimental validation of energy management strategies for vehicle electric power net. In *Proc. of the 8th Int. Symp. on Advanced Vehicle Control (AVEC)*, Taipei, Taiwan, August 2006.
- [45] J.T.B.A. Kessels, M.W.T. Koot, and P.P.J. van den Bosch. Optimal adaptive solution to powersplit problem in vehicles with integrated starter/generator. In *Proc. of the IEEE Vehicle Power and Propulsion Conference*, Windsor, UK, September 2006.
- [46] M.J. Kim, H. Peng, C.-C. Lin, E. Stamos, and D. Tran. Testing, modeling, and control of a fuel cell hybrid vehicle. In *Proc. of the American Control Conf.*, pages 3859–3864, Portland, OR, June 2005.
- [47] I. Kolmanovsky, I. Siverguina, and B. Lygoe. Optimization of powertrain operating policy for feasibility assessment and calibration: Stochastic dynamic programming approach. In *Proc. of the American Control Conf.*, volume 2, pages 1425–1430, Anchorage, AK, May 2002.
- [48] M. Koot, J. Kessels, and B. de Jager. Energy management in a vehicle with a dual storage power net. In *Proc. of the 16th IFAC World Congress*, Prague, Czech Republic, July 2005.
- [49] M. Koot, J. Kessels, B. de Jager, and P. van den Bosch. Fuel reduction potential of energy management for vehicular electric power systems. *International Journal of Alternative Propulsion*, 1(1):112–131, 2006.
- [50] M. Koot, J.T.B.A. Kessels, and B. de Jager. Fuel reduction of parallel hybrid electric vehicles. In *Proc. of the IEEE Vehicle Power and Propulsion Conference*, pages 99–104, Chicago, IL, September 2005.
- [51] M. Koot, J.T.B.A. Kessels, B. de Jager, W.P.M.H. Heemels, P.P.J. van den Bosch, and M. Steinbuch. Energy management strategies for vehicular electric power systems. *IEEE Trans. on Vehicular Technology*, 54(3):771–782, May 2005.
- [52] M.W.T. Koot. *Energy management for vehicular electric power systems*. PhD thesis, Department of Mechanical Engineering, Technische Universiteit Eindhoven, The Netherlands, 2006.
- [53] R. Langari and J.-S. Won. Intelligent energy management agent for a parallel hybrid vehicle, Part I: System architecture and design of the driving situation identification process. *IEEE Trans. on Vehicular Technology*, 54(3):925–934, May 2005.
- [54] C.-C. Lin, H. Peng, and J.W. Grizzle. A stochastic control strategy for hybrid electric vehicles. In *Proc. of the American Control Conf.*, pages 4710–4715, Boston, MI, June 2004.
- [55] C.-C. Lin, H. Peng, J.W. Grizzle, and J.-M. Kang. Power management strategy for a parallel hybrid electric truck. *IEEE Trans. on Control Systems Technology*, 11(6):839–849, November 2003.
- [56] J. Liu and H. Peng. Control optimization for a power-split hybrid vehicle. In *Proc. of the American Control Conf.*, pages 466–471, Minneapolis, June 2006.
- [57] Y. Luan and N.A. Henein. Contribution of cold and hot start transients in engine-out HC emissions. In *Int. Fall Fuels and Lubricants Meeting and Exposition*, San Francisco, CA, October 1998. SAE Paper 982645.

-
- [58] J.M. Miller. Hybrid electric vehicle propulsion system architectures of the e-CVT type. *IEEE Trans. on Power Electronics*, 21(3):756–767, May 2006.
- [59] J.M. Miller and M. Everett. Ultra-capacitor augmentation of the vehicle electrical system to reset its power budget. In *Proc. 8th IEEE Workshop on Power Electronics in Transportation*, pages 19–26, Detroit, October 2004.
- [60] J. Moreno, M.E. Ortúzar, and J.W. Dixon. Energy-management system for a hybrid electric vehicle, using ultracapacitors and neural networks. *IEEE Trans. on Industrial Electronics*, 53(2):614–623, April 2006.
- [61] C. Musardo, G. Rizzoni, and B. Staccia. A-ECMS: an adaptive algorithm for hybrid electric vehicle energy management. In *Proc. of the joint 44th IEEE Conf. on Decision and Control & European Control Conference*, pages 1816–1823, Seville, Spain, December 2005.
- [62] P. Nicastrì and H. Huang. 42V PowerNet: Providing the vehicle electrical power for the 21st century. In *Proc. of the SAE Future Transportation Technology Conf.*, Costa Mesa, CA, August 2000. SAE Paper 2000-01-3050.
- [63] T.H. Ortmeier and P. Pillay. Trends in transportation sector technology energy use and greenhouse gas emissions. *Proceedings of the IEEE*, 89(12):1837–1847, December 2001.
- [64] H.B. Pacejka. *Tyre and vehicle dynamics*. Amsterdam : Butterworth-Heinemann, second edition, 2006.
- [65] G. Paganelli, G. Ercole, A. Brahma, Y. Guezennec, and G. Rizzoni. General supervisory control policy for the energy optimization of charge-sustaining hybrid electric vehicles. *JSAE Review*, 22(4):511–518, April 2001.
- [66] P.E. Pascoe, H. Sirisena, and A.H. Anbuky. Coup de fouet based VRLA battery capacity estimation. In *Proc. 1st IEEE Int. Workshop on Power Electronic Design, Test and Applications*, pages 149–153, Christchurch, New Zealand, January 2002.
- [67] C.P. Quigley, R.J. Ball, A.M. Vinsome, and R.P. Jones. Predicting journey parameters for the intelligent control of a hybrid electric vehicle. In *Proc. of the IEEE Int. Symp. on Intelligent Control*, pages 402–407, September 1996.
- [68] J.J. Romm and A.A. Frank. Hybrid vehicles gain traction. *Scientific American*, pages 56–63, April 2006.
- [69] T. Sakamoto, T. Matsuda, and T. Minami. Evaluation of hybrid electric vehicle battery life in North American market. In *Proc. of the EVS 22 - Electric Vehicle Symposium*, Yokohama, Japan, October 2006.
- [70] H. Santoso and W.K. Cheng. Mixture preparation and hydrocarbon emissions behaviors in the first cycle of SI engine cranking. In *Powertrain & Fluid Systems Conference & Exhibition*, San Diego, CA, October 2002. SAE Paper 2002-01-2805.
- [71] H.-P. Schöner and P. Hille. Automotive power electronics - New challenges for power electronics. In *IEEE 31st Annual Power Electronics Specialists Conf., PESC 00*, volume 1, pages 6–11, June 2000.
- [72] N.J. Schouten, M.A. Salman, and N.A. Kheir. Fuzzy logic control for parallel hybrid vehicles. *IEEE Trans. on Control Systems Technology*, 10(3):460–468, May 2002.
- [73] A. Sciarretta, M. Back, and L. Guzzella. Optimal control of parallel hybrid electric vehicles. *IEEE Trans. on Control Systems Technology*, 12(3):352–362, May 2004.

- [74] A. Sciarretta, L. Guzzella, and M. Back. A real-time optimal control strategy for parallel hybrid vehicles with on-board estimation of the control parameters. In *Proc. of the IFAC Symp. on Advances In Automotive Control*, Salerno, Italy, April 19-23 2004.
- [75] L. Serrao, Z. Chehab, Y. Guezennec, and G. Rizzoni. An aging model of Ni-MH batteries for hybrid electric vehicles. In *Proc. of the IEEE Vehicle Power and Propulsion Conference*, pages 78–85, Chicago, IL, September 2005.
- [76] J. Shen, A. Masrur, V.K. Garg, and J. Monroe. Automotive electric power and energy management: A system approach. In *Business Briefing: Global Automotive Manufacturing and Technology*. Touch Briefings, April 2003.
- [77] G. Steinmaurer and L. del Re. Optimal energy management for mild hybrid operation of vehicles with an integrated starter generator. In *Proc. of the SAE World Congress*, Detroit, Michigan, April 2005. SAE Paper 2005-01-0280.
- [78] E.D. Tate and S.P. Boyd. Finding ultimate limits of performance for hybrid electric vehicles. In *Proc. of the SAE Future Transportation Technology Conf.*, Costa Mesa, CA, August 2000. SAE Paper 2000-01-3099.
- [79] M. Thele, E. Karden, E. Surewaard, and D.U. Sauer. Impedance-based overcharging and gassing model for vrla/agm batteries. *J. of Power Sources*, 158(2):953–963, August 2006.
- [80] K.G.O. van de Meerakker, P.C.J.N. Rosielle, B. Bonsen, T.W.G.L. Klaassen, and N.J.J. Liebrand. Mechanism proposed for ratio and clamping force control in a cvt. In *Proc. of the FISITA World Automotive Conf.*, Barcelona, Spain, May 2004.
- [81] P.P.J. van den Bosch and F.A. Lootsma. Scheduling of power generation via large-scale nonlinear optimization. *J. of Optimization Theory and Appl.*, 55:313–326, 1987.
- [82] C.A. Vincent and B. Scrosati. *Modern batteries : an introduction to electrochemical power sources*. Arnold, London, second edition, 1997.
- [83] M.J. West, C.M. Bingham, and N. Schofield. Predictive control for energy management in all/more electric vehicles with multiple energy storage units. In *Proc. of the IEEE Int. Electric Machines and Drives Conf.*, volume 1, pages 222–228, June 2003.
- [84] S.S. Williamson and A. Emadi. Comparative assessment of hybrid electric and fuel cell vehicles based on comprehensive well-to-wheels efficiency analysis. *IEEE Trans. on Vehicular Technology*, 54(3):856–862, May 2005.
- [85] K.B. Wipke, M.R. Cuddy, and S.D. Burch. ADVISOR 2.1: A user-friendly advanced powertrain simulation using a combined backward/forward approach. *IEEE Transactions on Vehicular Technology*, 48(6):1751–1761, November 1999.
- [86] J.-S. Won and R. Langari. Intelligent energy management agent for a parallel hybrid vehicle. In *Proc. of the American Control Conf.*, Denver, CO, June 2003.

Summary

Energy Management for Automotive Power Nets

Reducing fuel consumption has always been a major challenge to the automotive industry. Whereas first marketing aspects gave rise to innovative research, today the environmental regulations have become the main driving force behind new technologies. Historically, the research concentrated on improvements for the mechanical side of the vehicle. However, the introduction of Hybrid Electric Vehicles (HEV), where the propulsion power can also be delivered by an electric machine, definitely emphasizes the benefits of electro-mechanical solutions. With a secondary power source, the HEV can satisfy the vehicle power demand in various ways. An energy management (EM) strategy is needed to control this added freedom in a fuel-efficient way.

At present, a broad range of EM strategies has been proposed in literature and several concepts have been implemented in series-production vehicles. Typically, the academic solutions focus on complex optimization techniques, arising from well defined mathematical problems. The engineering approach offers a sub-optimal strategy, based on heuristic rules. Nevertheless, both policies fail when the important vehicle characteristics for EM are not well understood.

The main contribution of this thesis is to deduce a physical explanation of the EM problem for all HEV configurations, viz., the series-HEV, the parallel-HEV and the combined series/parallel-HEV. By having a good understanding of the vehicle properties of interest, it becomes possible to develop a model-based EM strategy that mimics the optimal solution, without the need for complex optimization routines, nor the necessity for having accurate predictions about the future driving cycle. The proposed causal strategy is directly suitable for on-line implementation in a vehicle.

The primary goal of an EM strategy is to maximize the fuel efficiency of the vehicle. In practice, this requirement is often associated with operating the internal combustion engine (ICE) in its highest efficiency region. Nevertheless, this thesis reveals that this concept is only partially true. A better understanding of how to operate the ICE follows from two other properties:

the slope of the fuel map and its fuel offset at idle speed. A formal optimization problem is formulated to prove that these properties also relate to a mathematical interpretation, and infer from the optimal solution.

For all the HEV configurations mentioned above, a power-oriented vehicle model is derived. Next, a suitable EM strategy is proposed. This strategy originates from a non-causal global optimization, but through a physical understanding of the parameters of interest, it is translated into a causal on-line strategy. To cope with uncertainties in the future power demand, a feedback mechanism is added which automatically regulates the energy in the battery near a reference value. Contrary to standard control experience, this feedback control loop has a better performance if it incorporates a small bandwidth and a large tracking error.

Simulation results for all HEVs demonstrate that the proposed EM strategy achieves a fuel economy which is almost equivalent to the optimal solution. Moreover, when the fuel costs for producing electric power are accurately known in advance, this strategy has the ability to further improve its performance. In practice, however, this requirement is inappropriate, since causality of the EM strategy is lost.

An alternative methodology is presented to include road predictions into the causal EM strategy. By means of an electronic horizon, the prediction information is translated into a preferred reference trajectory for the energy stored in the battery. However, it will be demonstrated that the added value of having knowledge about the future driving cycle is limited, compared to the situation without prediction information.

Finally, the EM concept can also be applied to the electric power net of vehicles with a traditional drive train, or micro HEVs. Here, the alternator takes the position of the electric machine. As a case-study, the EM strategy has been implemented in a Ford Mondeo vehicle. Vehicle experiments on a roller-dynamometer test-bench show that profits in fuel economy are achieved up to 2.6% for a typical driving cycle. Although the potential fuel benefits are limited for the vehicle under consideration, the return on investment is extremely high, since it requires primarily changes in the vehicle software.

Samenvatting

Binnen de automobielindustrie is brandstofbesparing altijd een belangrijk punt van aandacht geweest. Werd voorheen het onderzoek op dit gebied vooral geïnitieerd door marketing aspecten, tegenwoordig zijn met name de strenge milieu eisen vanuit de overheid de drijvende kracht achter nieuwe ontwikkelingen. In het verleden concentreerde het onderzoek zich voornamelijk op het verbeteren van de mechanische aspecten van het voertuig, maar met de introductie van hybride voertuigen (Hybrid Electric Vehicle, HEV), waarbij de aandrijving van het voertuig deels door een elektrische machine wordt gerealiseerd, werd duidelijk welke voordelen een elektro-mechanische oplossing biedt. Door de aanwezigheid van een tweede vermogensbron, is het voor een HEV mogelijk om het gevraagde vermogen op verschillende manieren te leveren. Een passende energie management (EM) strategie is noodzakelijk voor een optimaal brandstofverbruik.

In de afgelopen jaren is een breed scala aan EM strategieën beschreven in de literatuur en zijn diverse concepten inmiddels toegepast in serie-productie voertuigen. Daarbij richten de academische oplossingen zich vooral op complexe optimalisatie technieken, welke ontstaan uit een formele wiskundige probleemstelling. Anderzijds zijn vele sub-optimale strategieën toegepast, welke gebaseerd zijn op heuristische regels.

De bijdrage van dit proefschrift is een fysische afleiding van het EM probleem voor vele HEV configuraties, te weten de serie-HEV, de parallel-HEV en de serie/parallel-HEV. Middels het doorgronden van de belangrijke voertuig eigenschappen voor EM blijkt het mogelijk een model-gebaseerde EM strategie te ontwikkelen, welke in staat is om de optimale oplossing na te bootsen, zonder gebruik te maken van complexe optimalisatiemechanismen, of te beschikken over nauwkeurige voorspellingen van het toekomstige rijgedrag. Deze causale strategie is direct toepasbaar in een voertuig.

De hoofdtaak van de EM strategie is het minimaliseren van het brandstofverbruik. In de praktijk wordt deze doelstelling vaak gekoppeld aan de wens om de verbrandingsmotor enkel in zijn meest efficiënte werkgebied te bedrijven. Echter, dit proefschrift toont aan dat deze gedachtegang slechts gedeeltelijk juist is. Een beter inzicht in het gebruik van de verbrandingsmotor voor EM volgt uit de volgende twee karakteristieken: de helling

waarmee brandstof curves stijgen bij een toenemend motor vermogen en het brandstofverbruik bij een netto vermogen gelijk nul. Door een formeel optimalisatieprobleem te formuleren ontstaat tevens een wiskundige interpretatie van deze eigenschappen met betrekking tot de optimale oplossing.

Voor alle bovengenoemde HEV configuraties is een vermogensgebaseerd model afgeleid. Vervolgens is een passende EM strategie ontwikkeld. Deze strategieën gebruiken als startpunt een niet-causale globale optimalisatie, maar door fysische kennis van het EM probleem, wordt dit vertaald naar een causale strategie. Voor het omgaan met onzekerheden in de toekomstige rijcyclus wordt een terugkoppeling ingebracht, zodat de energie in de accu nabij een referentiewaarde blijft. In tegenstelling tot traditionele regellussen neemt hier de prestatie toe, wanneer een kleine bandbreedte met een grote volgfout wordt gekozen.

Simulatiesresultaten tonen aan dat de voorgestelde EM strategie voor elke HEV configuratie nagenoeg hetzelfde brandstofverbruik behaalt als de optimale oplossing. Evenwel wordt een nog betere prestatie geleverd, indien er nauwkeurige informatie is over de benodigde brandstof voor het toekomstig gevraagde elektrisch vermogen. Echter, deze eis is praktisch niet realiseerbaar, daar causaliteit niet gewaarborgd blijft. Om voorspellingen van het toekomstige rijgedrag mee te nemen in de voorgestelde causale EM strategie, wordt een alternatieve methode gepresenteerd. Middels een elektronische horizon worden de voorspellingen omgezet in een gewenst referentietraject voor de energie in de accu. Het blijkt dat het hebben van kennis over de toekomst slechts een zeer beperkte toegevoegde waarde heeft voor de prestaties van een EM strategie.

Tot slot is het EM concept ook toepasbaar op voertuigen met een traditionele aandrijflijn en zogenaamde micro-hybride voertuigen. Bij wijze van proef is het EM systeem in een Ford Mondeo geïmplementeerd. Middels een vaste rijcyclus op een gecertificeerde roller-bank is een brandstofbesparing gemeten van 2.6%. Hoewel de mogelijke besparing in dit voertuig beperkt is, is de gedane investering zeer effectief, aangezien voornamelijk aanpassingen in de software van het voertuig nodig zijn.

Dankwoord

Inmiddels is het alweer december geworden, maar van een echte winter is nog lang geen sprake. Vanaf de vierde verdieping van het Potentiaal gebouw (lees E-hoog) zie ik weer een mooie rode gloed aan de horizon verschijnen, waar zo dadelijk de zon gaat opkomen. Deze maandag morgen is een prima moment om terug te kijken op vier jaar onderzoek, waarin ik met veel plezier heb mogen samenwerken met een fijne groep mensen en die mij op legio manieren vooruit hebben geholpen. Allemaal bedankt daarvoor!

Toch zijn er enkele personen die ik graag speciaal wil noemen. Als eerste noem ik mijn promotor (en tevens co-promotor) Paul van den Bosch. Menig weekeinde heb jij je ingezet om mijn onderzoek vooruit te helpen. Door jouw onvoorwaardelijke steun en betrouwbaarheid, wist je mij zelfvertrouwen te geven en werden alle kansen maximaal benut. Bovendien heb ik veel mogen leren van jouw levenswijsheid.

Een andere belangrijke spil in de voortgang van mijn onderzoek was Will Hendrix. De rol van project leider is zeker niet voor iedereen weggelegd, maar bij jou past het echt! Ook denk ik met plezier terug aan het reizen naar Aken voor het uitvoeren van de voertuigexperimenten en waarbij we ondertussen konden bijpraten over de voortgang van mijn promotie. Een zelfde mate van dank gaat uit naar Maurice Heemels. Jouw sociale betrokkenheid is meer dan bijzonder te noemen en zal mij altijd bijblijven. Hopelijk mogen we nog lang met z'n drieën gaan zwemmen.

Een andere grote bijdrage in mijn werk komt van collega promovendus Michiel Koot. Michiel, dankzij jou raakte ik snel vertrouwd met de wereld der werktuigbouwkunde. Tevens bedankt om mij op sleptouw te nemen naar allerlei conferenties in het buitenland. Reizen met jou was super!

Daarnaast wil ik de wetenschappelijke bijdrage van Bram de Jager zeker niet onvermeld laten. Jouw kritische, doch eerlijke manier van kijken heeft mijn werk alleen maar beter gemaakt. Ook de waardevolle discussies met Theo Hofman droegen hiertoe bij. Uiteraard ben ik zeer erkentelijk voor de feedback die ik mocht ontvangen van de mensen uit mijn kerncommissie: Daniël Kok, Joop Pauwelussen, Maarten Steinbuch en Okko Bosgra.

Buiten de wetenschap heb ik veel plezier beleefd met de (ex-) promovendi van onze vakgroep. Een hechte club werd gevormd door: Andrej,

Nelis, Mark, Maarten, Heico, Mircea, Satya, Bart, Aleksandar, Patricia en Leo. Evenwel toch een bijzonder woordje van dank voor mijn kamer genoot Heico Sandee. Als geen ander had jij oog voor andere dingen dan promoveren en de gedrevenheid die jou omringt, leidt tot enthousiasme bij iedereen. Jammer dat we niet vaker samen muziek hebben gemaakt. Also thanks to Andrej Jokic for helping me with mathematics.

Naast alle promovendi heb ik ook veel mogen leren van de elektrostudenten Joris, Marc, Jan-Willem en Rachid. Zeker het koffie uurtje met Joris is een blijvende activiteit geworden.

Hoewel de CS-groep nog veel meer mensen omvat, wil ik speciaal Barbara en Udo noemen. Jullie toewijding tot het werk gaat veel verder dan enkel het verlenen van service; bedankt daarvoor! Daarnaast liep ik graag binnen bij Femke en Renée van de afdeling personeelszaken. Het is wel gebleken dat promoveren meer is dan alleen jezelf technisch ontwikkelen. Fijn dat jullie daar oog voor hadden. Überhaupt was de TU/e een fijne werkgever. De festiviteiten rond het 50 jarig bestaan van afgelopen jaar, zoals bijvoorbeeld het optreden van Rowwen-Hèze, waren geweldig.

Buiten de TU/e wil ik ook de mensen van Ford Forschungszentrum Aachen bedanken. Met Daniël als initiator, maar ook Edo, Engbert, Holger, Thomas en Mark ontstond een mooi project met veel ruimte om onze eigen ideeën in te brengen.

Ook mag in dit dankwoord het dagelijkse treingezelschap Mariëlle, Xander en Ron niet ontbreken. Om te beginnen wil ik Mariëlle van Veggel bedanken voor al die interessante gesprekken. Onze promoties verliepen vrijwel synchroon, waardoor we altijd wel iets te vertellen hadden. Maar gelukkig gingen deze gesprekken ook vaak over hele andere dingen dan werk; van muziek maken tot een betere zwemtechniek; van het kopen van een huis tot het vinden van een nieuwe baan. Ik wens Xander en Ron veel succes met hun promotie en het jaarlijkse schaatsen met Ron blijft gewoon leuk.

Als laatste volgt dan mijn dank aan de familie thuis. Pap en mam, bedankt voor al jullie goede zorgen in de afgelopen jaren. Dankzij jullie was er altijd iemand in de buurt om te vertellen wat de dag mij weer had gebracht. Mijn broer Wim wil ik heel erg bedanken voor de bouwactiviteiten die we altijd op zaterdag ontplooiden. Zo'n ontspanning blijkt hard nodig na vijf dagen bureau werk. Als allerlaatste bedank ik mijn zus Angelique. De e-mails die ik van 'JeZus' mocht ontvangen brachten altijd een brede glimlach rond mijn mond.

Eindhoven, december 2006.

Index

- bandwidth, 91, 105, 141, 144
- baseline (BL), 40, 56, 103, 122
- battery, 23, 30, 39, 55, 65
 - charge acceptance, 81
 - lead-acid, 23
 - start, light, and ignition (SLI), 30
 - valve-regulated lead-acid (VRLA), 30
- battery wear, 75, 114, 137
- brake specific fuel consumption (BSFC), 17
- CarSim, 16
- charge sustaining, 3, 46, 59, 72, 112, 146
- charging mode (C), 40, 43, 58
- circulating power, 68
- complementary sensitivity, 141
- continuously variable transmission (CVT), 62
 - electronically-controlled (eCVT), 63
- depth of discharge (DOD), 76
- drag torque, 19, 58
- drive train, 20, 26, 36, 54
- driver, 29, 128
- dSPACE MicroAutoBox, 121
- dynamic programming (DP), 10, 46
 - stochastic DP, 94
- e-line (economy line), 38, 68
- efficiency, 5
 - tank-to-wheel, 5
 - well-to-tank, 5
 - well-to-wheel, 5
- electric machine, 22, 36, 67
- electric vehicle (EV), 3
- electronic horizon (e-horizon), 93
- energy management (EM), 2, 35
- engine control unit (ECU), 18, 121, 128
- engine running signal, 39, 46
- engine stop/start, 7, 18, 138
- final drive, 20, 28, 66
- fourier transform, 145
- fuel cell hybrid vehicle (FCHV), 3
- fuel cut-off, 19, 58
- fuel economy, 45, 59, 71, 86, 112, 126
- fuel map, 17, 40, 55, 110
- generator, 22, 37
 - alternator, 111
- hybrid electric vehicle (HEV), 2, 3, 35
 - full HEV, 4, 53
 - micro HEV, 4, 53
 - mild/medium HEV, 4, 53
 - P-HEV, 4, 53
 - S-HEV, 4, 36
 - S/P-HEV, 4, 62
- hydrogen ICE, 3
- incremental fuel cost, 40, 56, 118
- integrated starter/generator (ISG), 19, 53, 55, 81

- internal combustion engine (ICE),
 - 2, 16, 38, 54, 66, 134
 - engine downsizing, 81
 - spark ignition (SI) engine, 17, 38
- Kharitonov theorem, 142
- Lagrangian, 48, 118
 - Lagrange multiplier, 49, 60, 73, 118
- linear programming (LP), 10, 109
- load scheduling, 7
- lower heating value, 17, 38, 98
- model predictive control (MPC),
 - 10, 117
- motor assist (MA), 7, 57
- motor only (MO), 40, 44, 57, 74
- neural network, 11, 95
- optimization problem, 11, 45, 59, 112
 - optimal control, 10
- piece-wise affine function, 40
- planetary gear train, 63
- plug-in vehicle, 3
- power distribution management (PDM),
 - 109, 122
 - flexible power demand, 108
- power net, 37, 55, 65
- power supply management (PSM),
 - 40, 43, 58, 109, 122
- probability density function (PDF),
 - 97
- proportional integral (PI) controller,
 - 29, 52, 62, 75, 105, 121, 140
- quadratic programming (QP), 10, 99, 109, 113
- reformer, 3
- regenerative braking (R), 6, 44, 50, 58, 74, 122
- spectrum, 105, 145
- stability, 142
 - stable polynomial, 142
- state of charge (SOC), 24
- state of energy (SOE), 24, 111
- sweet spot, 83
- Taylor approximation, 114
- vehicle model
 - backward vehicle model, 20
 - conventional vehicle, 110
 - dynamic vehicle model, 26
 - forward vehicle model, 20, 26
 - P-HEV, 54, 81
 - quasi-static vehicle model, 16
 - S-HEV, 36, 80
 - S/P-HEV, 65, 82

Curriculum Vitae



31 december 1977 Geboren te Venray.

1991 - 1992 Brugklas, Kath. MAVO „De Kolk”, Venray.

1992 - 1995 HAVO, Kath. Scholengemeenschap „Jerusalem”, Venray.

1995 - 1996 Propedeuse certificaat HTS Hogere Informatica,
Hogeschool Eindhoven.

1996 - 2000 HTS Elektrotechniek, Hogeschool Eindhoven / Fontys Hogescholen. Specialisatie Technische Computerkunde. Afstudeeropdracht bij ASML te Veldhoven. Onderwerp: ontwikkelen van besturingssoftware voor een precisie-mechanica meetinstrument.
Diploma behaald met lof.

2000 - 2003 Verkorte opleiding elektrotechniek, Technische Universiteit Eindhoven. Studierichting Informatietechnische Wetenschappen. Afstuderen binnen de sectie Control Systems. Onderwerp: “Model checking and nonlinear predictive control – A case-study on an energy management system for cars”. Diploma cum laude.

2003 - 2007 Promotie onderzoek / Assistent in opleiding (AIO), Technische Universiteit Eindhoven. Faculteit Elektrotechniek, capaciteitsgroep Meet- en Besturingssystemen; sectie Control Systems. Onderwerp: dit proefschrift.



Energy Management for Automotive Power Nets

John Kessels

Energy Management for Automotive Power Nets



John Kessels

UITNODIGING

tot het bijwonen van de openbare
verdediging van het proefschrift

**Energy Management
for Automotive Power Nets**

op woensdag
14 februari 2007
om 16:00 uur

in het Auditorium van de
Technische Universiteit Eindhoven

Den Dolech 2
5600 MB Eindhoven

Na afloop van de
promotieplechtigheid volgt
om 17:30 uur een receptie.
Ook daarvoor bent u van
harte uitgenodigd.

John Kessels
Heidseweg 47
5812 AA Heide
j.t.b.a.kessels@tue.nl



STELLINGEN

behorende bij het proefschrift

*Energy Management
for Automotive Power Nets*

door

John Kessels

Eindhoven, februari 2007

1. Een succesvol energie management systeem benut de volgende karakteristieken van een verbrandingsmotor:
 - a. een draaiende motor verbruikt brandstof bij stilstand van het voertuig;
 - b. het motorkenvel beschrijft een niet-lineaire relatie tussen brandstofgebruik en netto motorvermogen, gegeven een constant toerental;
 - c. het motorkenvel beschrijft een niet-constante relatie tussen brandstofgebruik en toerental, gegeven een constant motorvermogen;waarbij a en b tijdelijke energie opslag vereisen.

dit proefschrift, hoofdstuk 3

2. Een energie management strategie kan anticiperen op toekomstige motorbelasting, door aanpassing van de referentiewaarde voor de energietoestand van de accu.

dit proefschrift, hoofdstuk 5

3. Een goed energie management systeem heeft een slechte storingsonderdrukking.

dit proefschrift, appendix A

4. Bandbreedte is een te breed begrip.

5. Ontwerper's gebreken, worden dikwijls met regeltechniek glad gestreken.
6. Naarmate de promovendus teksten scherper formuleert, neemt het gewicht van het proefschrift voor een deskundige toe en voor de leek af.
7. De titellengte van een artikel of proefschrift is omgekeerd evenredig met de omvang van het probleem dat wordt opgelost.
8. De mens kijkt uitsluitend naar het verleden.
9. De liberalisering van zorg en energie, kost de burger zorg en energie.
10. Het zelf bouwen van een huis is het ultieme voorbeeld van concessies doen.
11. Waar het in het leven vooral om gaat, is hoe je met elkaar omgaat.
12. Als je in jezelf gelooft, gelooft een ander je ook.